Photo- and Electro-Chemistry Methods for Waterborne Pathogen Treatment and Detection in Environmental Water

Thesis by

Siwen Wang

In Partial Fulfillment of the Requirements for the Degree of

Doctor of Philosophy in Environmental Science and Engineering

CALIFORNIA INSTITUTE OF TECHNOLOGY

Pasadena, California

2020

(Defended September 16, 2020)

Siwen Wang
ORCID: 0000-0002-8553-425X

DEDICATION

To my husband, Yang, for always loving me, supporting me, and being at my side.

To my son, Edmund, without whom I would have written a better thesis, but my life would never have been complete.

ACKNOWLEDGEMENTS

I believe that I am not the only one who always imagined the moment of writing the acknowledgements for their PhD thesis during the many years of study. There truly are too many things to be grateful for and lots of people to thank, for making the completion of this thesis possible.

First and foremost, I would like to thank my thesis advisor, Michael R. Hoffmann, who has since become more than that, a friend of mine and my family, for his guidance, support, and trust throughout the five years of my PhD study. Mike provided me advice from the most basic chemical mechanisms to the grand picture of my career over our discussions on projects, manuscripts, and courses. His quoting on specific numbers in chemistry, such as pK_a, without a blink has always been fascinating to me during our discussions. We also shared opinions on life, politics, health, and technologies other than the ones we work on, and I am always inspired by his wisdom and humor. I want to thank Mike especially for being continuously supportive during my life-changing events in the past few years, including becoming a mother and moving across the country in my last year of study, as well as when I encountered discrimination during my pregnancy and maternity leave. His trust in my ability has been a consistent driving force for me to finish my thesis.

Thank you to Jared Leadbetter, David Tirrell, and Kaihang Wang for being members of my thesis advisory committee, and for providing guidance and advice on my thesis work. Thanks to Jared, for chairing my thesis advisory committee, and providing valuable advice as a microbiologist and detailed feedbacks on my manuscript draft starting from our very first meeting. Thanks to Dave, who is probably one of the busiest faculty members at Caltech, but always immediately replied to my emails for scheduling meetings, spent time discussing my research progress, and always directly pointing out the key problems. Thanks to Kaihang, whose enthusiasm and curiosity for science inspired me from the first time we met, though in Caltech daycare, for your patience with helping me learn the most basic concepts of DNA cloning and providing all the resources I needed for my work on antibiotic resistance genes in my later PhD years.

Thanks to Alex Sessions, who was the advisor of my second project for the first-year qualifying exam, for teaching me everything I know about isotopes, and for being present at every one of my oral exams and thesis advisory meetings ever since and always the first one to congratulate and encourage me.

I want to thank Andrew Thompson, who was our option representative for many years, for being constantly informative, supportive, and caring, for providing advice on my academic study and plan, and for sharing experiences of life.

Thank you to Simona Bordoni, for providing me imperative support to finish the course of Atmosphere Dynamics during my pregnancy, and for sharing her own experiences on raising children while completing her PhD study. Although I always knew that the PhD program is not welcoming to parents, and I came to understand that even better after I really became one. Simona's story greatly encouraged me and made me believe the possibility of balancing these two touch tasks at the same time. Her story has inspired and motivated me to become a female scientist like her.

I thank the past and present postdocs in the Hoffmann group, with whom I worked on the MEMs project, Xing Xie, Janina Bahnemann, Katharina Urmann, Xingyu Lin, Leda Katebian, and Jing Li, for all their advice on my projects and manuscripts. I learned a lot about microbiology and DNA detection from them. I want to thank Xing particularly for helping me and treating me as an independent peer researcher from the very beginning when I started research in this brand new area at Caltech.

It was such a pleasant journey to work with other past and present members of Hoffmann group, Yan Qu, Clement Cid, Kangwoo Cho, Hyunwoong Park (HP), Su Young Ryu, Justin Jasper, Cody Finke, Zaneib Jelif, Sara Rastosa, Sara (Lijie) Li, Eitam Shafran, Hugo Leandri, Nissim Gore-Datar, Junghun Lim, Alan Gu, Sean Kim, Axl LeVan, and many others. I am grateful for the joys and beers we shared together with the presentations and research discussions during our group meetings every Friday afternoon.

My thesis work could not have been completed without the great and continuous support from Caltech staff, who helped me with literally every detail in my academic study and life. I also thank Dr. Nathan Dalleska for his great technical support at the Environmental Analysis Center.

Thank you to my fellows, Yanzhe Zhu, Xunyi Wu, Jieun Shin, and Eunkyung Kim, who joined the Hoffmann group at the same time as, for those struggles on courses and exams we passed through together. Many thanks to Yanzhe and Xunyi, who shared the same office with me for four years, for those chats, laughter, snack time, coffee breaks, and trips that I really cherished.

Thank you to Yuanlong Huang, Ran Zhao, Jinqiang Chen, Hang Yu, and many other friends I met in the GPS Division, for your kindest help and all your enthusiasm for science, your own careers or even fitness and climbing that keeps inspiring me every day.

Thank you to Xiaomeng Xiu, Dongbin Wang, Hanliang Guo, Xing Zhang and Chengpeng Li, for the time we spent time together in Alhambra. Thanks to Xiaomeng and Dongbin for helping me settling down when I just arrived in LA.

Thanks to Hannah Yang and Charles Sanfiorenzo, for your patience, and all the help and support during my visits in Kaihang's group.

During my visit in Clarkson University for the last year of PhD, I want to thank many faculty members and fellows who generously helped me with lab setups, experiments, and moving stuff. Thank you to Shane Rogers, Stefan Grimberg, Thomas Holsen, Fengbin Huang, Shasha Yang, Xudong Su, Estefanny Quispe, and many others.

I am fortunate to have always had great advisors from the first day I started scientific research. A special thanks to my undergrad and Masters thesis advisor, Jun Huang in Tsinghua University, for accepting me as your Masters student, teaching me analytical chemistry and photo-chemistry, offering opportunities of visits abroad and leading field trips, and for those conversations and encouragements during my PhD study. I learned many, many things from Jun, not only about research, but also about, which is more importantly, how to be a good advisor, a parent, a friend, a colleague, and a good person.

I want to acknowledge the Bill and Melinda Gates Foundation for the funding supports for the work set forth in this thesis, and I remain grateful for the opportunity to work on such impactful projects.

Thanks to my two dearest friends, Xing Zhang and Lisha Xi, with whom I spent the most time in LA during my early and later PhD years, respectively, for all the precious time we spent together. You are the sweetest chocolates in my box of life that I remember only the happiest moments for my years in LA.

Lastly, thank you to my family for your enduring love and support. Thank you to my mother, an independent woman, for raising me to another independent woman. Despite those incomprehensible and paradoxical arguments and complaints on my independence for the years after I made my own family, I just want you to know that I always love you. To my husband, Yang, who is my partner for both life and work, for your listening and understanding, love and support, and for all the ups and downs we experienced together. To my son, Edmund, who is the light of my life even in my darkest days.

ABSTRACT

Waterborne disease is a global burden, which is mainly caused by waterborne pathogens disseminated through unsafe water, inadequate sanitation, and hygiene. Antibiotic resistance, which can also spread in water, has become an increasingly serious global health threat as it can prevent the effective treatment of infectious diseases. Improvements on water treatment and detection are the two critical strategies to control the surveillance of waterborne pathogens as well as antibiotic resistance bacteria and genes. The advancement in photo- and electro-chemical methods may provide more opportunities on decentralized water treatment and on-site pathogen monitoring under source-limited conditions. This thesis is dedicated to exploring the possible solutions to automatic, rapid, and easy-to-use *in situ* pathogen analysis for environmental water by adopting photo- or electro-chemical method, and to enhanced removal of antibiotic resistance bacteria (ARB) and antibiotic resistance genes (ARGs) from wastewater by combining photo- and electro-chemical techniques. These include removal of ARB and ARGs by UV-assisted electrochemical treatment, electrochemical cell lysis (ECL) for DNA extraction from bacteria, and sunlight-activated propidium monoazide (PMA) pretreatment for live/dead bacteria differentiation by quantitative real-time polymerase chain reaction (qPCR) detection. Both experimental approaches and computational modelling were used to evaluate the performance of the techniques and to bring more insights into the mechanism. Each study presents a demonstration on real environmental or wastewater to access the potential of their applications under complex environmental parameters.

UV-assisted electrochemical treatment for ARB and ARGs was conducted using a blue TiO_2 nanotube array (BNTA) anode. The inactivation of tetracycline- and SMX-resistant *E. coli* and the corresponding plasmid coded genes (*tetA* and *sul1*) damage was measured by plate counting on selective agar and qPCR, respectively. As a comparison of UV treatment alone, the enhanced reduction of both ARB and ARGs was achieved by UV-assisted electrochemical oxidation (UV-EO) without Cl^- and was further facilitated with the presence of Cl^-, which is attributed to the *in-situ* generated oxidants by electrochemical process. Significantly slower removal of ARG than ARB was observed for both UV irradiation alone and UV-EO treatment, wherein intracellular ARG generally reduced slower than extracellular ones, and short amplicons reduced significantly

slower than long ones. The predominant nucleotide damage by UV irradiation and conformational change by UV-EO treatment was visualized by DNA gel electrophoresis for treated extracellular ARGs. The mechanism on ARB and ARGs damage was further understood by computational chemical modeling. The slower reduction was found for the native bacteria and genes, *tetA* and *sul1*, in the latrine wastewater than that in laboratory-prepared buffered samples. The result emphasizes that all the UV-based techniques may only apply after other treatments to avoid the impairment by the transmittance, color, and particulate material in environmental or wastewater.

A comprehensive investigation was conducted for ECL in terms of its performance on DNA extraction from gram-negative bacteria (*Escherichia coli* and *Salmonella* Typhi) and gram-positive bacteria (*Enterococcus durans* and *Bacillus subtilis*). A milliliter-output ECL device was developed based on the disruption of the cell membrane by OH^- that can be generated locally at the cathode and accumulated improvingly through a cation exchange membrane. Both gram-negative and gram-positive bacteria were successfully lysed within 1 min at a low voltage of ~5 V. To better understand the pH effects on cell lysis, the pH profile at the cathode surface and in bulk cathodic effluent was simulated via hydroxide transport in the cathodic chamber. The demonstration of ECL on various environmental water sample types (including pond water, treated wastewater, and untreated wastewater) showed its potential as a prelude to nucleic-acid based analyses of waterborne bacteria in the field.

Propidium monoazide (PMA), a nucleic acid-binding dye, has been used to distinguish live from dead cells prior to PCR-based detection. To explore the off-the-grid application of PMA, sunlight was investigated for PMA activation as an alternative light source to a typical halogen lamp. PMA was successfully activated by a solar simulator, and the pretreatment conditions were optimized with respect to the PMA concentration as 80 μM and the exposure time as 10 min. The optimal PMA pretreatment was tested on four different bacteria species (two gram-positive and two gram-negative), and the effects of sunlight intensity and multi-sequential treatment were studied. Sunlight-activated PMA pretreatment was eventually demonstrated on latrine wastewater samples with natural sunlight on both sunny and cloudy days. The results showed the potential of sunlight-

activated PMA pretreatment to be integrated into a lab-on-a-chip (LOAC) PCR device for off-the-grid microbial detection and quantification.

PUBLISHED CONTENT AND CONTRIBUTIONS

Wang, S., Yang, S., Wang, K., Yang, H., Sanfiorenzo, C., Rogers, S., Yang, Y. and Hoffmann, M. R. "Removal of antibiotic resistant bacteria and genes by UV-assisted electrolysis on degenerative TiO_2 nanotube array". *To be submitted*.

Wang, S conceived the project, performed the experiments, interpreted the data, and wrote the manuscript.

Wang, S., Zhu, Y., Yang, Y., Li, J., Hoffmann, M. R. (2020). "Electrochemical cell lysis of gram-positive and gram-negative bacteria: DNA extraction from environmental water samples". In: *Electrochimica Acta*, 2020, 338, 135864. https://doi.org/10.1016/j.electacta.2020.135864.

Wang, S conceived the project, performed the experiments, interpreted the data, and wrote the manuscript.

Zhu, Y., Huang, X., Xie, X., Bahnemann, J., Lin, X., Wu, X., Wang, S., Hoffmann, M. R. (2018). "Propidium monoazide pretreatment on a 3D-printed microfluidic device for efficient PCR determination of 'live versus dead' microbial cells". In: *Environmental Science: Water Research & Technology* 2018, 4, (7), 956-963. https://doi.org/10.1039/C8EW00058A.

Wang S. participated in experiments of propidium monoazide pretreatment.

Xie, X.; Bahnemann, J.; Wang, S.; Yang, Y.; Hoffmann, M. R. (2016). " 'Nanofiltration' Enabled by Super-Absorbent Polymer Beads for Concentrating Microorganisms in Water Samples". In: *Scientific Reports* 2016, 6, 20516. https://doi.org/10.1038/srep20516.

Wang S. participated in culturing microorganisms, concentration experiments with super-absorbent polymers, reviewed and edited the manuscript.

Xie, X.; Wang, S.; Jiang, S. C.; Bahnemann, J.; Hoffmann, M. R. (2016). "Sunlight-Activated Propidium Monoazide Pretreatment for Differentiation of Viable and Dead Bacteria by Quantitative Real-Time Polymerase Chain Reaction". In: *Environmental Science & Technology Letters* 2016, 3, (2), 57-61. https://doi.org/10.1021/acs.estlett.5b00348.

Wang S. participated in experiment design for the optimization of propidium monoazide treatment using simulated sunlight, contributed in DNA extraction and detection, data analysis, and participated in the manuscript.

TABLE OF CONTENTS

LIST OF ILLUSTRATIONS

Number *Page*

LIST OF TABLES

Number *Page*

Chapter 1

INTRODUCTION

1.1 Background and motivation

Every year, there are more than 2.2 million deaths and cases of severe illnesses caused by waterborne diseases, including diarrhea, gastrointestinal diseases, and systematic illnesses. Most of these deaths are children under five, approximately 4,000 every day (World Health Organization, 2015; Ramírez-Castillo, F.Y. *et al.*, 2015). The vast majority of these young victims died of illnesses attributable to their water source contaminated by raw sewage. Unsafe water, inadequate sanitation, and hygiene were responsible for their deaths, which are preventable. It is estimated that 780 million people do not have access to improved water sources, and 2.5 billion people (*i.e.*, 35% of the world's population) lack access to improved sanitation (Centers for Disease Control and Prevention, 2018). The World Health Organization (WHO) has reported that the improvements to drinking-water, sanitation, hygiene, and water resource management could reduce almost 10% of the total burden of disease worldwide (World Health Organization, 2016). The Hoffmann research group was motivated by this urgent need, and has been continuously undertaking efforts on the development of decentralized wastewater treatment technologies and on-site pathogen monitoring systems that can be applied under source-limited conditions. A self-contained solar-powered toilet (Caltech Solar Toilet) based on electrochemical wastewater treatment was invented by our group, as a response to the "Reinvent the Toilet Challenge" announced by The Bill & Melinda Gates Foundation in 2011. As the core unit, the electrochemical reactor of the Caltech Solar Toilet utilizes semiconductor anodes for oxidization of chloride to chlorine, leading to the disinfection of microorganisms (Huang *et al.*, 2016). Hereafter, a "Portable Pathogen Analysis System (PPAS)" based on nucleic acid detection was proposed to integrate sample concentration, preparation, and detection for the fast and cost-effective pathogen analysis of wastewater. In this thesis, I present my work on the photo- and electrochemical methods for the treatment and detection of waterborne pathogens.

Bacteria, virus, and parasites have been the leading causes for waterborne disease outbreaks. In 2011 to 2012, waterborne diseases caused 431 cases of illness in United States, wherein 47% were caused by bacteria, 32% by viruses, and 11% by parasites (Beer *et al.*, 2015). Municipal wastewater treatment plants are designed to target these pathogens. However, another major threat to human health that can spread in water, antibiotic resistance, has been overlooked for years until the last decade. Antibiotics have revolutionized the field of medicine and saved millions of lives since the discovery of penicillin by Alexander Fleming in 1928 (Martens and Demain, 2017; Ventola, 2015). Almost one century after, we are facing a global crisis: many antibiotics are no longer effective for treating even the simplest infection (Martens and Demain, 2017). The antibiotic resistance crisis has been considered attributable to overuse and misuse of antibiotics. In addition, the lack of new antibiotic discovery has also made the matters worse. Worldwide, at least 700,000 people die from drug-resistant diseases each year (World Health Organization, 2019). In the United States, more than 2.8 million antibiotic resistant infections occur each year, which results in 35,000 cases of death (Centers for Disease Control and Prevention, 2019). In 2015, the WHO announced a global action that urges international participation on controlling and monitoring the spread of all forms of antimicrobial resistance, including antibiotic resistance, the most urgent drug-resistance trend (World Health Organization, 2015).

Wastewater treatment plants (WWTPs) have been identified as a significant source of both antibiotic resistance bacteria (ARB) and antibiotic resistance genes (ARGs) that are released into the environment. Wastewater and WWTPs act as reservoirs of antibiotic resistance that originates from different sources, *e.g.,* municipal, hospital and livestock waste, and also as the hotspots for horizontal gene transfer (HGT), which enables broader dissemination of ARGs (Karkman *et al.*, 2018). HGT can occur through different mechanisms including: 1) transformation, where competent bacteria uptake free DNA from their surroundings; 2) transduction, where DNA is transferred from a bacteriophage-infected bacterium into a bacteriophage-susceptible bacterium; and 3) conjugation, where DNA passes from a donor cell to an acceptor cell through direct cell-cell contact (Thomas and Nielsen, 2005). Transformation allows the spread of ARGs without a viable or infective donor microbe. As a result, wastewater treatment processes that kill the microbe containing ARGs do not necessarily eliminate the discharge of ARGs to downstream, as they are

not designed to damage nucleic acids (Chang *et al*., 2017). A number of studies have reported that individual commonly-used disinfectants, including chlorine, ozone, and UV irradiation, do not have ideal performances for the elimination of ARGs due to ineffective deactivation with regular doses for treatment of other pathogens. The incomplete degradation for ARB and ARGs may promote horizontal gene transfer, *e.g.,* by chlorine, (Shi *et al*., 2013; Zhang *et al*., 2017; Zhuang *et al*., 2015) or microbial selection of ARB, *e.g.,* by UV (Guo *et al*., 2013; Z. Zhang *et al*., 2019). Recently, there has been a trend of combined techniques for more efficient control of ARB and ARGs, especially UV combined with high redox potential oxidants, *e.g.,* UV/chlorine, UV/H_2O_2, UV/peroxymonosulfate and UV/$S_2O_8^{2-}$ (Zhang *et al*., 2015; Lin *et al*., 2016; Pang *et al*., 2016; Yoon *et al*., 2017; Guo *et al*., 2017; Yoon *et al*., 2018; He *et al*., 2019; T. Zhang *et al*., 2019; Nihemaiti *et al*., 2020). Higher reduction rates of ARGs were found for most of the UV-combined treatment methods than UV alone or the oxidant alone. We were motivated by these observations and interested in combining UV with an electrochemical method for the treatment of ARB and ARGs in wastewater, considering that electrochemical processes lead to the *in situ* generation of the aforementioned oxidants.

Detection methods play a major role in monitoring water quality, surveillance, and quantitative microbial risk assessment. Proper assessment of pathogens during water quality monitoring is also critical for decision-making regarding water distribution system infrastructure and the choice of the best water treatment practices for the prevention of waterborne disease outbreaks (Straub and Chandler, 2003). The most important requirements for reliable assessment include specificity, sensitivity, reproducibility, speed, automation, and low cost (Kostić *et al*., 2011). Traditional cultivation-based methods are extensively used for pathogen detection in water quality monitoring, which are, however, labor intensive, time consuming, and often compromised by low sensitivity. Furthermore, viable but non-culturable pathogen cells may also cause false negative results by cultivation-based methods (Law *et al*., 2014; Zhao *et al*., 2014).

However, there have been numerous advances in biomolecular methods for the detection of pathogens. For example, quantitative real-time polymerase chain reactions (qPCR or real-time PCR) provide much faster, more sensitive, and more accurate detection of pathogens than the traditional cultivation-based methods. Such biomolecular techniques also present the

unprecedented possibilities for automatic, real-time, and *in situ* pathogen analysis for microbial risk assessment purposes. To explore these possibilities, the sample preparation step involves the most time-consuming, labor-intensive and expensive steps rather than detection itself. The challenges of the sample preparation followed by downstream nucleic acid-based detection (*e.g.,* qPCR) are the low concentration of pathogens in large volumes of water, the complexity of nucleic acids extraction and purification, and the viability differentiation. Our overarching goal is to develop techniques to solve these challenges and to adapt and integrate into portable pathogen analysis systems that can be used under source limited conditions.

1.2 Thesis Organization

Chapter 2 of this thesis presents the inactivation of antibiotic resistance bacteria (ARB) and degradation of antibiotic resistance genes (ARG) by UV-assisted electrochemical method using a blue TiO_2 nanotube array (BNTA) anode. UV combined techniques (*e.g.,* UV/chlorine and UV/H_2O_2) have been reported to be more efficient for ARG elimination than individual disinfection oxidants alone. In this chapter, we combine UV and electrochemical methods, which can generate the oxidants *in situ*. Both intracellular and extracellular ARGs have been investigated for relative degradation efficiency of the UV-assisted electrochemical methods with a comparison of UV irradiation alone. Comparison of the treatment effectiveness with and without Cl^- as the contributor to reactive chlorine production and, as a consequence, ARG elimination or reduction is evaluated. We provide the fluence-based first-order kinetic rates for gene damage as measured by qPCR. The mechanism of gene damage by this method is visualized by gel electrophoresis. By demonstrating on the latrine wastewater sampled from the solar-powered toilet located at the Caltech campus, we suggest that the UV-assisted electrochemical methods have the potential for efficient ARG elimination as the last step in wastewater treatment.

In **Chapter 3**, we describe the development of a cost-effective, high-throughput electrochemical cell lysis (ECL) device for DNA extraction of bacteria in environmental water. ECL provides a rapid, reagent-free method for cell lysis in contrast to the most commonly used chemical lysis approaches. The ECL technique relies on the cathodic production of hydroxide ions leading to cell membrane disruption. ECL operates low applied voltages that can be easily applied under source-

limited conditions. Unlike the previous ECL studies which mainly focused on clinical samples with a focus on micro-device fabrication, we explore and optimize the environmental applications of this technique. Herein, we present a comprehensive study on performance characterization of ECL with respect to the DNA extraction efficiency for both gram-positive and gram-negative bacteria. We compare the ECL method with homogeneous alkaline lysis at various pH values and suggest that ECL can achieve higher DNA extraction efficiencies with shorter reaction times. The simulations of the hydroxide transport in the cathodic chamber provide additional insight into the advantages and optimal operation conditions of ECL. We demonstrate the ECL method for DNA extraction from microbes present in various environmental water samples, including pond water, treated wastewater, and untreated wastewater. The results confirm the potential of ECL as a rapid sample preparation technique for microbial monitoring in the field.

In **Chapter 4**, we present a modification of propidium monoazide (PMA) pretreatment for viability differentiation followed by qPCR detection. Photoactivation of PMA is normally achieved by exposure to the bright visible light generated by a halogen lamp, which is energy consuming and requires a grid-based source of electricity. A halogen lamp is difficult to integrate into the advanced lab-on-chip PCR devices aiming for microbial detection under source-limited conditions. Instead, we propose to apply sunlight for photoactivation of PMA without the necessity of grid electricity. We optimize the pretreatment conditions in terms of PMA concentrations and sunlight exposure time. The result shows that the signal of DNA in dead cells was successfully reduced by sunlight-activated PMA under the optimal operation condition. We provide more details on the effect of sunlight intensity and multiple sequential treatments on the performance of PMA pretreatment. We also present the demonstration of the optimized PMA-qPCR assays on latrine wastewater samples on both sunny and cloudy days.

Chapter 2

REMOVAL OF ANTIBIOTIC RESISTANT BACTERIA AND GENES BY UV ASSISTED ELECTROLYSIS ON DEGENERATIVE TiO_2 NANOTUBE ARRAYS

Wang, S.; Yang, S.; Wang, K.; Yang, H.; Sanfiorenzo, C.; Rogers, S.; Yang, Y; Hoffmann, M.R. (2020). Removal of antibiotic resistant bacteria and genes by UV-assisted electrolysis on degenerative TiO_2 nanotube arrays. *To be submitted*.

Abstract

Antibiotic resistance has become a global crisis in recent years, while wastewater treatment plants (WWTPs) have been identified as a significant source of both antibiotic resistance bacteria (ARB) and antibiotic resistance genes (ARGs). However, commonly-used disinfectants have been shown to be ineffective for the elimination of ARGs. In this study, we investigated a method that utilizes UV-assisted electrochemical oxidation (UV-EO) that employs blue TiO_2 nanotube array (BNTA) anodes for the removal of ARB and ARGs. Inactivation of tetracycline- and sulfamethoxazole-resistant *E. coli* along with the corresponding plasmid coded genes (*tetA* and *sul1*) damage is measured by plate counting on selective agar and qPCR, respectively. In comparison with UV irradiation alone, enhanced reduction of both ARB and ARGs is achieved by UV-EO without Cl^-, although the process is facilitated in the presence of Cl^-, which is oxidized *in situ* to an array of oxidants generated electrochemically. Substantially slower degradation rates for ARGs than ARB are observed for both UV irradiation alone and UV-EO, wherein intracellular ARGs generally are reduced slower than extracellular ARGs, while shorter amplicons are reduced significantly slower than longer ones. Nucleotide damage by UV irradiation and conformational change by UV-EO were visualized using DNA gel electrophoresis for treated extracellular ARGs. The mechanism of ARB and ARGs damage is further explored using computational chemical modeling. Slower degradation is found for the bacteria and genes, *tetA* and *sul1*, in the latrine wastewater than that in laboratory prepared buffered samples. Results indicate that UV-based techniques should only be applied after conventional secondary and/or tertiary water treatment in order to avoid light

transmission attenuation due to turbidity and color in environmental waters or wastewaters.

2.1 Introduction

Antibiotic resistance can arise in microbes due to the misuse of antibiotics, as warned early by Alexander Fleming in his Nobel Prize Lecture of 1945 (Fleming, 1942). Antibiotic resistance has grown into a global health concern as the spreading of antibiotic resistance has outpaced the discovery and development of new antibiotics over the last half century (Walsh and Wencewicz, 2014). Each year, antibiotic resistance in bacteria caused at least 700,000 deaths globally (O'Neill, 2017). Furthermore, deaths due to antibiotic resistance could increase to 10 million per year by 2050, if no action is taken to control the growth of antibiotic resistance (Review on Antimicrobial Resistance, 2016). Wastewater treatment plants (WWTPs) have been identified as significant sources of antibiotic resistance bacteria (ARB) and antibiotic resistance genes (ARGs) released into environment. ARB and ARGs originate from various sources, *e.g.,* municipal, hospital, and livestock wastes that ultimately become influents into WWTPs (Karkman *et al*., 2018). However, recent studies indicate that traditional wastewater treatment does not effectively eliminate ARB and ARGs, even though the overall levels of both may be reduced (Joy *et al*., 2014; Xu *et al*., 2015). In addition, the presence of untreated antibiotics (Oberoi *et al*., 2019) and other compounds (*e.g.,* pharmaceuticals and heavy metals) together in a nutrient-rich engineered system makes WWTPs the hotspots for selection of antibiotic resistance and horizontal gene transfer, including conjugation, transduction, and transformation (Karkman *et al*., 2018; Mohammadali and Davies, 2017). In particular, transformation enables microbes to gain antibiotic resistance by taking up free DNA containing ARGs from their surroundings (*e.g.,* during a sequence of unit operations of a WWTP) and thereby propagate resistance (Chang *et al*., 2017; Karkman *et al*., 2018).

Commonly used disinfectants/oxidants, which include chlorine (Guo *et al*., 2015, p. 2; Yoon *et al*., 2017), ozone (Czekalski *et al*., 2016; He *et al*., 2019), and UV irradiation (Chang *et al*., 2017; He *et al*., 2019; McKinney and Pruden, 2012; Yoon *et al*., 2017), have been investigated for inactivating ARB and ARGs. Chlorine is the most widely used disinfectant for water disinfection due to the simplicity of use and its cost effectiveness. A number of studies have investigated the inactivation of ARB and ARGs by chlorine, showing that both ARB and ARGs can be reduced but

not completely removed after water treatment (Guo *et al*., 2015; He *et al*., 2019; Shi *et al*., 2013; Yoon *et al*., 2017; T. Zhang *et al*., 2019; Zhang *et al*., 2015; Zhuang *et al*., 2015). Horizontal gene transfer can also be promoted by low concentrations of chlorine and chloramines (Shi *et al*., 2013; Zhang *et al*., 2017; Zhuang *et al*., 2015), which makes it more difficult for ARB and ARGs inactivation. Ozonation is used both for wastewater and drinking water treatment for the removal of organic micropollutants (*e.g.,* antibiotics and pharmaceuticals) and inactivation of pathogens (Lee *et al*., 2016; Von Sonntag and Von Gunten, 2012; Xu *et al*., 2002). Complete inactivation of ARB and ARGs could be achieved by applying higher ozone doses and longer hydraulic retention times than those normally used in conventional treatment plants. However, higher O_3 dosages result in higher toxicity of the produced water due to ozonation by-products (Czekalski *et al*., 2016; Iakovides *et al*., 2019; Michael-Kordatou *et al*., 2017). Additional treatment steps after ozonation may be required to avoid the regrowth of ARB (Iakovides *et al*., 2019). UV disinfection is a popular alternative to chlorination/chloramination that is utilized by full-scale WWTPs around the world (Umar *et al*., 2019; US Environmental Protection Agency, 2006; van der Hoek *et al*., 2014) due to negligible production to toxic disinfection by-products (Z. Zhang *et al*., 2019). UV irradiation is considered to be a promising approach for eliminating ARB and ARGs in wastewater effluents without causing horizontal gene transfer (Umar *et al*., 2019; Z. Zhang *et al*., 2019). UV-C (wavelength $\leq$ 280 nm) light can penetrate the cell walls of bacteria and directly damage nucleic acids by forming dimers of adjacent thymines (McKinney and Pruden, 2012; Z. Zhang *et al*., 2019). However, UV disinfection has lower inactivation kinetic rates than other disinfectants, *e.g.,* chlorine and ozone (Zhuang *et al*., 2015), and the extent of ARGs damage is limited under the water treatment conditions (McKinney and Pruden, 2012; T. Zhang *et al*., 2019). Moreover, UV irradiation may result in microbial selection of ARB (Guo *et al*., 2013; Z. Zhang *et al*., 2019). Alternatively, UV irradiation combined with high redox potential oxidants (*e.g.,* UV/H_2O_2, UV/chlorine, UV/peroxymonosulfate and UV/photocatlysis) is found to be more efficient for the control of ARB and ARGs (Zhang *et al*., 2015; Lin *et al*., 2016; Pang *et al*., 2016; Yoon *et al*., 2017; Guo *et al*., 2017; Yoon *et al*., 2018; He *et al*., 2019; Hu *et al*., 2019; Zhang *et al*., 2019). Among these alternatives, UV/chlorine treatment has been shown to result in greater ARGs removal than either the use of UV or chlorine alone, even though similar elimination rates were found for ARB inactivation (Zhang *et al*., 2019).

Photoelectrochemical processing that combines electrolysis and photocatalysis with UV or visible light irradiation is known to enhance the efficiency of generating active oxidants, *e.g.,* reactive chlorine species (Cl_2, HOCl, ClO^-, $Cl^{\cdot}$ and $Cl^{2-\cdot}$) and $^{\cdot}OH$ radicals (Feng *et al*., 2016). Photoelectrochemical treatment techniques have been shown to effectively degrade a wide variety of pollutants, *e.g.,* dyes, pesticides, pharmaceuticals, and antibiotics (Pelegrini *et al*., 2001; Pinhedo *et al*., 2005; Catanho *et al*., 2006; Malpass *et al*., 2007, 2009; Xiao *et al*., 2009; Souza *et al*., 2014; Koo *et al*., 2017a; Mohite *et al*., 2017; Li *et al*., 2018; Zhou *et al*., 2019; Qi *et al*., 2020), as well as disinfection of *E. coli* (Christensen *et al*., 2003; Harper *et al*., 2001; Ma *et al*., 2016). However, few studies have reported on the inactivation of ARB and ARGs by photoelectrochemical methods. In particular, TiO_2 has been one of the most attractive photocatalysts for water splitting and pollution control due to the high reduction potential of its valence band edge (> +2.5 V), excellent chemical stability, low cost, and nontoxicity (Fujishima and Honda, 1972; Koo *et al*., 2017a; Mollavali *et al*., 2018; Yang *et al*., 2018a; Xu *et al*., 2020). However, its application on photo-assisted electrochemical process is limited due to fast recombination of electrons and holes generated by photoactivation, wide band gap, and low electrical conductivity. Recently, Blue TiO_2 nanotube array electrodes (BNTA) have been developed by electrochemical self-doping that leads to significant enhancements of photocatalytic activity, structural stability, electrical conductivity, and active oxidant generation (Yang and Hoffmann, 2016a). A limited number of studies have reported on the photoelectrochemical characteristics of BNTA for pollutant degradation (Koo *et al*., 2017a; Xu *et al*., 2020). To the best of our knowledge, BTNA has never been used for photoelectrochemical removal of ARB and ARGs.

In this study, we adopted BNTA for UV-assisted electrochemical inactivation of two different ARGs, *tetA* and *sul1*, which were acquired and amplified from latrine wastewater and cloned into vector plasmids, respectively, and the ARB were transformed with these vector plasmids. UV-assisted electrochemical oxidation (UV-EO) experiments designed to inactivate ARB and intracellular ARG (i-ARGs) were conducted for varied constant currents with the same UV irradiation intensity in both perchlorate and chloride solutions in order to examine the role of chlorine in further inactivation of ARB and ARGs. Optimized UV-EO conditions were then

applied for inactivating extracellular ARGs (e-ARGs) and for treating latrine wastewater directly. Plate counts were used for quantifying ARB inactivation kinetics, and quantitative polymerase chain reaction (qPCR) was used for quantifying the inactivation kinetics of one long and one short amplicon for each ARG. In addition to qPCR, DNA damage and transformation ability during e-ARG inactivation were also examined by gel electrophoresis and transformation assays, respectively. This study was designed to explore the potential of using UV-EO methods for ARB and ARGs removal in wastewater in order to substantially reduce ARB and ARGs discharge into the aquatic environment.

2.2 Experimental

2.2.1 Chemicals and Materials

Sodium perchlorate ($NaClO_4$), sodium chloride (NaCl), and benzoic acid were purchased from Sigma Aldrich (USA). Tetracycline hydrochloride, agarose (Molecular Biology Grade), and TBE buffer (Tris-Borate-EDTA, 10X) were purchased from Fisher BioReagents (Thermo Fisher Scientific, USA). Sulfamethoxazole (SMX), a sulfonamide, was purchased from TCI America (USA). Luria-Bertani (LB) Broth and LB Agar were purchased from Becton, Dickinson and Company (USA). SYBR Safe DNA Gel Stain and Ultra-pure DNase/RNase-free distilled water (dH_2O) was purchased from Invitrogen (Invitrogen by Thermo Fisher Scientific, USA). Quick-Load® Purple 1 kb Plus DNA Ladder was purchased from New England Biolabs, Inc. (USA). Milli-Q water ($\geq$ 18 MΩ) produced from a Millipore system (Millipore Co., USA). 0.5 M Borate buffer (pH 9.5) and potassium iodate (KIO_3) was purchased from Alfa Aesar (USA). Potassium iodide was purchased from Fisher Chemical (Thermo Fisher Scientific, USA).

2.2.2 Construction and Preparation of Plasmids

The two target genes, *tetA* and *sul1*, were selected due to their relatively high concentrations in the latrine wastewater that was tested in this study. They were subsequently PCR amplified from the latrine wastewater with the primers *tetA*-long and *sul1*-full. All the primers used in this study are listed in Table 2.4 of Section 2.5.4. The plasmid construction for pEB1-tetA and pEB1-sul1 was performed by substituting *tetA* and *sul1* for the GFP (green fluorescent protein) gene in pEB1-

sfGFP (kindly provided by Professor Kaihang Wang, Caltech, Addgene plasmid #103983), respectively (as shown in Figure 2.1). The detailed method of plasmid construction is described in Section 2.5.1. *E. coli* MegaX DH10B T1^{R} Electrocomp cells (Invitrogen by Thermo Fisher Scientific, USA) were used as host cells for all the transformation assays in this study, including the initial propagation of pEB1-sfGFP and construction of pEB1-tetA and pEB1-sul1, and were also involved in the experiments of i-ARGs and the plasmid extraction for the experiments of e-ARGs. Electroporation transformation was carefully performed in a 0.2-cm electroporation cuvette at 2500 V using the Eppendorf Eporator (Eppendorf, Germany). All the plasmids were extracted by QIAprep Spin Miniprep Kit (QIAGEN, USA) following the manufacturer's instruction.

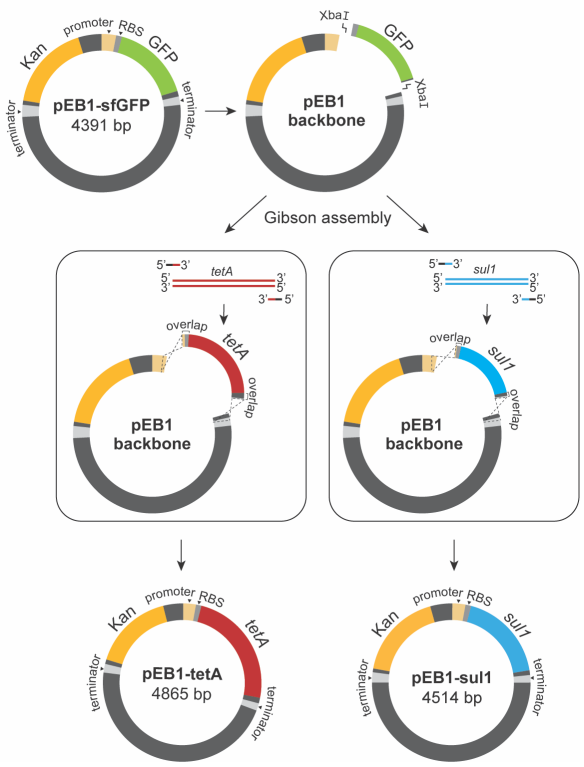

Figure 2.1: Plasmid construction performed for pEB1-tetA and pEB1-sul1.

2.2.3 Treatment of intracellular ARGs (i-ARGs)

All the UV-EO experiments were conducted in a batch reactor (Figure 2.2) consisting of a low-pressure mercury lamp emitting UV light mainly at 254 nm (16.5 cm of length, 9 W, Odyssea Aquarium Appliance Co., Ltd, China) and a glass reactor with a round quartz exposure window (3

cm of diameter). Electrolysis was performed by using a previously mentioned blue TiO_2 nanotube array (BNTA) (Yang and Hoffmann, 2016a) as the anode and platinum as the cathode. Detailed preparation and characterization of BNTA is also described in Section 2.5.2. For the degradation experiments involving i-ARGs, DH10B cells transformed with either pEB1-tetA or pEB1-sul1 were cultivated overnight to a log-phase growth at the optical density at 600-nm wavelength (OD_{600}) of 0.6-1.0, with the aforementioned method. The cells were then harvested by centrifugation at 5000 rpm for 10 min and then resuspended in 30 mM $NaClO_4$ or 30 mM NaCl to a final concentration of ~10^8 cells/mL. A cell suspension of 30 mL was added in the reactor with a stirrer for mixing. Varied constant direct currents of 6, 12, and 30 mA (equivalent to current densities of 2, 4, and 10 mA/cm^2, respectively; Potentiostat, BioLogic Science Instruments, France) were applied along with the same UV irradiation for 10 min. Aliquots of 500 µL were taken from the reaction solution at 0 s, 10 s, 30 s, 1 min, 5 min, and 10 min. As a comparison, the experiments were also conducted under UV-only conditions with the electrodes inserted in the solution to keep the same radiation flux. However, a Ti-metal electrode was substituted for BNTA to avoid photocatalysis by TiO_2. The UV irradiance at 254 nm was 5.0 ± 0.1 mW/cm^2, determined by chemical actinometry using a solution of 0.6 M potassium iodide and 0.1 M potassium iodate in 0.01 M borate buffer (pH 9.25) (Rahn, 1997). Plate counting was used to evaluate the viability of the DH10B cells after treatment. A series of ten-fold dilutions was prepared for each sample and then plated on LB agar with either 10 µg/mL tetracycline or 200 µg/mL SMX. The plates were cultivated at 37 ^oC for 16-18 hrs followed by manual counting. Plasmids of a 100-µL aliquot were also extracted for each sample with Fast DNA Spin Kit for Soil (MP Biomedicals, USA) following the manufacturer's instruction. The extracted plasmids were then quantified by qPCR to evaluate the gene damage.

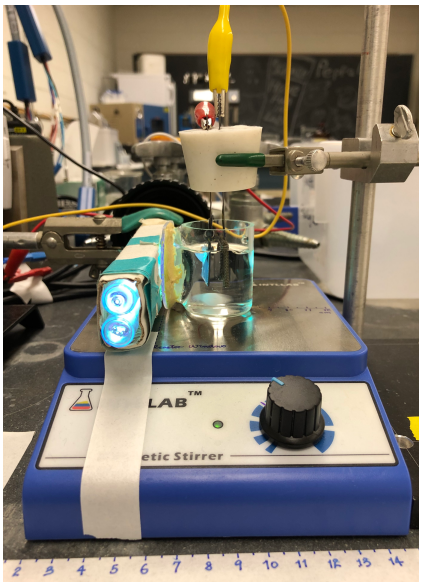

Figure 2.2: Photograph of the UV enhanced electrolytical reaction system.

2.2.4 Treatment of Extracellular ARGs (e-ARGs)

The plasmid stock for pEB1-tetA or pEB1-sul1 was spiked into 30 mM $NaClO_4$ or 30 mM NaCl to achieve a concentration of ~10 ng/µL. The electrolysis experiments were conducted under UV irradiation only or UV-EO at a constant current of 30 mA which was optimized in the experiments involving i-ARG. An aliquot of 500 µL was taken from the reaction solution at the same sampling point as used for i-ARG treatment.

The plasmid DNA damage was evaluated by both qPCR and gel electrophoresis. All the samples were directly used for qPCR measurement. An aliquot of each sample was treated by a restriction enzyme, SbfI (NEB #R0642), at 37 ^{o}C for 15 min to linearize the plasmid DNA with the position shown in Figure 2.3. Both the samples with and without restriction were carried out for gel electrophoresis on 1% TBE agarose gels at 100 V for 30 min using MyGel^{TM} InstaView Electrophoresis System (Accuris Instrstruments by Benchmark Scientific, USA). The DNA bands were visualized by SYBR Safe DNA Gel Stain (10,000X, Thermo Fisher Scientific, USA) with 1 kb plus ladder (New England Biolabs Inc., USA).

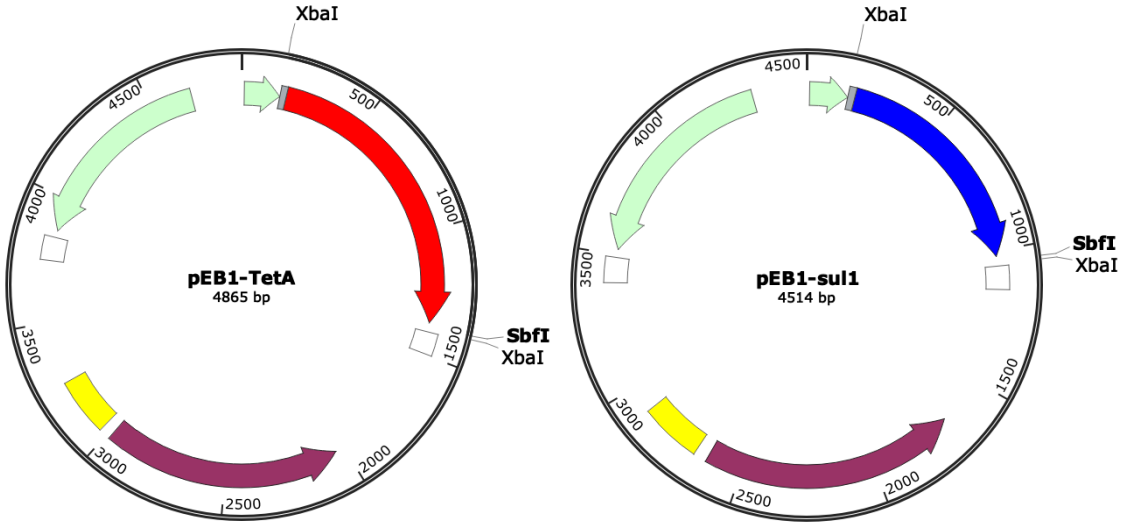

Figure 2.3: Plasmid DNA maps of pEB1-tetA and pEB1-sul1 showing the positions of the two restriction enzymes, XbaI and SbfI.

The effect of the electrolytes on gel electrophoresis and qPCR inhibition was investigated and described in Section 2.5.3. No difference was observed for gel electrophoresis or qPCR between the samples in the non-electrolyzed sample and those electrolyzed in NaCl.

2.2.5 Treatment of ARGs in Wastewater

The treated latrine wastewater was collected from a solar-powered recycling electrochemical toilet system located on Caltech campus (Pasadena, CA). The initial condition parameters of the wastewater are 236 mg/L for chemical oxygen demand (COD) and 26.2 mM for NH_4^+ as major pollutants, which are similar to those previously reported (Jasper *et al.*, 2017; Wang *et al.*, 2020; Yang and Hoffmann, 2016a). More details are listed in Table 2.2 of Section 2.3.4. Sterilized filter papers with 8.0-µm pore size (diameter, 55 mm; Cat No., 1002 055; Whatman) were used for filtration to remove big particles before the electrolysis experiments. The filtered wastewater with a volume of 30 mL was directly added into the reactor for UV-enhanced electrolysis under optimized electrical conditions, *i.e.,* the current density of 10 mA/cm^2, with a duration from 0-30 min. To determine the viability of ARB cells before and after treatment, an aliquot of each sample was plated on both non-selective and selective LB plates (with 10 µg/mL tetracycline or 200 µg/mL SMX) and incubated overnight at 37 ^{o}C. To monitor gene damage by the treatment, 200

μL of each sample was extracted using a Fast DNA Spin Kit for Soil (MP Biomedicals, USA) following the manufacturer's instruction. Following extraction, both the long and short amplicons of *tetA* and *sul1* genes were detected by qPCR and quantified using the calibration curves for plasmids, pEB1-tetA and pEB1-sul1, respectively.

2.2.6 Quantitative PCR

The gene damage of *tetA* and *sul1* after treatment was determined by qPCR (MasterCycler RealPlex 4, Eppendorf, USA). Both a short amplicon (216 bp for *tetA* and 162 bp for *sul1*) and a long amplicon (1200 bp for *tetA* and 827 by for *sul1*) were quantified for each gene using the primers previously reported (Chang *et al*., 2017; Czekalski *et al*., 2016; Xu *et al*., 2015) (Table 2.4 in Section 2.5.4). Each 20-μL reaction mixture contained 10 μL of Fast EvaGreen qPCR Master Mix (Biotium, USA), 0.5 μM of forward and reverse primers and 2 μL of template. The thermal cycling was for 2 min at 95 ^{o}C followed by 45 cycles of 5 s at 95 ^{o}C, 5 s at the annealing temperature (Table 2.4 in Section 2.5.4), and 15 s for short amplicons or 60 s for long amplicons at 72 ^{o}C. The qPCR amplification efficiency was 73% for *tetA*_long, 91% for *tetA*_short, 90% for *sul1*_long, and 96% for *sul1*_short. The R^2 value was above 0.99 for all the amplicons (Figure 2.4). A non-template control (NTC) was set up with each qPCR measurement. Among all the qPCR runs with 45 thermal cycles, no amplification was detected for two long amplicons, and 38.4 was detected as the lowest C_t value (the highest concentration) of NTC for two short amplicons. The limit of detection was determined as 8 copies/μL, which was the highest value among the 4 different amplicons measured in this study.

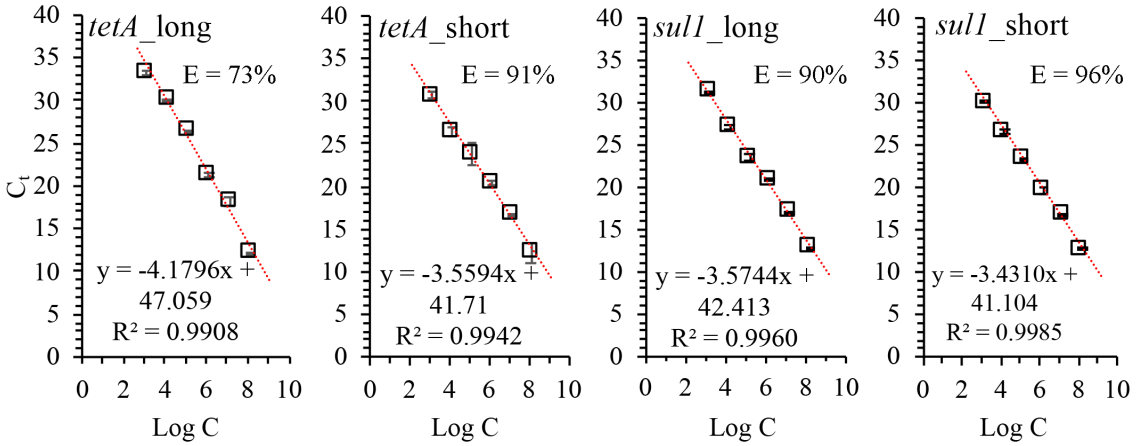

Figure 2.4: The qPCR calibration curves for 4 amplicons, *tetA*_long (1200 bp), *tetA*_short (216 bp), *sul1*_long (827 bp), and *sul1*_short (162 bp), with slope, y intercept, R^2, and PCR efficiency (E) calculated from $10^{(-1/slope)}$-1. The error bars represent one-standard deviation of triplicate measurements.

2.2.7 Radical Generation Probed by Benzoic Acid Degradation

Benzoic acid (BA) was used as a probe molecule to estimate radical production rates. Degradation of benzoic acid with an initial concentration of 1 mM was performed in 30 mM $NaClO_4$ or 30 mM NaCl for 1 hr, with treatments including UV only (in ClO_4^-), EO only (in ClO_4^- or in Cl^-), and UV-EO at 30 mA of constant current (equivalent to 10 mA/cm^2). The concentrations of benzoic acid were then analyzed by UPLC-MS/MS (Thermo Scientific, Vanquish-TSQ ALTIS) equipped with a Atlantis® HILIC Silica column (3 µm, 2.1 mm × 100 mm). The mass spectrometer was operated in the negative ionization (ESI) mode with a spray voltage of -2500 V and a vaporizer temperature of 350 °C. Quantification was performed using multiple reaction monitoring (MRM), and the MRM transition was m/z 121/77. The gradient solvent program started from 90% acetonitrile in 5 mM ammonium acetate with 1-min hold, then decreased to 50% acetonitrile over 4 min, followed by a return to 90% acetonitrile over 1 min, and equilibrium for 1.9 min. For quality assurance and quality control (QA/QC), samples diluted with methanol (10 µL of injection) were spiked with 10 µg of mass-labeled internal standard, benzoic acid-D5 (98%, Cambridge Isotope Laboratories, Inc., USA). The lower limit of quantification (LOQ) was set to 80 ng/L with signal to noise ratio of 10

to 1. Calibration standards and blanks were reinjected during the sequence to validate the instrument response and avoid benzoic acid carry over.

2.3 Results and Discussion

2.3.1 Inactivation of ARB and Degradation of ARGs

Figure 2.5 shows the changes in the logarithmic relative concentrations in cell culturability of ARB on selective agar plates and gene damage for both intracellular and extracellular plasmids measured by qPCR, as a function of UV dose and time. Different treatment conditions were investigated and compared, including UV irradiation only in 30 mM ClO_4^- (Figure 2.5a and d), UV-EO by BNTA anode in 30 mM ClO_4^- (Figure 2.5b and e), and in 30 mM Cl^- (Figure 2.5c and f). A constant direct current of 30 mA was applied for UV-EO treatment, which was optimized by the treatment of i-ARGs with varied currents (Figure 2.6). The initial cell concentrations of ARB measured on selective plates were ~2.3×10^7 and ~2.9×10^7 CFU/mL for tetracycline-resistant and SMX-resistant *E. coli*, respectively. For the treatment of extracellular plasmids, the initial concentrations were 8.0×10^8 and 1.3×10^9 copies/μL for pEB1-tetA and pEB1-sul1 quantified by qPCR, respectively. The plasmid DNA quantification by qPCR amplicons with different lengths were consistent with the average standard deviations between long and short amplicons of 5.4×10^7 and 1.6×10^8 copies/μL for pEB1-tetA and pEB1-sul1, respectively.

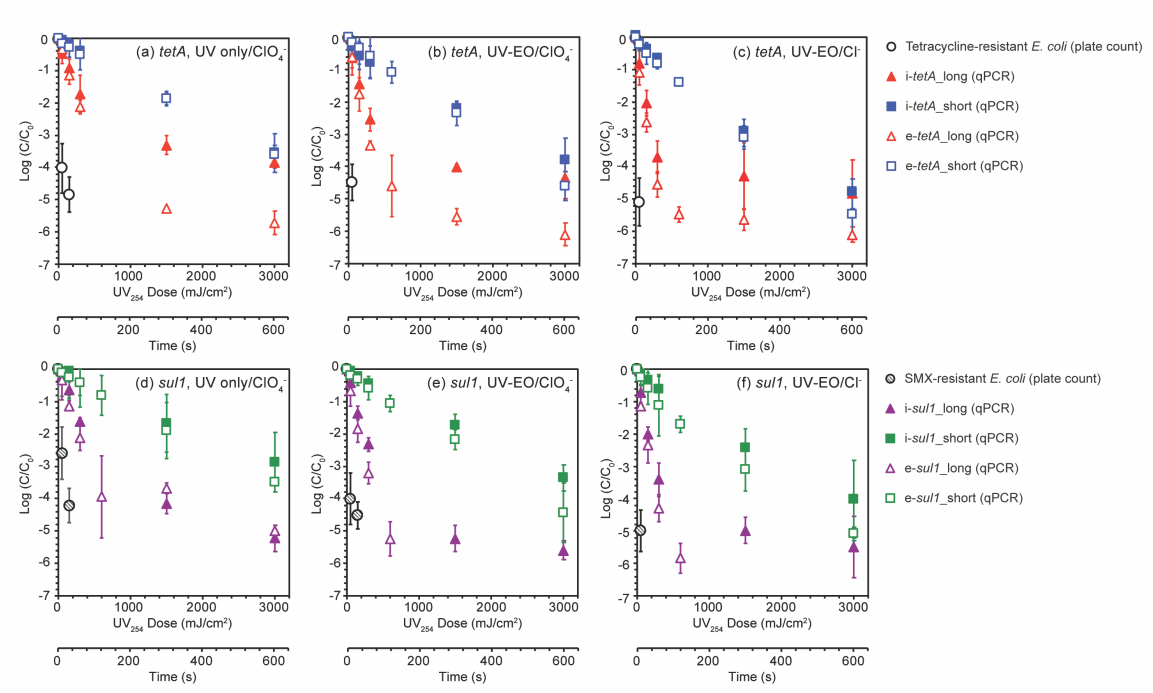

Figure 2.5: Inactivation of antibiotic resistant *E. coli* and degradation of *tetA* and *sul1* genes with UV irradiation or UV-EO treatment at an optimized current of 30 mA on the BNTA anode. The experiments were conducted in 30 mM $NaClO_4$ ("ClO_4^-") or 30 mM NaCl ("Cl^-"). The error bars represent standard deviation from triplicate experiments.

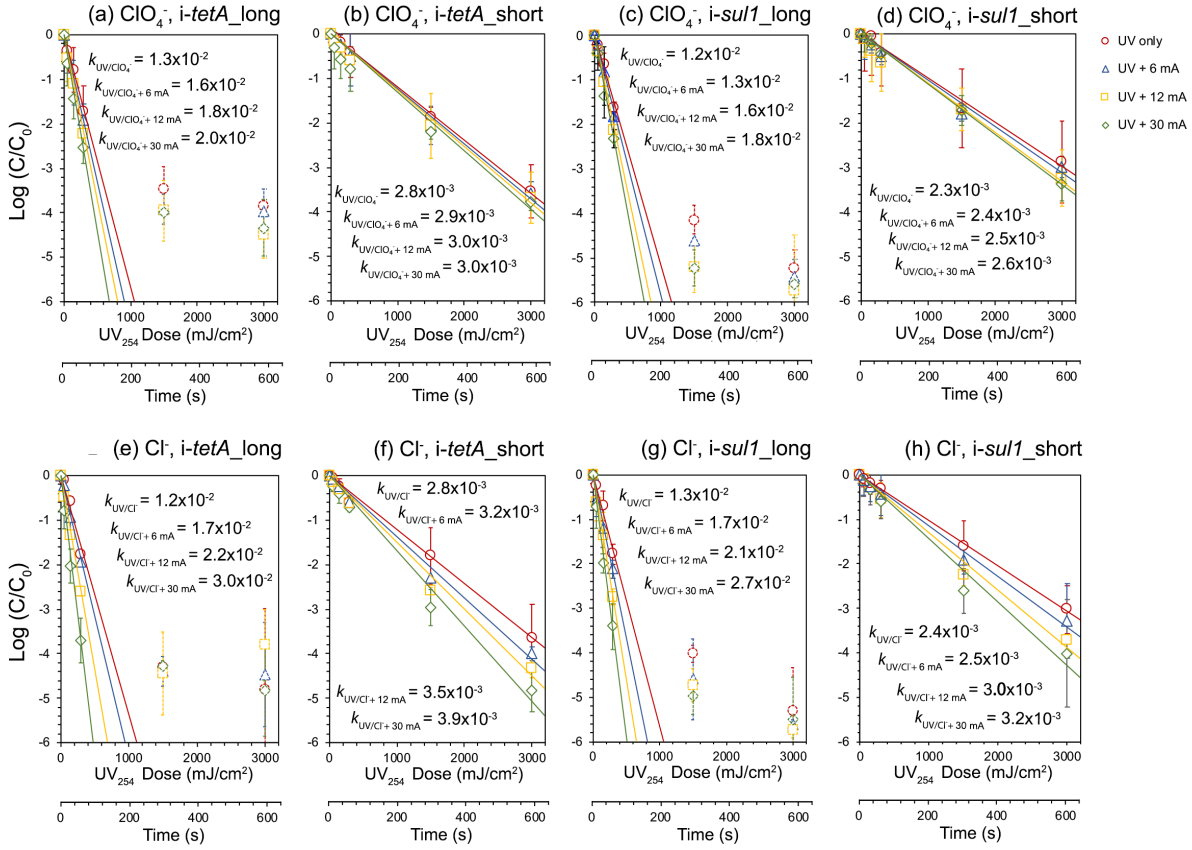

Figure 2.6: Logarithmic relative concentration of both long and short qPCR amplicons for *tetA* and *sul1* as a function of 1) UV_{254} dose and 2) time, during treatment of intracellular plasmids hosted in *E. coli* DH10B with UV and UV-enhanced electrolysis at various currents conducted in 30 mM $NaClO_4$ (a-d) and 30 mM NaCl (e-h). The error bars represent standard deviation from triplicate experiments, and the lines represent the linear regressions of the data. The fluence-based first-order kinetic rates, *k*, are derived from the slope of the linear curves and labeled in units of cm^2/mJ. Some data points are excluded from linear regression due to their deviation from first-order kinetics by observation and are labeled in dashed border.

2.3.1.1 Inactivation of ARB

In general, the inactivation of tetracycline- and SMX-resistant *E. coli* occurred rapidly under all the treatment conditions present in Figure 2.5. The logarithmic removal of ARB by different treatment conditions with the same duration has the order of UV < UV-EO/ClO_4^- < UV-EO/Cl^-. The required UV dosages for 2-log_{10} and 4-log_{10} removal of ARB and ARGs are summarized in Table 2.5 of Section 2.5.5. Included in Table 2.5 are relevant literature values that were obtained employing treatment techniques related to those used in this study. Under a UV_{254} dose of 50

mJ/cm^2 (10 s duration), 2.6-log$_{10}$ of SMX-resistant *E. coli* and 3.9-log$_{10}$ of tetracycline-resistant *E. coli* were removed by UV irradiation alone, and ≥ 4-log$_{10}$ removal was achieved for both types of ARB by UV-EO treatment. Furthermore, in the presence of Cl^- during UV-EO treatment ≥ 5-log$_{10}$ was obtained for ARB with UV dose of 50 mJ/cm^2 (10 s duration), and no surviving ARB were observed after a UV dose of 150 mJ/cm^2 (30 s duration). The enhanced elimination of ARB is attributed to the *in situ* generation of the HClO/ClO^- due to the anodic oxidation of chloride.

2.3.1.2 The Kinetics of ARG Damage

In contrast to the fast removal of ARB, significantly slower reduction was found for the corresponding gene damage measured by qPCR (Figure 2.5). This result is consistent with previous studies (He *et al*., 2019; Yoon *et al*., 2017; T. Zhang *et al*., 2019). Results show clearly that ARGs can survive from treatment and have the potential for dissemination through horizontal gene transfer even when the ARB are completely eliminated. Linear-regression fitting for the gene damage data is shown in Figure 2.5; the fluence-based first-order kinetic rate constants, *k*, were determined from the slopes, which are summarized in Table 2.5 of Section 2.5.5. In general, for a given amplicon, the same order among different treatments was found for kinetic rates of gene damage measured by qPCR as that found for ARB inactivation measured by plate counting, *i.e.,* UV < UV-EO/ClO_4^- < UV-EO /Cl^-. These results indicate that the oxidants generated by electrochemical oxidation of chloride and water, *i.e.,* ·OH and HClO/ClO^-, not only enhance ARB removal but they also lead to ARG damage. The latter result can be attributed to a greater number of target sites on the DNA strands. For a 2-log removal, the required UV dose was 271-384 mJ/cm^2 for long amplicons and 1645-2003 mJ/cm^2 for short amplicons with UV irradiation only. With UV-EO, doses of 177-256 mJ/cm^2 for long and 1245-1772 mJ/cm^2 for short amplicons in ClO_4^- were required, while doses of 128-154 mJ/cm^2 for long and 960-1181 mJ/cm^2 for short amplicons with UV-EO in Cl^- were needed (Table 2.5 in Section 2.5.5). The required UV doses for the removal of ARB and ARGs found in this study are much higher than those in previous studies at a comparable level of removal. The experimental setups, *i.e.*, a batch reactor used in this study and the petri dish used as a thin film reactor in previous studies (Chang *et al*., 2017; He *et al*., 2019; Nihemaiti *et al*., 2020b; Yoon *et al*., 2018, 2017; Zhang *et al*., 2019), may have accounted for the differences in reported kinetic rates.

2.3.1.3 Effect of Amplicon Length on ARG Damage

Both long (*tetA*_long, 1200 bp and *sul1*_long 827 bp) and short amplicons (*tetA*_short, 216 bp and *sul1*_short 162 bp) were measured for each target ARG. Although the short amplicon between 70-200 bp is optimal for the standard qPCR quantification, the longer amplicon with the length >1000 bp has the capability to capture DNA damage (Chang *et al*., 2017; Egan *et al*., 2007; T. Zhang *et al*., 2019). The development of the qPCR dye, EvaGreen, enabled the quantification of long amplicons by qPCR with less inhibition (Mao *et al*., 2007; McKinney and Pruden, 2012). It is noticeable that the short amplicons for both target ARGs followed first-order kinetics over the entire UV dose of 3000 mJ/cm^2 under all the different treatments applied in this study, however, the long amplicons appeared to have a tailing effect that deviated from first-order kinetics at exposure higher than 300 mJ/cm^2. Therefore, the rate constants for the long amplicons were determined only from the data that fit true first-order kinetics, *i.e.*, 0-300 mJ/cm^2. As expected, the longer amplicons have significantly higher rate constants than the short amplicons for all the cases due to the greater number of attacking targets in the long amplicons than for the short ones (Chang *et al*., 2017). The *k* values of long amplicons are larger than those of short ones by a factor of 5.4, 7.0, and 7.7 for UV only, UV-EO treatment in ClO_4^- and in Cl^-, respectively. This trend is consistent with the increasing *k* for a given amplicon in the order of UV-EO/Cl^- > UV-EO/ClO_4^- > UV, which can be explained in terms of the extra target DNA damage sites created by the oxidants (*i.e.,* $\cdot$OH and HClO/ClO^-) having greater impact on the long amplicons and thus larger *k* values.

2.3.1.4 Intracellular and Extracellular ARG Damage

Figure 2.5 shows that extracellular ARGs (e-*tetA* and e-*sul1*) reacted faster than the intracellular ones (i-*tetA* and i-*sul1*) for a given qPCR amplicon. The only exception was for the *tetA*_short under UV_{254} irradiation, which gave no significant difference (P = 0.9, n = 3) for *k* between intracellular and extracellular genes. All the other amplicons with the different treatments resulted in higher *k* values for the extracellular genes than for the intracellular ones by a factor from 1.21 to 1.36. For UV-only treatment, Yoon *et al*., (2017) reported a faster damage rate for e-ARGs than of i-ARGs by a factor of 1.7, while McKinney and Pruden (2012) found insignificant difference in the damage rates of e-ARGs and i-ARGs (McKinney and Pruden, 2012). The results obtained

in our study indicate that the cellular components can protect the intracellular genes from both UV- and oxidant-induced damage to some extent. The difference found in various studies may be attributed to different host bacterial strains, initial concentrations, and experimental setups.

2.3.2 Mechanisms on ARG damage

To further understand the mechanisms leading to plasmid damage, gel electrophoresis was conducted for both e-*tetA* and e-*sul1* before and after the treatment of UV alone and UV-EO, with a comparison of all the same samples but treated by the restriction enzyme SbfI (Figure 2.7). Untreated pEB1-tetA and pEB1-sul1 (*i.e.*, controls) are shown in lane 1 of each gel electrophoresis image that has bands between 4-5 kb and close to 4 kb, respectively. These were identified as the supercoiled form of the plasmids. The bands in lane 5 of all the images show an upward transition after the restriction of plasmids by enzyme SbfI that reflect the real sizes of the plasmids (4865 bp and 4514 bp for pEB1-tetA and pEB1-sul1, respectively), which were identified as the linearized form of the plasmids. For the treatment by UV alone (Figure 2.7a and d), the gel electrophoresis images do not show a significant conformational change of the plasmids until 5 min of the treatment (*i.e.,* a UV_{254} dose of 1.5 J/cm^2). The native supercoiled plasmids were significantly diminished when the UV dose was higher than 1.5 J/cm^2, as the fluorescence of the bands was much less intensive. A higher band on gel appeared for both plasmids simultaneously, which is identified as relaxed nicked circular form. Plasmid DNA mainly maintained a covalently circular, supercoiled form *in vivo* or in isolated extracts directly from bacterial cells (Hayes, 2003). The supercoiled plasmid migrates faster than linear DNA with the same base pair length due to their smaller size, resulting in a lower band on agarose gel. Relaxed nicked circular plasmids (caused by single-strand breaks) and linearized plasmids (caused by double-strand breaks) are the most common topological variations that cause the upward transition of the band compared to the supercoiled plasmid on an agarose gel. Thus, the relaxed nicked circular plasmid migrates slower with the uppermost band (Chen *et al*., 2007). Figure 2.7a and d clearly show that UV irradiation can induce a significant conformational change in the plasmid (*e.g.,* relaxed nicked circular form caused by single-strand breaks) when a sufficient UV fluence is applied, which was also observed in a previous study (Yoon *et al*., 2017). The native supercoiled bands almost disappeared after 10

min of the treatment (*i.e.,* the UV dose of 3 J/cm^2), which indicates that more extensive fragmentation of the plasmid was caused at this level of the UV dosage. However, the formation of UV-induced DNA damage visualized by gel electrophoresis appears to be much slower than the gene damage detected by qPCR (Figure 2.5). UV irradiation induces damage to DNA bases and results in pyrimidine dimerization at a lower dose.

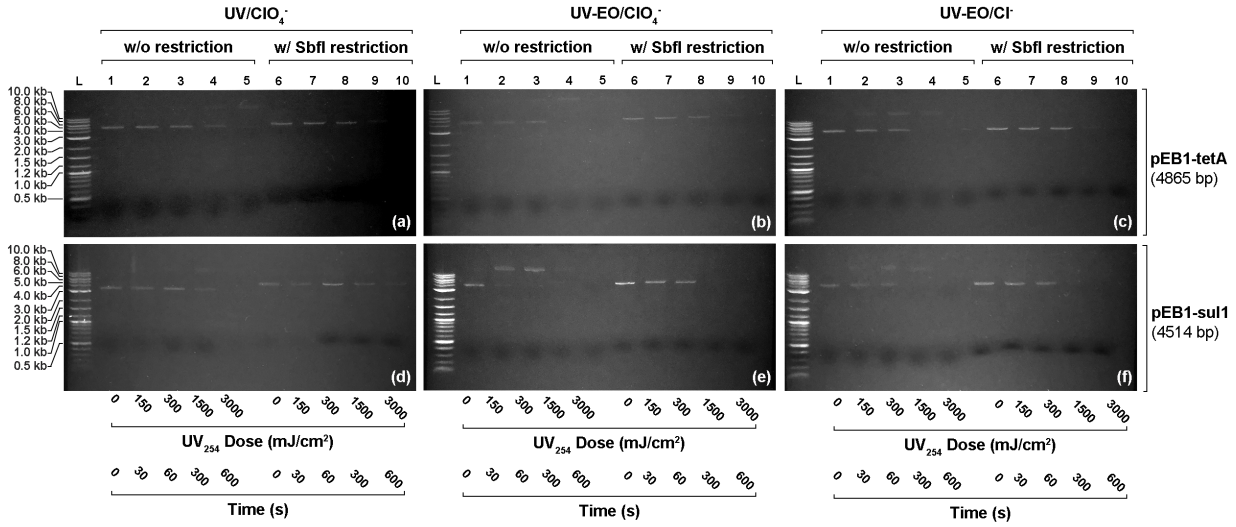

Figure 2.7: DNA electrophoresis gel of extracellular plasmids, pEB1-tetA (a-c) and pEB1-sul1 (d-f), as a function of UV dose in mJ/cm^2 and time in s, with different treatment including UV in ClO_4^- (a and d), UV-EO with BNTA at 30 mA in ClO_4^- (b and e) and in Cl^- (c and f). All the tests were carried out with an initial concentration of ~10 ng/µL plasmids in 30 mM $NaClO_4$ labeled as "ClO_4^-" or 30 mM NaCl labeled as "Cl^-". UV intensity was 5 mW/cm^2 at 254 nm. The first lane "L" of each image shows the standard 1kb plus DNA ladder. All the DNA samples are presented without (w/o) any enzyme treatment (lane 1-5) and with (w/) restriction by SbfI enzyme at 37 ^oC for 15 min (lane 6-10).

Gel electrophoresis shows that the UV-EO treatment process caused substantially faster plasmid conformational damage when compared to UV alone. This result is consistent with the higher kinetic rates of gene damage detected by qPCR. The bands at the higher DNA markers that appeared after only 30 s or 1 min of treatment (Figure 2.7b, c, e, and f) were identified as nicked circular plasmids. Overall, these results show significant oxidant-induced DNA damage, *i.e.*, single-strand breaks (Suquet *et al*., 2010; Yoon *et al*., 2017). The native supercoiled plasmids were noticeably diminished after 1 min of treatment, while the nicked circular plasmids showed a

noticeable diminishment after 5 min of treatment. Fragmentation of plasmid DNA was induced at a corresponding level of damage.

For pEB1-sul1, a greater degree of conformational change was observed for UV-EO without the presence of Cl^- (Figure 2.7e) than for the one with Cl^- (Figure 2.7f) (Suquet *et al*., 2010). In the presence of only ClO_4^- as an electrolyte, ·OH is the predominant oxidant generated by the UV-EO process, whereas HOCl/OCl^- predominate when Cl^- the electrolyte. Previous studies have shown that HOCl/OCl^- is relatively unreactive toward sugar or the polyphosphoribose backbone of DNA, although reactive chlorine causes nucleobase damage. (Burrows and Muller, 1998; Hawkins and Davies, 1998; Suquet *et al*., 2010) The nicked circular plasmid and the diminishment of both native supercoiled and nicked circular plasmids may indicate that the nucleobases were extensively damaged. On the other hand, ·OH, as well as other reactive oxygen species, can cause both types of damage, which could result in the more significant conformational change of plasmids observed in this study (Burrows and Muller, 1998; He *et al*., 2019; Kennedy *et al*., 1997; Suquet *et al*., 2010). In contrast, higher kinetic rates of gene damage as detected by qPCR were found for UV-EO in Cl^--than in ClO_4^-. It may be explained by the significantly higher amount of HOCl/OCl^- generated in Cl^- than ·OH levels in ClO_4^- at the same coulomb of charge. Such differences due to Cl^- oxidation were not observed for pEB1-tetA. As a note of caution, the plasmid DNA conformational changes that were observed by gel electrophoresis may also cause bias on qPCR quantification. For example, approximately 4.5-fold and 3-fold greater PCR amplification was found for nicked-circular and linear plasmids, respectively, than for the supercoiled plasmid due to the smaller tension that leads to easier denaturation in the PCR process (Lin *et al*., 2011). However, such an impact was not observed by the qPCR detection used in this study. DNA damage (*e.g.,* oxidant-induced DNA fragmentation and UV-induced pyrimidine dimer formation) may have caused a more dramatic elevation of qPCR C_t values.

2.3.3 Simulation of Radical Generation

Benzoic acid (BA: 1mM) was used as a radical probe with known rate constants for the various radicals ($k_{\cdot OH} = 5.90 \times 10^9\ M^{-1}\ s^{-1}$, $k_{Cl\cdot} = 1.8 \times 10^{10}\ M^{-1}\ s^{-1}$, $k_{Cl2\cdot-} = 2 \times 10^6\ M^{-1}\ s^{-1}$) (Buxton *et al*., 1988a; Gilbert *et al*., 1988; Mártire *et al*., 2001a). As shown in Figure 2.8, BA was not degraded

under UV irradiation. During EO treatment, BA was oxidized by electrochemically produced ·OH. The reaction between BA and ·OH follows second-order kinetics, which can be further simplified to a form of pseudo-order kinetics as Equation 2.1:

$$\frac{dC_{BA}}{dt} = k_{\cdot OH}[\cdot OH][BA] = k_{obs}[BA] \quad (2.1)$$

The observed rate constant (k_{obs}) fitted by linear regression is 2.58×10^{-4} s^{-1}. The corresponding steady-state ·OH concentration ($[\cdot OH]_{ss}$) is calculated to be 4.37×10^{-14} M according to Equation 2.2.

$$[\cdot OH]_{ss} = \frac{k_{obs}}{k_{\cdot OH}} \quad (2.2)$$

UV irradiation was found to accelerate the degradation of BA. The k_{obs} and $[\cdot OH]_{ss}$ are calculated as 5.16×10^{-4} s^{-1} and 8.75×10^{-14} M, respectively. The two-fold increase in $[\cdot OH]_{ss}$ after introducing UV irradiation into EO process implies that more ·OH radicals were produced in addition to those produced by electrolysis through electron tunneling. The synergistic ·OH production results from water oxidation by photogenerated holes (Figure 2.15 b vs. c in Section 2.5.2).

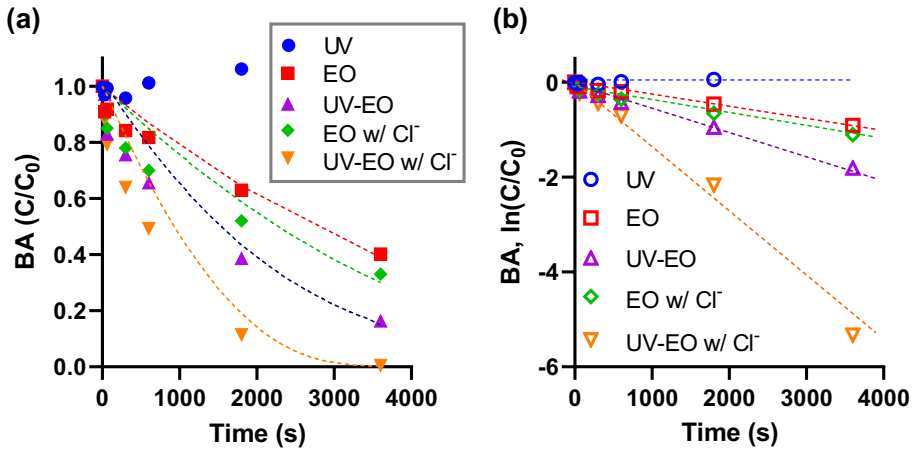

Figure 2.8: BA degradation by BNTA at 10 mA/cm^2 in the absence (EO) and presence (UV-EO) of UV. All tests were performed in 30 mM $NaClO_4$, except tests "EO w/ Cl^-" and "UV-EO w/ Cl^-" were conducted in 30 mM NaCl. (a): Dots and dashed lines represent experimental data and results of kinetic model simulation, respectively. (b): Experimental data fitted by the first-order kinetics.

In the presence of Cl^-, the EO degradation of BA was enhanced. Chloride can be oxidized to free chlorine ($HOCl/OCl^-$, $pK_a = 7.5$). It can readily react with ·OH to form Cl· and $Cl_2^{\cdot -}$ (Park *et al.*, 2009a; Yang *et al.*, 2016). Upon UV irradiation, the BA degradation was further enhanced. Free chlorine was produced during the UV-EO process. The concentrations of free chlorine are proportional to the electrolysis duration and current density (Figure 2.9). These results imply that chlorine was produced by the electrochemical oxidation of chloride rather than through the photochemical oxidation pathway. It is suspected that the extra radical inputs were produced from the UV photolysis of free chlorine ($HOCl \rightarrow \cdot OH + Cl\cdot$).

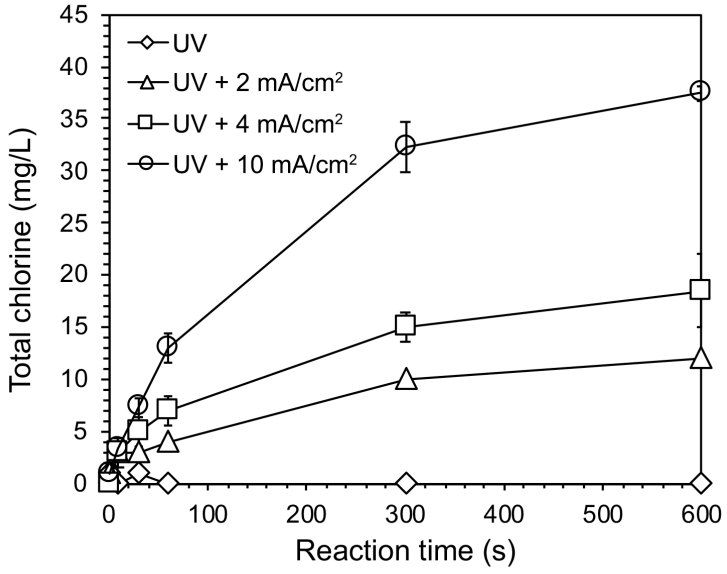

Figure 2.9: Chlorine evolution during UV-EO process in 30 mM NaCl at varied current densities. Error bars represent one standard deviation from triplicate experiments.

The presence of Cl^- significantly complicates the mechanisms of radical production, because Cl^- can be converted to multiple radicals (Cl·, $Cl_2^{\cdot -}$, $ClOH^{\cdot -}$, *etc.*). To unveil the speciation of these radicals, a computational kinetic model comprised of 39 zero-, first-, and second-order elementary kinetic reactions was developed (Table 2.1). The decay of BA as functions of reaction time under different test conditions is the outcomes of the interplays between BA and radicals. Therefore, fitting the data in Figure 2.8a by the kinetic model calibrates the unknown rate constants (*k*'s). As a consequence, the speciation of radicals can be back-calculated. Reaction 5 (*vide infra*) represents

the electrochemical production of ·OH. Given the ·OH radical production rate, the corresponding *k*'s were calibrated by the degradation of BA in test sets "UV" and "UV-EO". The *k* for reaction 6 was fitted by the degradation BA in test "EO w/Cl^-". We assume that the $Cl\cdot$ produced by BNT under UV irradiation is negligible because the previous study indicates that this pathway could be significant only if the TiO_2 is chlorinated by concentrated HCl (Yuan *et al.*, 2011). Therefore, the *k* for Reaction 6 remains constant under in test "UV-EO w/ Cl^-". Reaction 7 was introduced to account for radical input by the photolysis of HOCl. The *k* was obtained by fitting BA degradation data of test "UV-EO w/ Cl^-". For all the simulations that involve Cl^-, the $[Cl^-]$ was set as 30 mM. The [HOCl] was set as 35 mg/L, the plateau concentration observed after 600 s UV-EO treatment at 10 mA/cm^2.

Table 2.1: Critical reactions included in the kinetic model.

Reaction No.	**Reaction**	**Rate constant**	**Reference**
pH-dependent equilibrium			
1	$H^+ + OH^- \rightarrow H_2O$	1.00×10^{11} M^{-1} s^{-1}	Matthew and Anastasio, 2006
2	$H_2O \rightarrow H^+ + OH^-$	1.00×10^{-3} M^{-1} s^{-1}	Matthew and Anastasio, 2006
3	$OCl^- + H^+ \rightarrow HOCl$	5.00×10^{10} M^{-1} s^{-1}	Matthew and Anastasio, 2006
4	$HOCl \rightarrow OCl^- + H^+$	1.60×10^{3} M^{-1} s^{-1}	Matthew and Anastasio, 2006
Electrochemical reactions			
5[a]	$M\text{-}OH \rightarrow HO\cdot$	EO: 6.1×10^{-7} M s^{-1} UV-EO: 1.1×10^{-6} M s^{-1}	Fitted value
6[a]	$MO + Cl^- \rightarrow Cl\cdot$	8.8×10^{-5} s^{-1}	Fitted value
UV/chlorine			
7	$HOCl \rightarrow Cl\cdot + HO\cdot$	3×10^{-4} M s^{-1}	Fitted value

$Cl^{\cdot}$ generation			
8	$Cl^{-} + HO^{\cdot} \rightarrow ClOH^{\cdot}$	4.30×10^{9} M^{-1} s^{-1}	"NDRL/NIST Solution Kinetics Database," n.d.
9	$ClOH^{\cdot} \rightarrow Cl^{-} + HO^{\cdot}$	6.10×10^{9} M^{-1} s^{-1}	G. Jayson *et al*., 1973
10	$Cl^{\cdot} + OH^{-} \rightarrow ClOH^{\cdot -}$	1.80×10^{10} M^{-1} s^{-1}	Kläning and Wolff, 1985
11	$ClOH^{\cdot -} + H^{+} \rightarrow Cl^{\cdot} + H_2O$	2.10×10^{10} M^{-1} s^{-1}	G. Jayson *et al*., 1973
12	$ClOH^{\cdot -} + Cl^{-} \rightarrow Cl_2^{\cdot -} + OH^{-}$	1.00×10^{5} M^{-1} s^{-1}	Grebel *et al*., 2010
13	$Cl_2^{\cdot -} + OH^{-} \rightarrow ClOH^{\cdot -} + Cl^{-}$	4.50×10^{7} M^{-1} s^{-1}	Grebel *et al*., 2010
14	$Cl^{\cdot} + Cl^{-} \rightarrow Cl_2^{\cdot -}$	6.50×10^{9} M^{-1} s^{-1}	Kläning and Wolff, 1985
15	$Cl_2^{\cdot -} \rightarrow Cl^{\cdot} + Cl^{-}$	1.10×10^{5} M^{-1} s^{-1}	G. Jayson *et al*., 1973
Cl_2 generation			
16	$Cl^{\cdot} + Cl^{\cdot} \rightarrow Cl_2$	1.00×10^{8} M^{-1} s^{-1}	Wu *et al*., 1980
17	$Cl^{\cdot} + Cl_2^{\cdot -} \rightarrow Cl^{-} + Cl_2$	1.40×10^{9} M^{-1} s^{-1}	Park *et al*., 2009b
18	$Cl_2^{\cdot -} + Cl_2^{\cdot -} \rightarrow 2Cl^{-} + Cl_2$	8.30×10^{8} M^{-1} s^{-1}	"NDRL/NIST Solution Kinetics Database," n.d.
19	$Cl_2^{\cdot -} + HO^{\cdot} \rightarrow HOCl + Cl^{-}$	1.00×10^{9} M^{-1} s^{-1}	"NDRL/NIST Solution Kinetics Database," n.d.
Cl_2 dissolution			

20	$Cl_2 + H_2O \rightarrow Cl_2OH^- + H^+$	1.50×10^1 M^{-1} s^{-1}	Wang and Margerum, 1994
21	$Cl_2OH^- \rightarrow HOCl + Cl^-$	5.50×10^9 M^{-1} s^{-1}	Wang and Margerum, 1994
$HO^\cdot$ transformation			
22	$HO^\cdot \rightarrow O^{\cdot-} + H^+$	1.26×10^{12} M^{-1} s^{-1}	Buxton *et al*., 1988b
23	$O^{\cdot-} + H_2O \rightarrow HO^\cdot + OH^-$	1.80×10^6 M^{-1} s^{-1}	Buxton *et al*., 1988b
24	$HO^\cdot + OH^- \rightarrow O^{\cdot-} + H_2O$	1.30×10^{10} M^{-1} s^{-1}	Buxton *et al*., 1988b
HO_2^-, $HO_2^\cdot$, $O_2^{\cdot-}$ related			
25	$HO^\cdot + O^{\cdot-} \rightarrow HO_2^-$	1.00×10^{10} M^{-1} s^{-1}	Buxton *et al*., 1988b
26	$HO^\cdot + HO_2^- \rightarrow HO_2^\cdot + OH^-$	7.50×10^9 M^{-1} s^{-1}	Buxton *et al*., 1988b
27	$HO_2^\cdot + O_2^{\cdot-} \rightarrow HO_2^- + O_2$	9.70×10^7 M^{-1} s^{-1}	Buxton *et al*., 1988b
28	$HO^\cdot + HO_2^\cdot \rightarrow H_2O + O_2$	6.60×10^9 M^{-1} s^{-1}	Buxton *et al*., 1988b
29	$HO_2^\cdot + HO_2^\cdot \rightarrow H_2O_2 + O_2$	8.30×10^5 M^{-1} s^{-1}	Buxton *et al*., 1988b
30	$HO_2^\cdot \rightarrow H^+ + O_2^{\cdot-}$	1.60×10^5 M^{-1} s^{-1}	Bielski *et al*., 1985
31	$HO^\cdot + O_2^{\cdot-} \rightarrow OH^- + O_2$	8.00×10^9 M^{-1} s^{-1}	Buxton *et al*., 1988b
Radicals quenched by free chlorine			
32	$HO^\cdot + HOCl \rightarrow ClO^\cdot + H_2O$	2.00×10^9 M^{-1} s^{-1}	Matthew and Anastasio, 2006
33	$HO^\cdot + OCl^- \rightarrow ClO^\cdot + OH^-$	8.80×10^9 M^{-1} s^{-1}	Connick, 1947
34	$Cl^\cdot + HOCl \rightarrow ClO^\cdot + H^+ + Cl^-$	3.00×10^9 M^{-1} s^{-1}	Zehavi and Rabani, 1972

35	$Cl^{\cdot} + OCl^{-} \rightarrow ClO^{\cdot} + Cl^{-}$	8.20×10^{9} M^{-1} s^{-1}	G. Jayson *et al.*, 1973
Radicals quenched by benzoic acid			
36	$HO^{\cdot} + C_6H_5COO^{-} \rightarrow$ Products	5.90×10^{9} M^{-1} s^{-1}	Buxton *et al.*, 1988b
37	$Cl^{\cdot} + C_6H_5COO^{-} \rightarrow$ Products	1.80×10^{10} M^{-1} s^{-1}	Mártire *et al.*, 2001b
38	$Cl_2^{\cdot -} + C_6H_5COO^{-} \rightarrow$ Products	2.00×10^{6} M^{-1} s^{-1}	Hasegawa and Neta, 1978
39	$O^{\cdot -} + C_6H_5COO^{-} \rightarrow$ Products	4.00×10^{7} M^{-1} s^{-1}	Buxton *et al.*, 1988b

[a] The M-OH and MO represents the active sites of BNTA to generate ·OH radicals and oxidize Cl^-, respectively. The active sites are assumed to be infinite. Thus, {M-OH} and {MO} were set as one in the model. The reactions then follow zero-order kinetics.

As shown in Figure 2.8a, the kinetic model describes well the experimental data ($R^2 > 0.90$). We then use the calibrated model to estimate the speciation of radicals in the presence of Cl^-. For EO treatment in the presence of Cl^-, $Cl_2^{\cdot -}$ is the dominant radical, followed by ·OH and $Cl^{\cdot}$ (Figure 2.10a). With UV irradiation, concentrations of all radicals increased (Figure 2.10b), which is in agreement with our assumption that the photolysis of free chlorine produces more radicals.

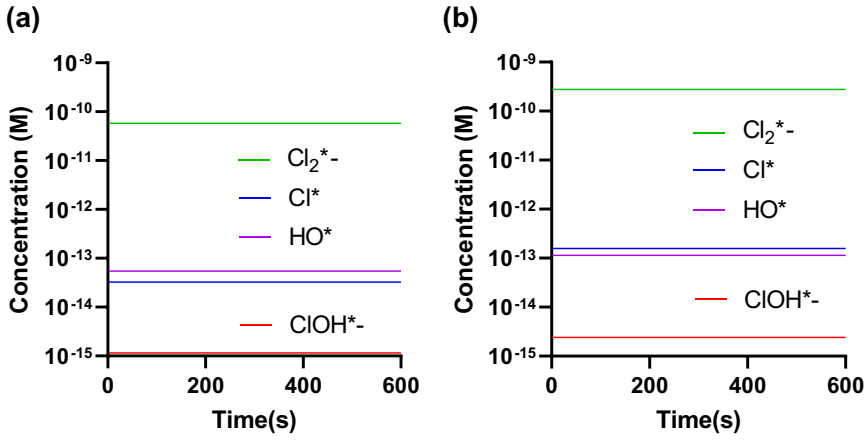

Figure 2.10: Radical speciation in tests (a) EO w/ Cl^- and (b) UV-EO w/Cl^- in the presence of 30 mM NaCl and 35 mg/L free chlorine.

2.3.4 UV-Assisted Electrochemical Oxidation of ARGs in Wastewater

The initial bacterial concentrations in wastewater are ~6.3×10^3 and ~2.4×10^3 CFU/mL counted on non-selective LB and selective LB agar with 200 µg/mL SMX, respectively. No colony was observed for the original wastewater plated on selective LB agar with 10 µg/mL tetracycline even after five days of incubation. There was no colony growing on SMX-selective LB agar after UV-EO treatment even for only 10 s. So only the change in relative logarithmic concentrations of total bacteria measured by non-selective LB agar plates is shown in Figure 2.11. The initial concentrations of four different amplicons were estimated as ~5.8×10^2, ~2.5×10^3, ~7.5×10^3, and ~2.2×10^4 copies/µL for *tetA*_long, *tetA*_short, *sul1*_long, and *sul1*_short, respectively.

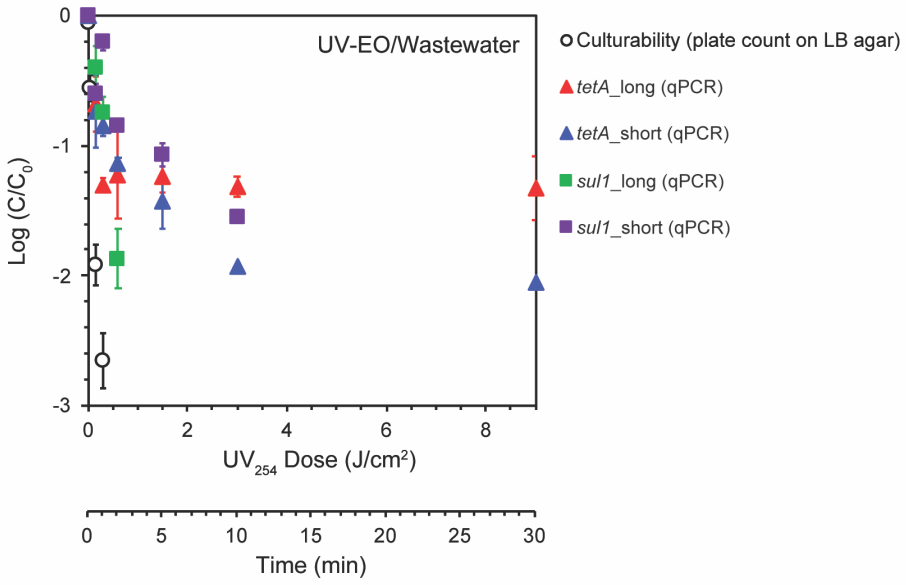

Figure 2.11: Reduction of total bacteria and ARGs by UV-EO treatment in wastewater.

With UV-EO treatment, 1.9- and 2.7-$\log_{10}$ removal of total bacteria was achieved under 150 and 300 mJ/cm^2 of UV doses, respectively. As most of the ARG amplicons in wastewater do not follow the first-order kinetics while being degraded (*i.e.*, reduction in viable number) (Figure 2.11), only the required UV doses for a certain level of removal are shown in Table 2.5 of Section 2.5.5. The tailing effects appeared for all the amplicons detected in wastewater except the sul1_long, which was reduced to the concentrations lower than the limit of detection (*i.e.,* 8 copies/µL) after the UV dose of 600 mJ/cm^2. A significantly slower reduction and higher required doses for a comparable level of removal were found for the native ARGs in wastewater as a comparison with that for the

clean buffered samples discussed *vide supra*. For the native ARGs in wastewater, with 600 mJ/cm^2 of UV dose, 1.1- and 2.9-log$_{10}$ removal was detected for *tetA*_long and *sul1*_long, respectively. Much higher UV doses of 3000 and 9000 mJ/cm^2 were required for 1.9- and 1.8-log$_{10}$ removal of *tetA*_short and *sul1*_short, respectively. For the spiked ARGs (including both intracellular and extracellular ones) in 30 mM NaCl, ~150 mJ/cm^2 and ~1100 mJ/cm^2 were measured as required for 2-log$_{10}$ removal of long and short amplicons, respectively. This difference, first, can be partially attributed to the consumption of the oxidants by other pollutants, *e.g.*, NH_3-N and wastewater organic matter. The concentrations of NH_3-N and chemical oxygen demand (COD) before and after 30 min of treatment are listed in Table 2.2. Second, just as UV disinfection, all the photo-based techniques may be significantly influenced by the water quality parameters, *e.g.,* the transmittance, color, and presence of particulate material (US Environmental Protection Agency, 2006). Third, the lower initial concentrations (10^2-10^4 copies/μL in wastewater whereas 10^8-10^9 copies/μL in clean samples) and different forms of native genes in wastewater may also considerably affect the reduction rates.

Table 2.2: Wastewater conditions before and after the UV-EO treatment by BNTA at 30 mA for 30 min.

	Before treatment	After treatment
NH_3-N (mg/L)	445	390
COD (mg/L)	236	174
pH	9.0	8.9
Total chlorine (mg/L)	0.0	4.0
Conductivity (mS/cm)	5.0	

2.4 Conclusion

In summary, we developed a UV-EO method with BNTA anodes for enhanced removal of ARB and ARGs in water. Reduction kinetics were evaluated by plate counting and qPCR for ARB and ARGs, respectively. Mechanisms on gene damage by UV, oxidants, or a combination thereof were visualized by gel electrophoresis. A further enhanced reduction of ARB and ARGs was shown by UV-EO experiments with the presence of Cl^- and further understood by simulation of radical generation. However, the demonstration of UV-EO on the latrine wastewater exhibits a much

slower degradation of ARGs. This result suggests that UV-EO treatment as well as other photo-based techniques should be applied as the last step after other water treatment for the effectiveness of ARB and ARGs removal. This finding also emphasizes the importance of field tests or demonstrations on natural ambient waters and engineered process waters for any environmental applications. Combinations of different techniques will certainly become more common in future water treatment processes targeted toward ARB and ARGs elimination. Further attempts should be taken to understand the effects of different water quality parameters on removal of ARB and ARGs treated by UV-EO and to track the ARB and ARGs with other traditional water treatment followed by UV-EO treatment. In addition, to better understand the performance of UV-EO treatment on ARG dissemination control and the accuracy of using qPCR to assess the elimination of ARGs, the change of transformation activity for ARGs treated by UV-EO should be investigated.

2.5 Supporting Information

2.5.1 Detailed Method on Plasmid Construction

The general idea of plasmid construction is to modify the template plasmid, pEB1-sfGFP (kindly provided by Professor Kaihang Wang, Caltech; Addgene plasmid #103983 ; http://n2t.net/addgene:103983) with the target gene inserts (*i.e.*, *tetA* and *sul1*) which were PCR-amplified from the latrine wastewater.

Preparation of the backbone from pEB1-sfGFP with digestion enzyme XbaI.

E. coli MegaX DH10B $T1^R$ Electrocomp cells (Invitrogen by Thermo Fisher Scientific, USA) was used for all the transformation in this study, including the initial propagation of pEB1-sfGFP, construction of all the plasmids. The transformation was carefully prepared following the instruction. The electroporation was performed in a 0.2-cm electroporation cuvette at 2500 V using the Eppendorf Eporator (Eppendorf, Germany). To propagate pEB1-sfGFP, the transformed cells with pEB1-sfGFP was plated on LB agar with 50 μg/mL kanamycin and incubated overnight at 37 ^oC. Cultures of 100 mL in LB Broth with 50 μg/mL kanamycin were inoculated with single colonies and incubated overnight at 37 ^oC, 200 rpm. The pEB1-sfGFP were then extracted with a

final concentration of ~124 ng/μL by QIAprep Spin Miniprep Kit (QIAGEN, USA) following the instruction.

The restriction enzyme XbaI (R0145T, New England Biolabs Inc., USA) was used for the digestion of pEB1-sfGFP to cut off the GFP gene. A total reaction volume of 100 μL was prepared with 10 μL of XbaI, 10 μL of CutSmart Buffer, 40 μL of pEB1-sfGFP stock solution, and 40 μL of nuclease-free water. The digestion reaction was performed overnight at 37 ^{o}C. Gel electrophoresis of the digested pEB1-sfGFP was conducted on 1% TBE agarose gels at 100 V for 30 min using MyGel^{TM} InstaView Electrophoresis System (Accuris Instrstruments by Benchmark Scientific, USA). The bands (Figure 2.12) were visualized by SYBR Safe DNA Gel Stain (10,000X, Thermo Fisher Scientific, USA) with 1 kb plus ladder (New England Biolabs Inc., USA). The gel with the band for the backbone pEB1 (3622 bp) was cut off and purified with GeneJET Gel Extraction Kit (Thermo Fisher Scientific, USA).

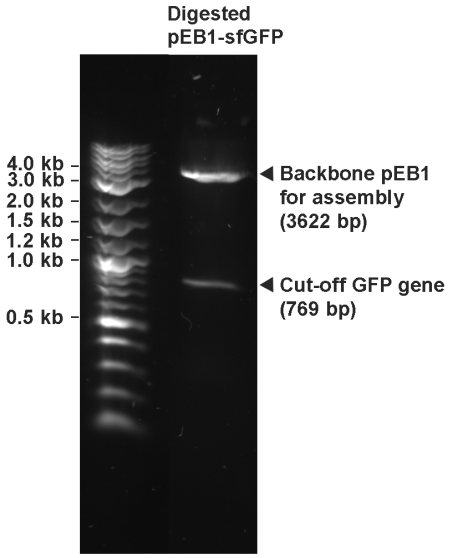

Figure 2.12: DNA gel electrophoresis of pEB1-sfGFP after digestion by XbaI.

Preparation of tetA and sul1 inserts from wastewater.

The two target genes, *tetA* and *sul1*, was first PCR amplified from the latrine wastewater with the primers *tetA*-long and *sul1*-full (Table 2.4 of Section 2.5.4). The PCR products were then purified with the QIAquick PCR Purification Kit (QIAGEN, USA). To include an overlap with the backbone pEB1 for assembly, the purified *tetA* and *sul1* genes were then modified with the primers pEB1-tetA and pEB1-sul1 (Table 2.4 in Section 2.5.4), respectively, by PCR amplification and then purified with with QIAquick PCR Purification Kit again. The PCR amplification was performed on a Biometra TRIO Thermal Cycler (Analytik Jena, Germany) using PrimeSTAR HS DNA Polymerase (Takara Bio Inc., USA). Each 50 µL PCR reaction contains 10 µL 5X PCR buffer, 4 µL 2.5 mM dNTP, 1 µL of forward and reverse primers at 10 µM, 1 µL template DNA, 0.5 µL PrimeSTAR and 32.5 µL sterilized dH_2O. The thermocycling program was 98 ^oC for 1 min followed by 36 cycles of 98 ^oC for 10 s, annealing temperature (Table 2.4 in Section 2.5.4) for 15 s with the primers of *tetA*-long and *sul1*-full or 10 s with longer primers, 72 ^oC for 1 min, and 72 ^oC for 30 s after cycles.

Gibson assembly for preparing target plasmids

Then, the complete fragments of *tetA* (1191 bp) and *sul1* (840 bp) were incorporated into backbone pEB1 by Gibson Assembly (Gibson *et al.*, 2009) forming the resulting plasmids pEB1-tetA and pEB1-sul1, respectively (shown in Figure 2.1 in Section 2.2.2).

Functionality analysis and structural sequencing for constructed plasmids

The plasmids were then transformed into DH10B and then plated on LB agar with 50 µg/mL Kanamycin and incubated overnight at 37 ^oC. Twenty-three colonies were picked from the plates for each cloned plasmid and suspended in 40 µL dH_2O. The culture suspension of DH10B transformed with pEB1-sfGFP was also prepared as negative control. Then 5 µL of each culture suspension was stamped on plain LB agar and LB agar with 10 µg/mL tetracycline for pEB1-tetA or LB agar with 200 µg/L sulfamethoxazole for pEB1-sul1. Two randomly selected positive colonies stamped on selective LB agar plate for each cloned plasmid are shown in Figure 2.13.

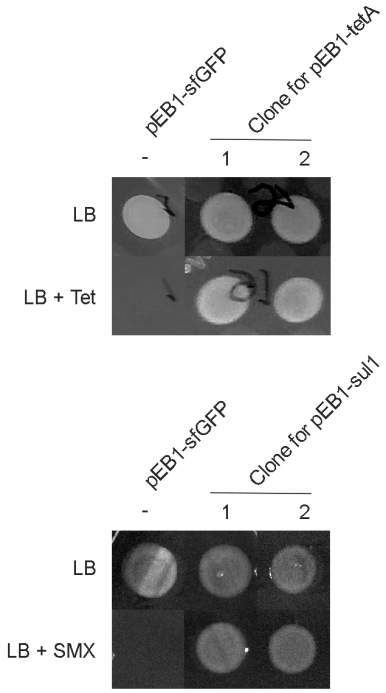

Figure 2.13: Growth of DH10B transformed by pEB1-sfGFP (-) and by the cloned pEB1-tetA and pEB1-sul1 (Tet, teracycline; SMX, sulfamethoxazole).

The two colonies were inoculated in selected LB media and grown overnight at 37 ^{o}C, 200 rpm. Plasmids were extracted from the culture and subsequently sequenced using Sanger sequencing (Laragen Sequencing and Genotyping, USA). For the target plasmid pEB1-tetA, 4 primers (pEB1-Bb-FW, pEB1-Bb-RV, *tetA*-long-FW, and *tetA*-short-RV, shown in Table 2.4 of Section 2.5.4) were used for sequencing. A sequence length of 1420 bp (including 181 bp before *tetA*, the first 528 bp of *tetA*, the last 592 bp of *tetA*, and 49 bp after *tetA*) was aligned using SnapGene (USA) and 8 base pair mutations resulting in 3 amino acid mutations were observed; all occurred in the *tetA* gene. The positions of all the mutations are listed in Table 2.3 and shown in Figure 2.14. Since the similarity of the aligned sequence is 99.5% and the tetracycline-resistance was successfully expressed by DH10B cells, we keep the gene as *tetA* in this study. For the target plasmid pEB1-sul1, 4 primers (pEB1-Bb-FW, pEB1-Bb-RV, *sul1*-full-FW and *sul1*-full-RV, shown in Table 2.4 of Section 2.5.4) were used for sequencing. A sequence length of 1105 bp (including the complete 840 bp of *sul1* gene with 198 bp before and 67 bp after *sul1*) were aligned using SnapGene (USA), and no mismatch was found (100% similarity).

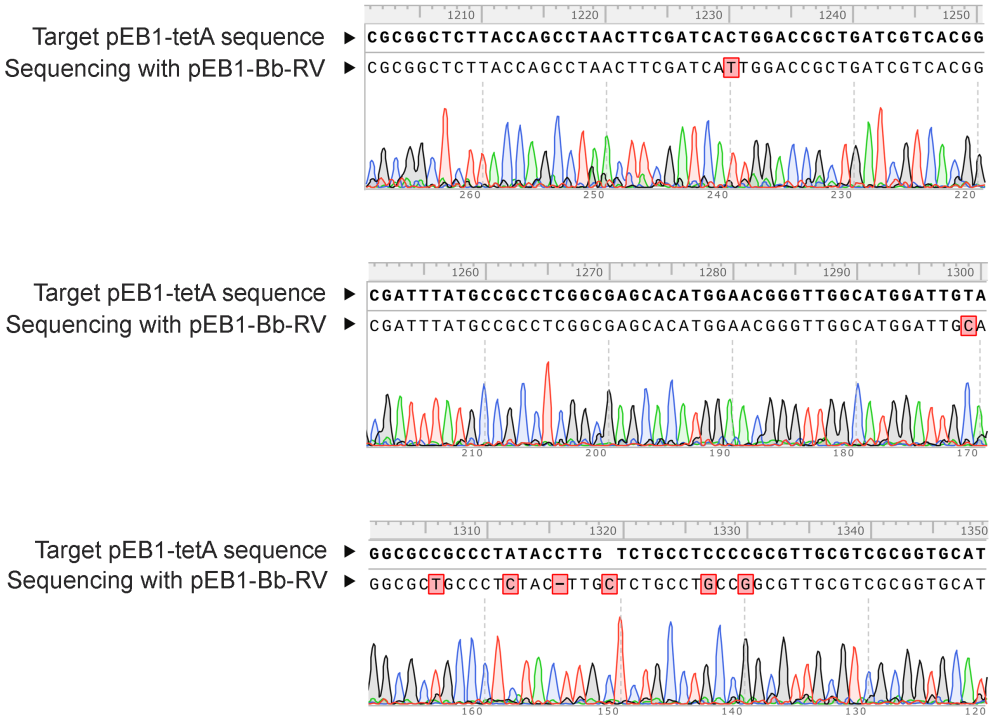

Figure 2.14: Chromatogram of Sanger sequencing for cloned pEB1-tetA with annotated mutations.

Table 2.3: Mutations in pEB1-tetA detected by Sanger sequencing.

Position in pEB1-tetA	Position in *tetA* gene	Mutation	Amino acid mutation in pEB1-tetA
1230	1049	C → T	Threonine (350)→Isoleucine
1299	1118	T → C	Valine (373)→Alanine
1306	1125	C → T	Alanine (375)→Alanine
1312	1131	A → C	Leucine (377)-Leucine
1316	1135	C → -	Leucine (379)-Leucine
1320	1139	- →C	Valine (380)→Leucine
1327	1146	C → G	Leucine (382)→Leucine
1330	1149	C → G	Proline (383)-Proline

Plasmid extraction

The transformed DH10B culture with the cloned pEB1-tetA or pEB1-sul1 was stored at -80 °C in 15% glycerol as stock. All the cell cultures thereafter were cultivated directly from the stocks in LB Broth with 10 µg/mL tetracycline or 200 µg/mL SMX at 37 °C, 200 rpm overnight. To prepare plasmid stocks, several extractions were conducted for both pEB1-tetA and pEBA-sul1. The

concentrations of the plasmid DNA in the plasmid stocks are 80-170 ng/μL as measured a Nanodrop One C (Thermo Fisher Scientific, USA).

2.5.2 Preparation and Characterization of Blue Nanotube Array (BNTA)

TiO_2 nanotube array (NTA) electrode was synthesized by the anodization as reported previously (Yang and Hoffmann, 2016b). A 6-cm^2 titanium (Ti) metal plate was coupled with a 6-cm^2 stainless-steel cathode, immersed in an ethylene glycol electrolyte containing 0.25 wt% NH_4F and 2 wt% H_2O. A constant voltage of 40 V was applied between the Ti plate anode and the stainless-steel cathode for 6 h. A layer of NTA film with a thickness of 16 μm grew on the surface of the Ti plate. The NTA electrode was then calcinated at 450 °C in air for 1 h to convert the amorphous TiO_2 to the anatase phase. The blue NTA (BNTA) was prepared by applying a cathodic current of 5 mA/cm^2 to the NTA in 15 mM Na_2SO_4 for 5 min.

The band structure and the mechanism of electron conduction of NTA and BNTA have been extensively studied previously (Koo *et al*., 2017b; Yang *et al*., 2018b; Yang and Hoffmann, 2016b). Figure 2.15 illustrates the band structures of NTA and BNTA. The NTA electrode with TiO_2 as the building blocks has the properties of n-type semiconductor. Its Fermi level was located beneath the conduction band. In an electrochemical system, the change of anodic potential leads to the shift of E_F of the semiconductor. As shown in Figure 2.15a, the application of anodic potential (*e.g.,* 4 V_{RHE}) results in the downward shifting of E_F and upward bending of edges of CB and VB. The band bending produces a space charge layer at the electrode/electrolyte interface, which serves as an energy barrier prohibiting the electron transfer. Therefore, the pristine NTA barely exhibited current response at anodic potentials.

The cathodization of NTA to BNTA reduced part of the Ti^{4+} to Ti^{3+} and created oxygen vacancies (O_{vac}) in the lattice structure. The Ti^{3+}-O_{vac} pairs are electron donor states that increase the doping level within TiO_2. Consequently, the E_F, which represents the average electron energy level, was shifted to above the CB edge. At anodic potentials, the space change layer was significantly reduced, enabling the conduction of electrons via tunneling mechanisms (Figure 2.15b). As a result,

BNTA shows significant current response at anodic potentials and high reactivity to produce oxidants such as free chlorine and hydroxyl radicals during electrolysis.

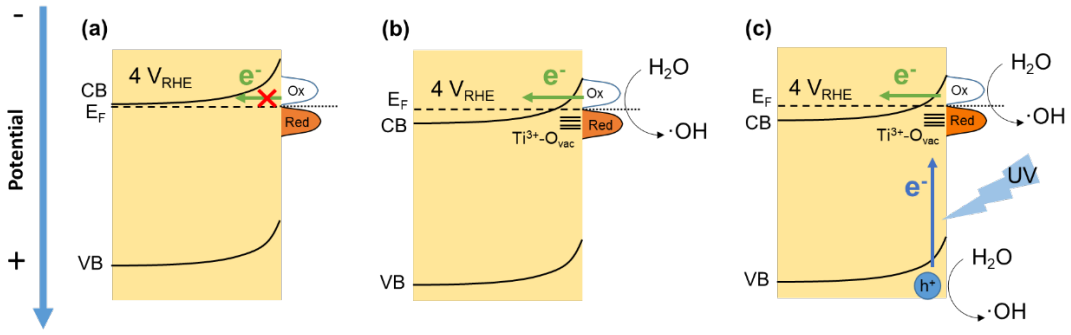

Figure 2.15: Schematic illustration of the position of the conduction band (CB), valence band (VB), and Fermi energy level (E_F) at an anodic potential of 4 V_{RHE} for (a) NTA, (b) BNTA, and (c) BNTA under UV irradiation.

Electrolysis using the BNTA anode was performed 30 mM $NaClO_4$ at 10 mA/cm^2, leading to an initial anodic potential of 4 V_{RHE}. The anodic potential gradually increases with the increase of electrolysis time, indicative of the rise of internal resistance to electron transfer. This is because of the oxidation of Ti^{3+}-O_{vac} pair back to Ti^{4+} (*i.e.,* the conversion from conductive TiO_{2-x} to insulative TiO_2). The results are in line with previous studies. A strategy proposed to regenerate the deactivated BTNA is to reverse polarity. However, this approach increases the complexity and cost of the power supply systems. In light of this, it is critical to develop facile methods to stabilize the Ti^{3+}-O_{vac} pair to maintain the conductivity of BNTA.

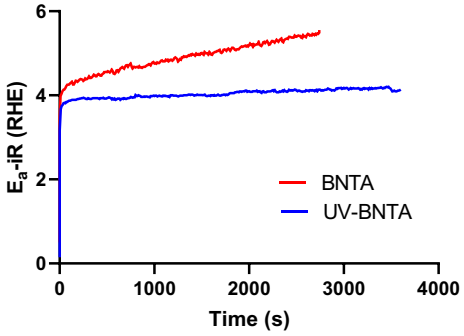

Figure 2.16: Stability tests performed in 15 mM Na_2SO_4 at 10 mA/cm^2.

UV irradiation can induce the electron-hole separation on TiO_2. The photogenerated electron can be trapped by bulk $>Ti^{IV}$ or surface $Ti^{IV}OH$ to form Ti^{3+} defect sites, while holes will be trapped by $Ti^{IV}OH$ to produce surface bound ·OH radicals ($Ti^{IV}OH\cdot$) (Hoffmann *et al*., 1995; Linsebigler *et al*., 1995). It is reasonable to speculate that photo-activation and cathodization treatment both produce the Ti^{3+}-O_{vac} pairs. The key hypothesis is that, by combining UV irradiation with electrolysis, the gradually depleted Ti^{3+}-O_{vac} under anodic potential can be *in situ* regenerated by photo-electrons.

The hypothesis was verified in the stability test (Figure 2.16). Under UV irradiation, no sign of inactivation was observed in a one hour test period. The XPS analysis provides direct evidence. As shown in Figure 2.17, the peak of O1s orbital can be deconvoluted to a main peak centered at 531 eV and shoulder peak centered at 532 eV. The former can be assigned to fully coordinated lattice oxygen while the latter corresponds to oxygen vacancies (Yang *et al*., 2018b, 2015). After cathodization, BNTA contains higher O_v than NTA (11 vs. 6%). BNTA samples were subjected to 1 h stability tests with and without UV irradiation. The abundance of O_v was preserved on spent BNTA with UV irradiation. In contrast, O_v was depleted on spent BNTA in the absence of UV.

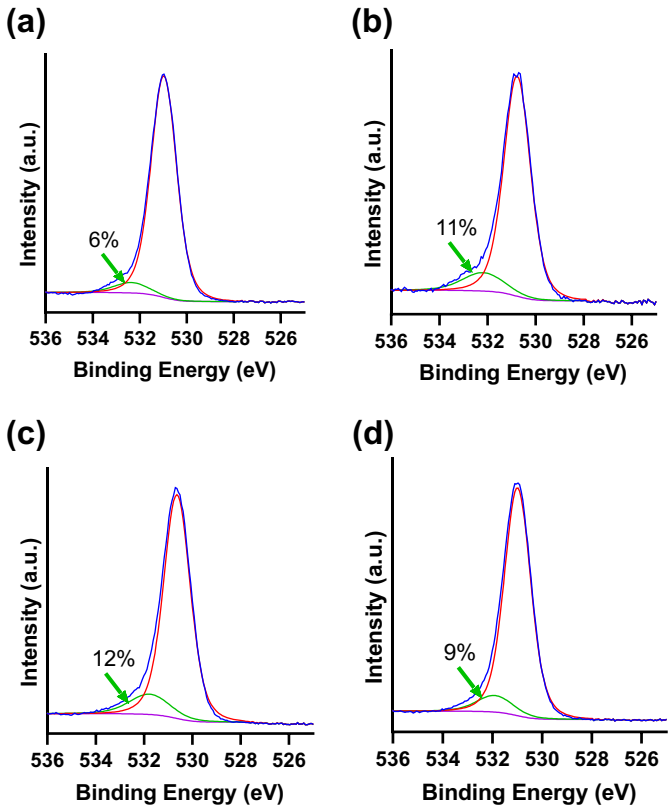

Figure 2.17: O1s XPS orbitals of (a) NTA, (b) BNTA, (c) BNTA after 1 h electrolysis with UV irradiation, and (d) BNTA after 1 h electrolysis without UV irradiation.

2.5.3 Effect of electrolytes on the DNA analysis by gel electrophoresis and qPCR inhibition

The effect of the electrolytes on gel electrophoresis and qPCR inhibition was investigated. The background electrolyte, NaCl, at an initial concentration of 30 mM was electrolyzed under a constant direct current of 30 mA with UV radiation for 0 s, 1 min, 5 min, and 10 min. Then the stock samples of pEB1-sul1 and purified PCR amplicon of *sul1* (840 bp) were spiked into the electrolyzed NaCl with varied electrolysis durations. They were then analyzed by gel electrophoresis and qPCR measurement. No differences were observed in the gel electrophoresis results (Figure 2.18) or qPCR (Figure 2.19) between the samples taken during the zero applied potential electrolysis (*i.e.*, no electrolysis) experiments and electrolyzed NaCl.

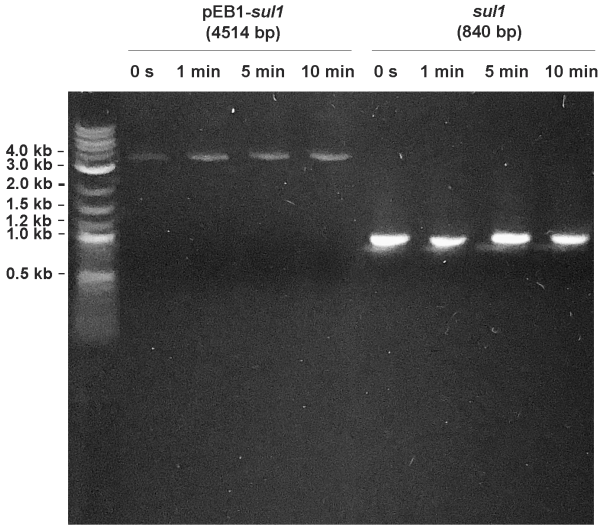

Figure 2.18: Gel electrophoresis of pEB1-sul1 and *sul1* spiked in electrolyzed NaCl (30 mM) with different electrolysis durations.

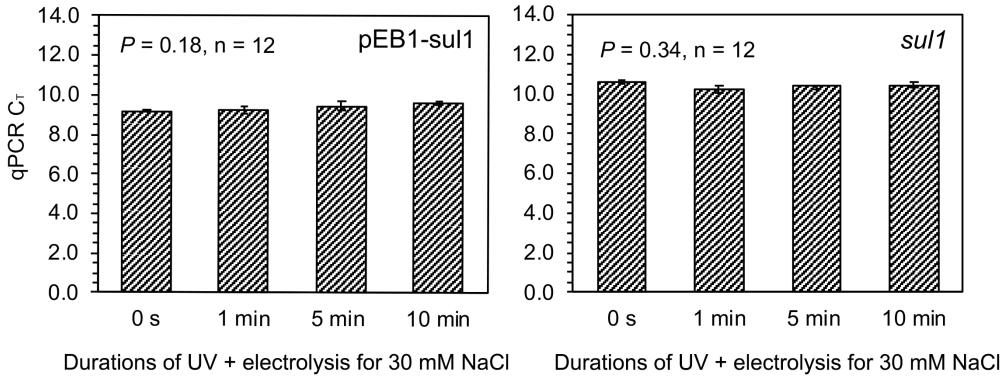

Figure 2.19: C_T values (*sul1*_long) of spiked pEB1-sul1 and *sul1* as a function of varied durations for UV-EO treated NaCl with an initial concentration of 30 mM. No difference was observed between the samples in untreated and treated NaCl with *P* values of 0.18 and 0.34 for pEB1-sul1 and *sul1*, respectively (ANOVA test).

2.5.4 List of Primers

Table 2.4: List of primers used in this study.

Primer	Sequence (5'-3')		Oligo size (nt)	Annealing temperature (°C)	Amplicon size (bp)	Annotation	Reference
tetA-long	FW:	CGT GTA TGA AAT CTA ACA ATG CGC T	25	51.9	1200	For qPCR quatification of *tetA* long amplicon, amplifying full-length tetA gene from wastewater, and sanger sequencing to check on the constructed plasmid	Chang *et al*., 2017
	RV:	CCA TTC AGG TCG AGG TGG C	19				
tetA-short	FW:	GAC TAT CGT CGC CGC ACT TA	20	53.9	216	For qPCR quatification of *tetA* short amplicon	Chang *et al*., 2017
	RV:	ATA ATG GCC TGC TTC TCG CC	20				
sul1-long	FW:	GAC GGT GTT CGG CAT TCT	18	60	827	For qPCR quatification of *sul1* long amplicon	Czekalski *et al*., 2016
	RV:	GAT CTA ACC CTC GGT CTC TGG	21				

sul1-short	FW:	CGC ACC GGA AAC ATC GCT GCA C	22	60	162	For qPCR quatification of *sul1* short amplicon	Xu *et al*., 2015
	RV:	TGA AGT TCC GCC GCA AGG CTC G	22				
sul1-full	FW:	ATG GTG ACG GTG TTC GGC ATT CTG AAT CT	29	60	840	For amplifying full-length sul1 gene from wastewater and sanger sequencing to check on the constructed plasmid	this study
	RV:	CTA GGC ATG ATC TAA CCC TCG GTC TCT GGC	30				
pEB1-Bb-tetA	FW:	TCT ACA AAT AAT TTT GTT TAA CTT TTC TAG ATT TAA GAA GGA GAT ATA CAT ATG AAA TCT AAC AAT GCG	87	60.0	1294	For adding an overlap of pEB1 backbone on each end of tetA genes	this study

		CTC ATC GTC ATC CTC GGC					
	RV:	CTT TCG TTT TAT TTG ATG CCT CTA GAG CTT GCA TGC CTG CAG GTC TGG ACA TTC AGG TCG AGG TGG CCC GGC TCC ATG	78				
pEB1-Bb-sul1	FW:	TCT ACA AAT AAT TTT GTT TAA CTT TTC TAG ATT TAA GAA GGA GAT ATA CAT ATG GTG ACG GTG TTC GGC ATT CTG AAT CT	80	60	942	For adding an overlap of pEB1 backbone on each end of sul1 genes	this study

	RV:	TTT CGT TTT ATT TGA TGC CTC TAG AGC TTG CAT GCC TGC AGG TCT GGA CAT CTA GGC ATG ATC TAA CCC TCG GTC TCT GGC	81				
pEB1-Bb	FW:	TTT GCA GGG CTT CCC AAC CTT ACC AGA GGG	30	65	1261	For sanger sequencing to check on the constructed plasmid	this study
	RV:	CGG ATT TGT CCT ACT CAG GAG AGC GTT CA	29				

2.5.5 Summary of Kinetic Parameters from Literature and This Study

Table 2.5: Summary of kinetic parameters for ARB deactivation and ARG degradation/deactivation from literature and this study, with the treatment related to this study of UV alone, UV-combined techniques, H_2O_2, and chlorine.

Gene	Gene length (bp)	DNA type	DNA name	DNA location	DNA length (bp)	Host cell	Inactivation type	Initial DNA/ cell concentration	Amplicon length (bp)	Reagent for treatment	Kinetic rates (cm^2/mJ for UV; $M^{-1} s^{-1}$ for H_2O_2; L/(mg•min) for chlorine)	Regression model	Required dose for 2-log10 reduction (mJ/cm^2 for UV; M・s for H_2O_2; mg/L•min for chlorine)	Required dose for 4-log10 reduction (mJ/cm^2 for UV; M・s for H_2O_2; mg/L•min for chlorine)	Reference
UV_{254}															
tetA	1191	plasmid	pEB1-tetA		4865	*E. coli* DH10B	culturability (selective agar)	~2.3×10^7 CFU/mL		30 mM $NaClO_4$		fluence-based first order		50 (3.9 log10)	This study
sul1	840	plasmid	pEB1-sul1		4514	*E. coli* DH10B	culturability (selective agar)	~2.8×10^7 CFU/mL		30 mM $NaClO_4$		fluence-based first order	50 (2.6-log_{10})	150 (4.2 log10)	
tetA	1191	plasmid	pEB1-tetA	intracellular	4865	*E. coli* DH10B	gene damage (by qPCR)	~2.3×10^7 CFU/mL	1200	30 mM $NaClO_4$	$1.3 (\pm 0.10)\times10^{-2}$	fluence-based first order	354	>3000	
tetA	1191	plasmid	pEB1-tetA	intracellular	4865	*E. coli* DH10B	gene damage (by qPCR)	~2.3×10^7 CFU/mL	216	30 mM $NaClO_4$	$2.8 (\pm 0.03)\times10^{-3}$	fluence-based first order	1645	>3000	
tetA	1191	plasmid	pEB1-tetA	extracellular	4865	*E. coli* DH10B	gene damage (by qPCR)	8×10^8 copies/µL	1200	30 mM $NaClO_4$	$1.7 (\pm 0.02)\times10^{-2}$	fluence-based first order	271	>542	
tetA	1191	plasmid	pEB1-tetA	extracellular	4865	*E. coli* DH10B	gene damage (by qPCR)	8×10^8 copies/µL	216	30 mM $NaClO_4$	$2.8 (\pm 0.03)\times10^{-3}$	fluence-based first order	1645	>3000	
sul1	840	plasmid	pEB1-sul1	intracellular	4514	*E. coli* DH10B	gene damage (by qPCR)	~$2.8e\times10^7$ CFU/mL	827	30 mM $NaClO_4$	$1.2 (\pm 0.02)\times10^{-2}$	fluence-based first order	384	~600	
sul1	840	plasmid	pEB1-sul1	intracellular	4514	*E. coli* DH10B	gene damage (by qPCR)	~$2.8e\times10^7$ CFU/mL	162	30 mM $NaClO_4$	$2.3 (\pm 0.02)\times10^{-3}$	fluence-based first order	2003	>3000	
sul1	840	plasmid	pEB1-sul1	extracellular	4514	*E. coli* DH10B	gene damage (by qPCR)	$1.3e\times10^9$ copies/µL	827	30 mM $NaClO_4$	$1.6 (\pm 0.05)\times10^{-2}$	fluence-based first order	288	~1500	
sul1	840	plasmid	pEB1-sul1	extracellular	4514	*E. coli* DH10B	gene damage (by qPCR)	1.3×10^9 copies/µL	162	30 mM $NaClO_4$	$2.8 (\pm 0.02)\times10^{-3}$	fluence-based first order	1645	>3000	
ampR	861	plasmid	pUC19	extracellular	2686	*E. coli* DH5*α*	gene damage (by qPCR)	1 µg/mL	192	2 mM PBS; pH 7	$2.0 (\pm 0.05)\times10^{-2}$	fluence-based first order	N.A.	N.A.	Nihemaiti *et al.*, 2020
ampR	861	plasmid	pUC19	extracellular	2686	*E. coli* DH5*α*	gene damage (by qPCR)	1 µg/mL	400	2 mM PBS; pH 7	$3.4 (\pm 0.07)\times10^{-2}$	fluence-based first order	135	N.A.	

ampR	861	plasmid	pUC19	extracellular	2686	*E. coli* DH5α	gene damage (by qPCR)	1 µg/mL	603	2 mM PBS; pH 7	5.8 (± 0.11)×10^{-2}	fluence-based first order	79	N.A.	
ampR	861	plasmid	pUC19	extracellular	2686	*E. coli* DH5α	gene damage (by qPCR)	1 µg/mL	851	2 mM PBS; pH 7	8.9 (± 0.16)×10^{-2}	fluence-based first order	52	104	
ampR	861	plasmid	pUC19	extracellular	2686	*E. coli* DH5α	transformation activity	1 µg/mL		2 mM PBS; pH 7	6.5 (± 0.21) ×10^{-2}	fluence-based first order	71	N.A.	
ampR	861	plasmid	pUC19	extracellular	2686	*E. coli* DH5α	transformation activity	1 µg/mL		2 mM PBS; pH 7	1.0 (± 0.03)×10^{-1}	fluence-based first order	46	92	
ampR	861	plasmid	pUC19	extracellular	2686	*E. coli* DH5α	transformation activity	1 µg/mL		2 mM PBS; pH 7	2.4 (± 0.06) ×10^{-1}	fluence-based first order	19	38	
ampR	861	plasmid	pUC19	extracellular	2686	*E. coli* DH5α	transformation activity	1 µg/mL		2 mM PBS; pH 7	1.6 (± 0.06)×10^{-1}	fluence-based first order	29	N.A.	
ampR	861	plasmid	pUC19	extracellular	2686	*E. coli* DH5α	transformation activity	1 µg/mL		2 mM PBS; pH 7	N.A. (too fast)				
sul1	840			intracellular		*Pseudomonas* HLS-6	gene damage (by qPCR)	$1×10^6$ CFU/mL	162	PBS; pH 7	1.96×10^{-2}	fluence-based first order	235	N.A.	Zhang *et al*., 2019
intl1				intracellular		*Pseudomonas* HLS-6	gene damage (by qPCR)	~$1×10^6$ CFU/mL	146	PBS; pH 7	2.99×10^{-2}	fluence-based first order	154	N.A.	
blt		chromosome		extracellular			gene damage (by qPCR)	1 ng/µL	266	10 mM PBS;pH 7	2.0 (± 0.1) ×10^{-2}	fluence-based first order	> 88 (0.6-$\log_{10}$)	N.A.	He *et al*., 2019
blt		chromosome		extracellular			gene damage (by qPCR)	1 ng/µL	832	10 mM PBS;pH 7	5.2 (± 0.2) ×10^{-2}	fluence-based first order	> 88(1.6-$\log_{10}$)	N.A.	
blt		chromosome		extracellular			gene damage (by qPCR)	1 ng/µL	870	10 mM PBS pH 7	7.8 (± 0.4) ×10^{-2}	fluence-based first order	66	N.A.	
blt		chromosome		extracellular			gene damage (by qPCR)	1 ng/µL	1017	10 mM PBS;pH 7	8.8 (± 0.4) ×10^{-2}	fluence-based first order	53	N.A.	
blt		chromosome		extracellular		*Bacillus subtilis* 1A189	transformation activity	1 ng/µL		10 mM PBS;pH 7			109	N.A.	
blt		chromosome		intracellular		*Bacillus subtilis* 1A189	transformation activity	$1×10^6$ CFU/mL		10 mM PBS;pH 7			> 66 (1.9-$\log_{10}$)	N.A.	
ampR	860	plasmid	pUC19	extracellular	2686	*E. coli* DH5α	gene damage (by qPCR)	~$1×10^{11}$ copies/mL	192	2 mM PBS; pH 7	1.9 (± 0.11) ×10^{-2}	fluence-based first order			Yoon *et al*., 2018
ampR	860	plasmid	pUC19	extracellular	2686	*E. coli* DH5α	gene damage (by qPCR)	~$1×10^{11}$ copies/mL	400	2 mM PBS; pH 7	3.1 (± 0.09) ×10^{-2}	fluence-based first order			
ampR	860	plasmid	pUC19	extracellular	2686	*E. coli* DH5α	gene damage (by qPCR)	~$1×10^{11}$ copies/mL	603	2 mM PBS; pH 7	5.4 (± 0.16) ×10^{-2}	fluence-based first order			
ampR	860	plasmid	pUC19	extracellular	2686	*E. coli* DH5α	gene damage (by qPCR)	~$1×10^{11}$ copies/mL	851	2 mM PBS; pH 7	1.0 (± 0.03) ×10^{-1}	fluence-based first order			
ampR	860	plasmid	pUC19	extracellular	2686	*E. coli* DH5α	transformation activity	~$1×10^{11}$ copies/mL		2 mM PBS; pH 7	6.1 (± 0.30)×10^{-2}	fluence-based first order	76	151	

ampR	860	plasmid	pUC19	intracellular	2686	*E. coli* DH5α	gene damage (by qPCR)	~5×10^{6} CFU/mL	192	2 mM PBS; pH 7	1.7 (± 0.09)×10^{-2}	fluence-based first order			
ampR	860	plasmid	pUC19	intracellular	2686	*E. coli* DH5α	gene damage (by qPCR)	~5×10^{6} CFU/mL	400	2 mM PBS; pH 7	2.8 (± 0.06)×10^{-2}	fluence-based first order			
ampR	860	plasmid	pUC19	intracellular	2686	*E. coli* DH5α	gene damage (by qPCR)	~5×10^{6} CFU/mL	603	2 mM PBS; pH 7	4.6 (± 0.18)×10^{-2}	fluence-based first order			
ampR	860	plasmid	pUC19	intracellular	2686	*E. coli* DH5α	gene damage (by qPCR)	~5×10^{6} CFU/mL	851	2 mM PBS; pH 7	7.2 (± 0.35)×10^{-2}	fluence-based first order			
ori	589	plasmid	pUC19	extracellular	2686	*E. coli* DH5α	gene damage (by qPCR)	~1×10^{11} copies/mL	190	2 mM PBS; pH 7	1.7 (± 0.09)×10^{-2}	fluence-based first order			
ori	589	plasmid	pUC19	extracellular	2686	*E. coli* DH5α	gene damage (by qPCR)	~1×10^{11} copies/mL	390	2 mM PBS; pH 7	2.9 (± 0.12) ×10^{-2}	fluence-based first order			
ori	589	plasmid	pUC19	extracellular	2686	*E. coli* DH5α	gene damage (by qPCR)	~1×10^{11} copies/mL	530	2 mM PBS; pH 7	4.0 (± 0.24) ×10^{-2}	fluence-based first order			
ori	589	plasmid	pUC19	intracellular	2686	*E. coli* DH5α	transformation activity	~5×10^{6} CFU/mL		2 mM PBS; pH 7	6.2 (± 0.4) ×10^{-2}	fluence-based first order	74	151	
ampR	860	plasmid	pUC4k	extracellular	3914	*E. coli* DH5α	gene damage (by qPCR)	~1×10^{10} copies/mL	850	2 mM PBS; pH 7	1.1 (± 0.01) ×10^{-1}	fluence-based first order	42	84	Yoon *et al*., 2017
kanR	815	plasmid	pUC4k	extracellular	3914	*E. coli* DH5α	gene damage (by qPCR)	~1×10^{10} copies/mL	806	2 mM PBS; pH 7	1.5 (± 0.06) ×10^{-1}	fluence-based first order	31	61	
ampR	860	plasmid	pUC4k	intracellular	3914	*E. coli* DH5α	gene damage (by qPCR)	~5×10^{5} CFU/mL	850	2 mM PBS; pH 7	7.0 (± 0.3) ×10^{-2}	fluence-based first order	66	132	
kanR	815	plasmid	pUC4k	intracellular	3914	*E. coli* DH5α	gene damage (by qPCR)	~5×10^{5} CFU/mL	806	2 mM PBS; pH 7	9.0 (± 1.4) ×10^{-2}	fluence-based first order	51	102	
ampR	860	plasmid	pUC4k	extracellular	3914	*E. coli* DH5α	gene damage (by qPCR)	~1×10^{10} copies/mL	850	2 mM PBS; pH 8	1.0 (± 0.06) ×10^{-1}	fluence-based first order	46	92	
kanR	815	plasmid	pUC4k	extracellular	3914	*E. coli* DH5α	gene damage (by qPCR)	~1×10^{10} copies/mL	806	2 mM PBS; pH 8	1.3 (± 0.1)×10^{-1}	fluence-based first order	35	71	
ampR	860	plasmid	pUC4k	intracellular	3914	*E. coli* DH5α	gene damage (by qPCR)	~5×10^{5} CFU/mL	850	2 mM PBS; pH 8	6.5 (± 0.9) ×10^{-2}	fluence-based first order	71	142	
kanR	815	plasmid	pUC4k	intracellular	3914	*E. coli* DH5α	gene damage (by qPCR)	~5×10^{5} CFU/mL	806	2 mM PBS; pH 8	7.2 (± 0.9)×10^{-2}	fluence-based first order	64	128	
ampR and *kanR*						*E. coli* DH5α	Culturability (selective agar)	~5×10^{5} CFU/mL		2 mM PBS; pH 7	2.1 (± 0.1)	fluence-based first order	2.2	4.4	
ampR	860	plasmid	pUC4k	extracellular	3914	*E. coli* DH5α	gene damage (by qPCR)	~1×10^{10} copies/mL	850	Spiked municiple wastewater effluent (activated sludge); pH 7	1.1×10^{-1}	fluence-based first order	42	< LOQ	
kanR	815	plasmid	pUC4k	extracellular	3914	*E. coli* DH5α	gene damage (by qPCR)	~1×10^{10} copies/mL	806	spiked municiple wastewater effluent (activated sludge); pH 7	9.5×10^{-2}	fluence-based first order	31	< LOQ	

ampR	860	plasmid	pUC4k	intracellular	3914	*E. coli* DH5α	gene damage (by qPCR)	~5×10^5 CFU/mL	850	spiked municiple wastewater effluent (activated sludge); pH 7	6.2×10^{-2}	fluence-based first order	66	< LOQ	
kanR	815	plasmid	pUC4k	intracellular	3914	*E. coli* DH5α	gene damage (by qPCR)	~5×10^5 CFU/mL	806	spiked municiple wastewater effluent (activated sludge); pH 7	6.3×10^{-2}	fluence-based first order	51	< LOQ	
tetA	1191	plasmid	pWH1266	extracellular		*E. coli* TOP10	gene damage (by qPCR)	10 ng/µL	1200	DNase free water	$5.8 (\pm 0.6)\times10^{-2}$	fluence-based first order	> 108 (1.7-$\log_{10}$)	N.A.	Chang *et al.*, 2017
tetA	1191	plasmid	pWH1266	extracellular		*E. coli* TOP10	gene damage (by qPCR)	10 ng/µL	216	DNase free water	$4.0 (\pm 0.5)\times10^{-3}$	fluence-based first order	> 430 (0.75-$\log_{10}$)	N.A.	
tetA	1191	plasmid	pWH1266	extracellular		*E. coli* TOP10	ARG transformation activity	10 ng/µL		DNase free water	$1.02 (\pm 0.19)\times10^{-1}$	fluence-based first order	45	N.A.	
*blaT*EM-1	861	plasmid	pWH1266	extracellular		*E. coli* TOP10	gene damage (by qPCR)	10 ng/µL	861	DNase free water	$6.8 (\pm 0.4)\times10^{-2}$	fluence-based first order	68	N.A.	
*blaT*EM-1	861	plasmid	pWH1266	extracellular		*E. coli* TOP10	gene damage (by qPCR)	10 ng/µL	209	DNase free water	$5.5 (\pm 0.6)\times10^{-3}$	fluence-based first order	> 430 (1-$\log_{10}$)	N.A.	
*blaT*EM-1	861	plasmid	pWH1266	extracellular		*E. coli* TOP10	transformation activity	10 ng/µL		DNase free water	$1.13 (\pm 0.09)\times10^{-1}$	fluence-based first order	40	N.A.	
ampC		chromosome	Unkown Type IV staphylococcal chromosomal cassette mec	extracellular		multiantibiotic-resistant *Pseudomonas aeruginosa* 01	gene damage (by qPCR)	1×10^4- 1×10^7 copies/µL	1006	Nanopure water	N.A.		~180	N.A.	Mckinney *et al.*, 2012
mecA		chromosome		extracellular		methicillin-resistant *Staphylococcus aureus* (MRSA)	gene damage (by qPCR)	1×10^4- 1×10^7 copies/µL	1018	Nanopure water	N.A.		~70	N.A.	
tetA		plasmid	pSMS35_130	extracellular		multiantibiotic-resistant *E. coli* SMS-3-5	gene damage (by qPCR)	1×10^4- 1×10^7 copies/µL	1054	Nanopure water	N.A.		~180	N.A.	
vanA		chromosome or plasmid		extracellular		vancomycin-resistant *Enterococcus faecium*	gene damage (by qPCR)	1×10^4- 1×10^7 copies/µL	1030	Nanopure water	N.A.		~75	N.A.	

ampC		chromosome		intracellular		multiantibiotic-resistant *Pseudomonas aeruginosa* 01	gene damage (by qPCR)		1006	PBS/filtered wastewater	N.A.		~240	N.A.		
mecA		chromosome	Type IV staphylococcal chromosomal cassette mec	intracellular		methicillin-resistant *Staphylococcus aureus* (MRSA)	gene damage (by qPCR)		1018	PBS/filtered wastewater	N.A.		~70	N.A.		
tetA		plasmid	pSMS35_130	intracellular		multiantibiotic-resistant *E. coli* SMS-3-5	gene damage (by qPCR)		1054	PBS/filtered wastewater	N.A.		~200	N.A.		
vanA		chromosome or plasmid		intracellular		vancomycin-resistant *Enterococcus faecium*	gene damage (by qPCR)		1030	PBS/filtered wastewater	N.A.		~80	N.A.		
UV_{254}/H_2O_2																
$[H_2O_2]_0$=0.5 mm																
ampR	861	plasmid	pUC19	extracellular	2686	*E. coli* DH5α	gene damage (by qPCR)	0.3 μg/mL	192	2 mM PBS; pH 7	10.34 (± 0.21) $\times 10^{-2}$	fluence-based first order	45	89	Nihemaiti *et al.*, 2020	
ampR	861	plasmid	pUC19	extracellular	2686	*E. coli* DH5α	gene damage (by qPCR)	0.3 μg/mL	400	2 mM PBS; pH 7	14.81 (± 0.78) $\times 10^{-2}$	fluence-based first order	31	N.A.		
ampR	861	plasmid	pUC19	extracellular	2686	*E. coli* DH5α	gene damage (by qPCR)	0.3 μg/mL	603	2 mM PBS; pH 7	19.34 (± 0.97) $\times 10^{-2}$	fluence-based first order	24	48		
ampR	861	plasmid	pUC19	extracellular	2686	*E. coli* DH5α	gene damage (by qPCR)	0.3 μg/mL	851	2 mM PBS; pH 7	29.99 (± 2.10) $\times 10^{-2}$	fluence-based first order	15	31		
ampR	861	plasmid	pUC19	extracellular	2686	*E. coli* DH5α	transformation activity	0.3 μg/mL		2 mM PBS; pH 7	5.11 (± 0.18) $\times 10^{-2}$	fluence-based first order	90	~180		
$[[H_2O_2]_0$=10 mg/L																
ampR	860	plasmid	pUC19	extracellular	2686	*E. coli* DH5α	gene damage (by qPCR)	~1×10^{11} copies/mL	192	2 mM PBS; pH 7	2.5 (± 0.14) $\times 10^{-2}$	fluence-based first order			Yoon *et al.*, 2018	
ampR	860	plasmid	pUC19	extracellular	2686	*E. coli* DH5α	gene damage (by qPCR)	~1×10^{11} copies/mL	400	2 mM PBS; pH 7	4.1 (± 0.16) $\times 10^{-2}$	fluence-based first order				
ampR	860	plasmid	pUC19	extracellular	2686	*E. coli* DH5α	gene damage (by qPCR)	~1×10^{11} copies/mL	603	2 mM PBS; pH 7	6.7 (± 0.28) $\times 10^{-2}$	fluence-based first order				

ampR	860	plasmid	pUC19	extracellular	2686	*E. coli* DH5α	gene damage (by qPCR)	~1×10^{11} copies/mL	851	2 mM PBS; pH 7	1.8 (± 0.06) $\times10^{-1}$	fluence-based first order			
ampR	860	plasmid	pUC19	extracellular	2686	*E. coli* DH5α	transformation activity	~1×10^{11} copies/mL		2 mM PBS; pH 7	7.3 (± 0.4) $\times10^{-2}$	fluence-based first order	63	126	
ampR	860	plasmid	pUC19	intracellular	2686	*E. coli* DH5α	gene damage (by qPCR)	~5×10^{6} CFU/mL	192	2 mM PBS; pH 7	1.6 (± 0.09)$\times10^{-2}$	fluence-based first order			
ampR	860	plasmid	pUC19	intracellular	2686	*E. coli* DH5α	gene damage (by qPCR)	~5×10^{6} CFU/mL	400	2 mM PBS; pH 7	2.9 (± 0.12) $\times10^{-2}$	fluence-based first order			
ampR	860	plasmid	pUC19	intracellular	2686	*E. coli* DH5α	gene damage (by qPCR)	~5×10^{6} CFU/mL	603	2 mM PBS; pH 7	4.8 (± 0.28) $\times10^{-2}$	fluence-based first order			
ampR	860	plasmid	pUC19	intracellular	2686	*E. coli* DH5α	gene damage (by qPCR)	~5×10^{6} CFU/mL	851	2 mM PBS; pH 7	7.3 (± 0.30) $\times10^{-2}$	fluence-based first order			
ori	589	plasmid	pUC19	extracellular	2686	*E. coli* DH5α	gene damage (by qPCR)	~1×10^{11} copies/mL	190	2 mM PBS; pH 7	2.3 (± 0.05) $\times10^{-2}$	fluence-based first order			
ori	589	plasmid	pUC19	extracellular	2686	*E. coli* DH5α	gene damage (by qPCR)	~1×10^{11} copies/mL	390	2 mM PBS; pH 7	3.9 (± 0.14) $\times10^{-2}$	fluence-based first order			
ori	589	plasmid	pUC19	extracellular	2686	*E. coli* DH5α	gene damage (by qPCR)	~1×10^{11} copies/mL	530	2 mM PBS; pH 7	4.7 (± 0.21) $\times10^{-2}$	fluence-based first order			
ori	589	plasmid	pUC19	intracellular	2686	*E. coli* DH5α	transformation activity	~5×10^{6} CFU/mL		2 mM PBS; pH 7	6.4 (± 0.4) $\times10^{-2}$	fluence-based first order	72	144	
$[H_2O_2]_0$==10 mg/L															
ampR	860	plasmid	pUC4k	extracellular	3914	*E. coli* DH5α	gene damage (by qPCR)	~1×10^{10} copies/mL	850	2 mM PBS; pH 7	2.1 (± 0.2) $\times10^{-1}$	fluence-based first order	22	44	Yoon *et al*., 2017
kanR	815	plasmid	pUC4k	extracellular	3914	*E. coli* DH5α	gene damage (by qPCR)	~1×10^{10} copies/mL	806	2 mM PBS; pH 7	2.1 (± 0.3) $\times10^{-1}$	fluence-based first order	22	44	
ampR	860	plasmid	pUC4k	intracellular	3914	*E. coli* DH5α	gene damage (by qPCR)	~5×10^{5} CFU/mL	850	2 mM PBS; pH 7	6.3 (± 0.6) $\times10^{-2}$	fluence-based first order	73	146	
kanR	815	plasmid	pUC4k	intracellular	3914	*E. coli* DH5α	gene damage (by qPCR)	~5×10^{5} CFU/mL	806	2 mM PBS; pH 7	7.1 (± 0.3) $\times10^{-2}$	fluence-based first order	65	130	
ampR	860	plasmid	pUC4k	extracellular	3914	*E. coli* DH5α	gene damage (by qPCR)	~1×10^{10} copies/mL	850	2 mM PBS; pH 8	1.3 (± 0.4) $\times10^{-1}$	fluence-based first order	35	71	
kanR	815	plasmid	pUC4k	extracellular	3914	*E. coli* DH5α	gene damage (by qPCR)	~1×10^{10} copies/mL	806	2 mM PBS; pH 8	2.0 (± 0.2) $\times10^{-1}$	fluence-based first order	23	46	
ampR	860	plasmid	pUC4k	intracellular	3914	*E. coli* DH5α	gene damage (by qPCR)	~5×10^{5} CFU/mL	850	2 mM PBS; pH 8	7.0 (± 3.5) $\times10^{-2}$	fluence-based first order	66	132	
kanR	815	plasmid	pUC4k	intracellular	3914	*E. coli* DH5α	gene damage (by qPCR)	~5×10^{5} CFU/mL	806	2 mM PBS; pH 8	8.8 (± 0.6) $\times10^{-2}$	fluence-based first order	52	105	
ampR and *kanR*						*E. coli* DH5α	culturability (selective agar)	~5×10^{5} CFU/mL		2 mM PBS; pH 7	2.2 (± 0.1)	fluence-based first order	2.1	4.2	
ampR	860	plasmid	pUC4k	extracellular	3914	*E. coli* DH5α	gene damage (by qPCR)	~1×10^{10} copies/mL	850	spiked municiple wastewater effluent (activated sludge); pH 7	1.1×10^{-1}	fluence-based first order	42	< LOQ	

kanR	815	plasmid	pUC4k	extracellular	3914	*E. coli* DH5α	gene damage (by qPCR)	~1×10^{10} copies/mL	806	spiked municiple wastewater effluent (activated sludge); pH 7	1.0×10^{-1}	fluence-based first order	46	< LOQ	
ampR	860	plasmid	pUC4k	intracellular	3914	*E. coli* DH5α	gene damage (by qPCR)	~5×10^{5} CFU/mL	850	spiked municiple wastewater effluent (activated sludge); pH 7	5.4×10^{-2}	fluence-based first order	85	< LOQ	
kanR	815	plasmid	pUC4k	intracellular	3914	*E. coli* DH5α	gene damage (by qPCR)	~5×10^{5} CFU/mL	806	spiked municiple wastewater effluent (activated sludge); pH 7	6.2×10^{-2}	fluence-based first order	74	< LOQ	
$UV_{254}/S_2O_8^{2-}$															
$[S_2O_8^{2-}]_0$=0.5 mM															
ampR	861	plasmid	pUC19	extracellular	2686	*E. coli* DH5α	gene damage (by qPCR)	0.3 μg/mL	192	2 mM PBS; pH 7	10.50 (± 0.48)×10^{-2}	fluence-based first order	44	N.A.	Nihemaiti *et al*., 2020
ampR	861	plasmid	pUC19	extracellular	2686	*E. coli* DH5α	gene damage (by qPCR)	0.3 μg/mL	400	2 mM PBS; pH 7	17.09 (± 0.46)×10^{-2}	fluence-based first order	27	54	
ampR	861	plasmid	pUC19	extracellular	2686	*E. coli* DH5α	gene damage (by qPCR)	0.3 μg/mL	603	2 mM PBS; pH 7	22.87 (± 1.57)×10^{-2}	fluence-based first order	24	48	
ampR	861	plasmid	pUC19	extracellular	2686	*E. coli* DH5α	gene damage (by qPCR)	0.3 μg/mL	851	2 mM PBS; pH 7	31.85 (± 1.57)×10^{-2}	fluence-based first order	14	29	
ampR	861	plasmid	pUC19	extracellular	2686	*E. coli* DH5α	transformation activity	0.3 μg/mL		2 mM PBS; pH 7	5.16 (± 0.09)×10^{-2}	fluence-based first order	89	179	
UV_{254}/Cl_2															
$[Cl_2]_0$=20 mg/L															
sul1				intracellular		*Pseudomonas* HLS-6	gene damage (by qPCR)	~1×10^{6} CFU/mL	162	PBS; pH 7	1.27×10^{-1}	first order	36	N.A.	Zhang *et al*., 2019
intI1				intracellular		*Pseudomonas* HLS-6	gene damage (by qPCR)	~1×10^{6} CFU/mL	146	PBS; pH 7	1.42×10^{-1}	first order	33	N.A.	
UV_{254} assisted electrochemistry															
30 mA of DC															
tetA	1191	plasmid	pEB1-tetA		4865	*E. coli* DH10B	culturability (selective agar)	~2.3×10^{7} CFU/mL		30 mM $NaClO_4$				50 (4.1-$\log_{10}$)	This study
sul1	840	plasmid	pEB1-sul1		4514	*E. coli* DH10B	culturability (selective agar)	~2.8×10^{7} CFU/mL		30 mM $NaClO_4$				50 (4.0-$\log_{10}$)	
tetA	1191	plasmid	pEB1-tetA	intracellular	4865	*E. coli* DH10B	gene damage (by qPCR)	~2.3×10^{7} CFU/mL	1200	30 mM $NaClO_4$	2.0 (± 0.05)×10^{-2}	fluence-based first order	230	1500 (4.0-$\log_{10}$)	

tetA	1191	plasmid	pEB1-tetA	intracellular	4865	*E. coli* DH10B	gene damage (by qPCR)	~2.3×10^{7} CFU/mL	216	30 mM $NaClO_4$	3.0 (± 0.03) $\times10^{-3}$	fluence-based first order	1535	3000 (3.8-$\log_{10}$)
tetA	1191	plasmid	pEB1-tetA	extracellular	4865	*E. coli* DH10B	gene damage (by qPCR)	8×10^{8} copies/µL	1200	30 mM $NaClO_4$	2.6 (± 0.07) $\times10^{-2}$	fluence-based first order	177	600 (4.6-$\log_{10}$)
tetA	1191	plasmid	pEB1-tetA	extracellular	4865	*E. coli* DH10B	gene damage (by qPCR)	8×10^{8} copies/µL	216	30 mM $NaClO_4$	3.7 (± 0.02) $\times10^{-3}$	fluence-based first order	1245	2490
sul1	840	plasmid	pEB1-sul1	intracellular	4514	*E. coli* DH10B	gene damage (by qPCR)	~$2.8e\times10^{7}$ CFU/mL	827	30 mM $NaClO_4$	1.8 (± 0.03) $\times10^{-2}$	fluence-based first order	256	1500 (5.2-$\log_{10}$)
sul1	840	plasmid	pEB1-sul1	intracellular	4514	*E. coli* DH10B	gene damage (by qPCR)	~$2.8e\times10^{7}$ CFU/mL	162	30 mM $NaClO_4$	2.6 (± 0.03) $\times10^{-3}$	fluence-based first order	1772	3000 (3.4-$\log_{10}$)
sul1	840	plasmid	pEB1-sul1	extracellular	4514	*E. coli* DH10B	gene damage (by qPCR)	$1.3e\times10^{9}$ copies/µL	827	30 mM $NaClO_4$	2.6 (± 0.03) $\times10^{-2}$	fluence-based first order	177	354
sul1	840	plasmid	pEB1-sul1	extracellular	4514	*E. coli* DH10B	gene damage (by qPCR)	1.3×10^{9} copies/µL	162	30 mM $NaClO_4$	3.5 (± 0.02) $\times10^{-3}$	fluence-based first order	1316	2632
tetA	1191	plasmid	pEB1-tetA		4865	*E. coli* DH10B	culturability (selective agar)	~2.3×10^{7} CFU/mL		30 mM NaCl		fluence-based first order		50 (4.8-$\log_{10}$)
sul1	840	plasmid	pEB1-sul1		4514	*E. coli* DH10B	culturability (selective agar)	~2.8×10^{7} CFU/mL		30 mM NaCl		fluence-based first order		50 (5.0-$\log_{10}$)
tetA	1191	plasmid	pEB1-tetA	intracellular	4865	*E. coli* DH10B	gene damage (by qPCR)	~2.3×10^{7} CFU/mL	1200	30 mM NaCl	3.0 (± 0.10)$\times10^{-2}$	fluence-based first order	154	300 (3.7-$\log_{10}$)
tetA	1191	plasmid	pEB1-tetA	intracellular	4865	*E. coli* DH10B	gene damage (by qPCR)	~2.3×10^{7} CFU/mL	216	30 mM NaCl	4.6(± 0.02) $\times10^{-3}$	fluence-based first order	1001	2003
tetA	1191	plasmid	pEB1-tetA	extracellular	4865	*E. coli* DH10B	gene damage (by qPCR)	8×10^{8} copies/µL	1200	30 mM NaCl	3.6 (± 0.03) $\times10^{-2}$	fluence-based first order	128	256
tetA	1191	plasmid	pEB1-tetA	extracellular	4865	*E. coli* DH10B	gene damage (by qPCR)	8×10^{8} copies/µL	216	30 mM NaCl	4.8 (± 0.02) $\times10^{-3}$	fluence-based first order	960	1919
sul1	840	plasmid	pEB1-sul1	intracellular	4514	*E. coli* DH10B	gene damage (by qPCR)	~2.8×10^{7}` CFU/mL	827	30 mM NaCl	2.7 (± 0.07) $\times10^{-2}$	fluence-based first order	171	300 (3.4-$\log_{10}$)
sul1	840	plasmid	pEB1-sul1	intracellular	4514	*E. coli* DH10B	gene damage (by qPCR)	~2.8×10^{7} CFU/mL	162	30 mM NaCl	3.9 (± 0.02) $\times10^{-3}$	fluence-based first order	1181	2362
sul1	840	plasmid	pEB1-sul1	extracellular	4514	*E. coli* DH10B	gene damage (by qPCR)	1.3×10^{9} copies/µL	827	30 mM NaCl	3.4 (± 0.07) $\times10^{-2}$	fluence-based first order	135	271
sul1	840	plasmid	pEB1-sul1	extracellular	4514	*E. coli* DH10B	gene damage (by qPCR)	1.3×10^{9} copies/µL	162	30 mM NaCl	4.1 (± 0.02) $\times10^{-3}$	fluence-based first order	1123	1123
						native bacteria in wastewater	culturability (non-selective agar)	~6.4×10^{3} CFU/mL		latrine wastewater			150 (1.9-$\log_{10}$)	300 (2.7-$\log_{10}$)
tetA	1191					native bacteria in	gene damage (by qPCR)	$5.8e\times10^{2}$ copies/µL	1200	latrine wastewater			600 (1.1-$\log_{10}$)	

						wastewater									
tetA	1191					native bacteria in wastewater	gene damage (by qPCR)	$2.5e\times10^{3}$ copies/μL	216	latrine wastewater			3000 (1.9-$\log_{10}$)		
sul1	840					native bacteria in wastewater	gene damage (by qPCR)	7.5×10^{3} copies/μL	827	latrine wastewater			600 (1.9-$\log_{10}$)		
sul1	840					native bacteria in wastewater	gene damage (by qPCR)	2.2×10^{4} copies/μL	162	latrine wastewater			9000 (1.8-$\log_{10}$)		
UV>290/H_2O_2															
$[H_2O_2]_0$=10 mM															
ampR	861	plasmid	pUC19	extracellular	2686	*E. coli* DH5α	gene damage (by qPCR)	1 μg/mL	192	2 mM PBS; pH 7	$8.1 (\pm 0.69)\times10^{9}$	fluence-based first order	N.A.	N.A.	Nihemaiti *et al.*, 2020
ampR	861	plasmid	pUC19	extracellular	2686	*E. coli* DH5α	gene damage (by qPCR)	1 μg/mL	400	2 mM PBS; pH 7	$2.2 (\pm 0.07)\times10^{10}$	fluence-based first order	N.A.	N.A.	
ampR	861	plasmid	pUC19	extracellular	2686	*E. coli* DH5α	gene damage (by qPCR)	1 μg/mL	603	2 mM PBS; pH 7	$3.5 (\pm 0.10)\times10^{10}$	fluence-based first order	1.32×10^{-10}	N.A.	
ampR	861	plasmid	pUC19	extracellular	2686	*E. coli* DH5α	gene damage (by qPCR)	1 μg/mL	851	2 mM PBS; pH 7	$5.6 (\pm 0.27)\times10^{10}$	fluence-based first order	8.23×10^{-11}	1.65×10^{-10}	
ampR	861	plasmid	pUC19	extracellular	2686	*E. coli* DH5α	transformation activity	1 μg/mL		2 mM PBS; pH 7	$2.7 (\pm 0.05)\times10^{10}$	fluence-based first order	1.71×10^{-10}	N.A.	
ampR	861	plasmid	pUC19	extracellular	2686	*E. coli* AB1157	transformation activity	1 μg/mL		2 mM PBS; pH 7	$4.1 (\pm 0.14)\times10^{10}$	fluence-based first order	1.12×10^{-10}	N.A.	
ampR	861	plasmid	pUC19	extracellular	2686	*E. coli* AB1886	transformation activity	1 μg/mL		2 mM PBS; pH 7	$6.5 (\pm 0.18)\times10^{10}$	fluence-based first order	7.09×10^{-11}	N.A.	
ampR	861	plasmid	pUC19	extracellular	2686	*E. coli* AB2463	transformation activity	1 μg/mL		2 mM PBS; pH 7	$8.2 (\pm 0.23)\times10^{10}$	fluence-based first order	5.62×10^{-11}	N.A.	
ampR	861	plasmid	pUC19	extracellular	2686	*E. coli* AB2480	transformation activity	1 μg/mL		2 mM PBS; pH 7	N.A. (too fast)				
blt		chromosome		extracellular			gene damage (by qPCR)	1 ng/μL	266	10 mM PBS;pH 7	$5.9 (\pm 0.8)\times10^{10}$	second order	$> 2.6\times10^{-11}$(0.8-$\log_{10}$)		He *et al.*, 2019
blt		chromosome		extracellular			gene damage (by qPCR)	1 ng/μL	832	10 mM PBS;pH 7	$1.9 (\pm 0.2)\times10^{11}$	second order	2.1×10^{-11}		
blt		chromosome		extracellular			gene damage (by qPCR)	1 ng/μL	870	10 mM PBSpH 7	$2.0 (\pm 0.2)\times10^{11}$	second order	2.1×10^{-11}		

blt		chromosome		extracellular			gene damage (by qPCR)	1 ng/µL	1017	10 mM PBS;pH 7	2.3 (± 0.3) ×10^{11}	second order	1.8×10^{-11}		
blt		chromosome		extracellular		*Bacillus subtilis* 1A189	transformation activity	1 ng/µL		10 mM PBS;pH 7			> 6.5 ×10^{-12} (1.7-$\log_{10}$)		
				intracellular		*Bacillus subtilis* 1A189	culturability	1×10^{6} CFU/mL		10 mM PBS; pH 7					
				intracellular		*Bacillus subtilis* 1A189	transformation activity	1×10^{6} CFU/mL		10 mM PBS; pH 7			> 66 (1.9-$\log_{10}$)		
Chlorine															
$[Cl_2]_0$=20 mg/L															
sul1				intracellular		*Pseudomonas* HLS-6	gene damage (by qPCR)	~1×10^{6} CFU/mL	162	PBS; pH 7	4.08×10^{-2}	first order	38	N.A.	Zhang *et al*., 2019
intl1				intracellular		*Pseudomonas* HLS-6	gene damage (by qPCR)	~1×10^{6} CFU/mL	146	PBS; pH 7	5.67×10^{-2}	first order	27	N.A.	
blt		chromosome		extracellular			gene damage (by qPCR)	1 ng/µL	266	NaOCl; pH 7	3.3 (± 0.3)	second order	100	N.A.	He *et al*., 2019
blt		chromosome		extracellular			gene damage (by qPCR)	1 ng/µL	832	NaOCl; pH 7	7.1 (± 0.4)	second order	70	N.A.	
blt		chromosome		extracellular			gene damage (by qPCR)	1 ng/µL	870	NaOCl; pH 7	6.8 (± 0.4)	second order	67	N.A.	
blt		chromosome		extracellular			gene damage (by qPCR)	1 ng/µL	1017	NaOCl; pH 7	7.7 (± 0.4)	second order	65	N.A.	
blt		chromosome		extracellular		*Bacillus subtilis* 1A189	transformation activity	1 ng/µL		NaOCl; pH 7			> 60 (1.5-$\log_{10}$)	N.A.	
blt		chromosome		intracellular		*Bacillus subtilis* 1A189	transformation activity	1×10^{6} CFU/mL		NaOCl; pH 7			> 46 (1-$\log_{10}$)	N.A.	
$[Cl_2]_0$=5 mg/L															
ampR	860	plasmid	pUC4k	extracellular	3914	*E. coli* DH5*α*	gene damage (by qPCR)	~1×10^{10} copies/mL	850	2 mM PBS; pH 7	2.1 (± 0.2) ×10^{-1}	fluence-based first order	22	37	Yoon *et al*., 2017
kanR	815	plasmid	pUC4k	extracellular	3914	*E. coli* DH5*α*	gene damage (by qPCR)	~1×10^{10} copies/mL	806	2 mM PBS; pH 7	3.1 (± 0.2) ×10^{-1}	fluence-based first order	28	50	
ampR	860	plasmid	pUC4k	intracellular	3914	*E. coli* DH5*α*	gene damage (by qPCR)	~5×10^{5} CFU/mL	850	2 mM PBS; pH 7	1.0 (± 0.1) ×10^{-1}	fluence-based first order	21	67	
kanR	815	plasmid	pUC4k	intracellular	3914	*E. coli* DH5*α*	gene damage (by qPCR)	~5×10^{5} CFU/mL	806	2 mM PBS; pH 7	1.0 (± 0.1) ×10^{-1}	fluence-based first order	26	72	

ampR	860	plasmid	pUC4k	extracellular	3914	*E. coli* DH5α	gene damage (by qPCR)	~1×10^{10} copies/mL	850	2 mM PBS; pH 8	7.4 (± 0.1) $\times10^{-2}$	fluence-based first order	89	152
kanR	815	plasmid	pUC4k	extracellular	3914	*E. coli* DH5α	gene damage (by qPCR)	~1×10^{10} copies/mL	806	2 mM PBS; pH 8	2.7 (± 0.2) $\times10^{-2}$	fluence-based first order	205	376
ampR	860	plasmid	pUC4k	intracellular	3914	*E. coli* DH5α	gene damage (by qPCR)	~5×10^{5} CFU/mL	850	2 mM PBS; pH 8	9.0 (± 0.7) $\times10^{-2}$	fluence-based first order	41	92
kanR	815	plasmid	pUC4k	intracellular	3914	*E. coli* DH5α	gene damage (by qPCR)	~5×10^{5} CFU/mL	806	2 mM PBS; pH 8	1.0 (± 0.2) $\times10^{-1}$	fluence-based first order	35	81
ampR and *kanR*		plasmid	pUC4k			*E. coli* DH5α	culturability (selective agar)	~5×10^{5} CFU/mL		2 mM PBS; pH 7	8.7 (± 0.9)	fluence-based first order	0.05	0.11
ampR	860	plasmid	pUC4k	extracellular	3914	*E. coli* DH5α	gene damage (by qPCR)	~1×10^{10} copies/mL	850	municiple wastewater effluent; pH 7	~300	fluence-based first order		Generally, 20 mg/L of chlorine dose was required (1 h duration)
kanR	815	plasmid	pUC4k	extracellular	3914	*E. coli* DH5α	gene damage (by qPCR)	~1×10^{10} copies/mL	806	municiple wastewater effluent; pH 7	~300	fluence-based first order		Generally, 20 mg/L of chlorine dose was required (1 h duration)
ampR	860	plasmid	pUC4k	intracellular	3914	*E. coli* DH5α	gene damage (by qPCR)	~5×10^{5} CFU/mL	850	municiple wastewater effluent; pH 7	~120	fluence-based first order		Generally, 20 mg/L of chlorine dose was required (1 h duration)
kanR	815	plasmid	pUC4k	intracellular	3914	*E. coli* DH5α	gene damage (by qPCR)	~5×10^{5} CFU/mL	806	municiple wastewater effluent; pH 7	~120	fluence-based first order		Generally, 20 mg/L of chlorine dose was required (1 h duration)

when the required dose for 2-log or 4-log removal falls off the linear regression data range, the data most nearby is reported.

Chapter 3

ELECTROCHEMICAL CELL LYSIS OF GRAM-POSITIVE AND GRAM-NEGATIVE BACTERIA: DNA EXTRACTION FROM ENVIRONMENTAL WATER SAMPLES

Wang, S., Zhu, Y., Yang, Y., Li, J., Hoffmann, M. R. (2020). Electrochemical cell lysis of gram-positive and gram-negative bacteria: DNA extraction from environmental water samples. In: *Electrochimica Acta*, 2020, 338, 135864.

Abstract

Cell lysis is an essential step for the nucleic acid-based surveillance of bacteriological water quality. Recently, electrochemical cell lysis (ECL), which is based on the local generation of hydroxide at a cathode surface, has been reported to be a rapid and reagent-free method for cell lysis. Herein, we describe the development of a milliliter-output ECL device and its performance characterization with respect to the DNA extraction efficiency for gram-negative bacteria (*Escherichia coli* and *Salmonella* Typhi) and gram-positive bacteria (*Enterococcus durans* and *Bacillus subtilis*). Both gram-negative and gram-positive bacteria were successfully lysed within a short but optimal duration of 1 min at a low voltage of ~5 V. The ECL method described herein, is demonstrated to be applicable to various environmental water sample types, including pond water, treated wastewater, and untreated wastewater with DNA extraction efficiencies similar to a commercial DNA extraction kit. The ECL system outperformed homogeneous chemical lysis in terms of reaction times and DNA extraction efficiencies, due in part to the high pH generated at the cathode surface, which was predicted by simulations of the hydroxide transport in the cathodic chamber. Our work indicates that the ECL method for DNA extraction is rapid, simplified, and low-cost with no need for complex instrumentation. It has demonstrable potential as a prelude to PCR analyses of waterborne bacteria in the field, especially for the gram-negative ones.

3.1 Introduction

During water electrolysis, the micro-environment at the electrode/electrolyte interface has different properties compared to that of the bulk electrolyte. The cathodic proton reduction to

hydrogen significantly increases the pH at the surface of cathode. This mechanism plays important roles in various physio-chemical processes, such as NH_3 stripping (Zhang *et al*., 2018), phosphate recovery (Cid *et al*., 2018), and enhanced CO_2 reduction (Ahangari *et al*., 2019). However, the application of this mechanism in biomolecular analysis, especially the detection of waterborne bacteria, was relatively less explored.

In recent years, the application of biomolecular techniques such as the polymerase chain reaction (PCR) has resulted in rapid, accurate, and sensitive methods for the quantification of waterborne bacteria (Xie *et al*., 2016; Heid *et al*., 1996; Kim *et al*., 2013). The initial step before actual PCR analysis is cell lysis for the extraction of nucleic acids. One of the most common cell lysis techniques for microbial quantification is chemical lysis, which employs an alkaline buffer or other lytic reagents to disrupt cell walls. This technique requires an array of essential instruments and multi-step reagent additions which are time-consuming and labor-intensive. In addition, removal of the reagents after cell lysis is required in order to avoid interference with downstream detection (Di Carlo *et al*., 2005; Lee *et al*., 2010). Electroporation uses the sharp potential gradient to break down cell membrane. It is fast and agent-free, and it is able to leave intracellular components intact (Jaikla *et al*., 2012; Tsong, 1991; Lu *et al*., 2005; Geng and Lu, 2013; Shahini and Yeow, 2013; Poudineh *et al*., 2014; Gabardo *et al*., 2015; de Lange *et al*., 2016; Experton *et al*., 2016; Sedgwick *et al*., 2008). The downside of electroporation, however, is the use of high electric fields to achieve irreversible electroporation (*e.g.*, 10 kV/cm reported by Poudineh *et al*. in 2014). High power and voltage required to generate the high electric field, also leads to joule heating of the fluid (Poudineh *et al*., 2014; Kotnik *et al*., 2015; Pliquett, 2003; Davalos and Rubinsky, 2008; Gao *et al*., 2004). Lower electroporation voltages can be realized using nano-structured electrodes coupled with microfluidic devices. However, this approach would require a complicated fabrication process and precise operation (Lu *et al*., 2005; Shahini and Yeow , 2013; Poudineh *et al*., 2014; Gabardo *et al*., 2015; Experton *et al*., 2016; Nan *et al*., 2014; Shehadul Islam *et al*., 2017; Graham *et al*., 2011).

Electrochemical cell lysis (ECL) relies on the cathodically generated hydroxide (*i.e.*, localized high pH) to disrupt microbial cell membranes by breaking fatty acid-glycerol ester bonds in phospholipids (Di Carlo *et al*., 2005; Nevill *et al*., 2007). In contrast to high-voltage electroporation, *e.g.*, 500 V (Wang *et al*., 2006), ECL requires significantly lower voltages, *e.g.*,

2-5 V (Di Carlo *et al*., 2005; Lee *et al*., 2010; Nevill *et al*., 2007; Jha *et al*., 2011, 2012), which avoids joule heating, and thereby, can be easily applied under source-limited conditions encountered in remote field sampling locations. However, we note that the aforementioned studies of ECL were mainly focused on clinical samples, *e.g.*, human cells, and conducted in well-controlled systems with purified buffers (summarized in Table 3.1 of Section 3.6.4). Furthermore, all of these studies highlighted in the development of micro-scale devices with microliter or even nanoliter throughput. It is important to understand if ECL can be used for other target cells with more common throughput that are related to more extensive applications, *e.g.,* environment, food and agriculture, *etc*.

Herein, we now report on the development and application of an ECL device that functions using a small sample volume (~1 mL). Our overarching goal is to determine the DNA extraction efficiencies as a function of the key operational parameters (*i.e.*, pH ranges with varied treatment durations) for the use of ECL, as applied to DNA extraction and PCR amplification of gram-positive and gram-negative bacteria in real surface water and wastewater.

3.2 Experimental

3.2.1 Reagents

Sodium sulfate (Na_2SO_4) was purchased from EMD Millipore Corporation (Germany). Hydrochloric acid (HCl) and sodium hydroxide (NaOH) were purchased from Sigma-Aldrich (USA). 50 mM Na_2SO_4, HCl with varied concentrations (0.1 mM, 1 mM, 10 mM, 100 mM, and 1 M) and NaOH with varied concentrations (0.1 mM, 1 mM, 10 mM, 100 mM, and 1 M) were prepared using ≥ 18 MΩ Milli-Q water produced from a Millipore system (Millipore Co., USA). PBS (Gibco™, 1X, pH 7.2) was purchased from Thermo Fisher Scientific (USA). Luria-Bertani (LB) Broth, Tryptic Soy Broth (TSB), Brain Heart Infusion (BHI) Broth, and Nutrient Broth (NB) were purchased from Becton, Dickinson and Company (USA). Nuclease-free water for PCR was purchased from Promega Corporation (USA).

3.2.2 Bacterial Sample Preparation

The gram-negative bacteria species, *Escherichia coli* (ATCC 10798, *E. coli*), *Salmonella* Typhi (ATCC CVD909, *S.* Typhi), and gram-positive bacteria species, *Bacillus subtilis* (ATCC 6051, *B.*

subtilis) and *Enterococcus durans* (ATCC 6056, *E. durans*) were cultivated at 200 rpm (Innova 42 Incubator Shaker, New Brunswick Scientific, USA) for 12-14 hrs to log-phase growth at the optical density at λ = 600 nm (OD_{600}) of 0.6-1.0. *E. coli, S.* Typhi, and *E. durans* were grown at 37 ^{o}C in LB, TSB and BHI media, respectively. *Bacillus* was grown at 30 ^{o}C in NB media. After incubation, the bacterial cells were harvested by centrifugation (Eppendorf, Germany) at 5000 rpm, washed twice and resuspended in 50 mM Na_2SO_4 to a concentration of ~10^8 cells/mL (estimated by OD_{600} values).

3.2.3 Electrochemical Cell Lysis Experiment

The ECL device consists of a dimensionally stable IrO_2/Ti anode (synthesis was reported previously by Yang *et al*. in 2016), a Ti cathode, and a cation exchange membrane (Nafion 117, Dupont, USA), as shown in Figure 3.1a. The reactor was made of polycarbonate, and a photograph of the ECL device is also shown in Figure 3.2. The mechanism on the breakdown of microbial cell membrane by ECL is illustrated in Figure 3.1b and Figure 3.1c. The membrane separates the device into an anodic chamber (1.6 mL) and a cathodic chamber (0.8 mL). One outlet was added on the top of each chamber to enable gas ventilation. For ECL reactions, 50 mM Na_2SO_4 and bacterial suspensions were injected from the bottom into the anodic and cathodic chamber, respectively, using syringes. A constant direct current of 40 mA (16 mA/cm^2, Potentiostat, BioLogic Science Instruments, France) was applied for 30 s -10 min. The cathodic effluents were collected, using syringes after each reaction, and the chambers were washed three times with DI water between each reaction. The pH values were measured for all cathodic effluents and initial samples with a pH meter (Orion Star A215, Thermo Fisher Scientific, USA) with a semi-micro pH probe (Orion 9110DJWP, Thermo Fisher Scientific, USA).

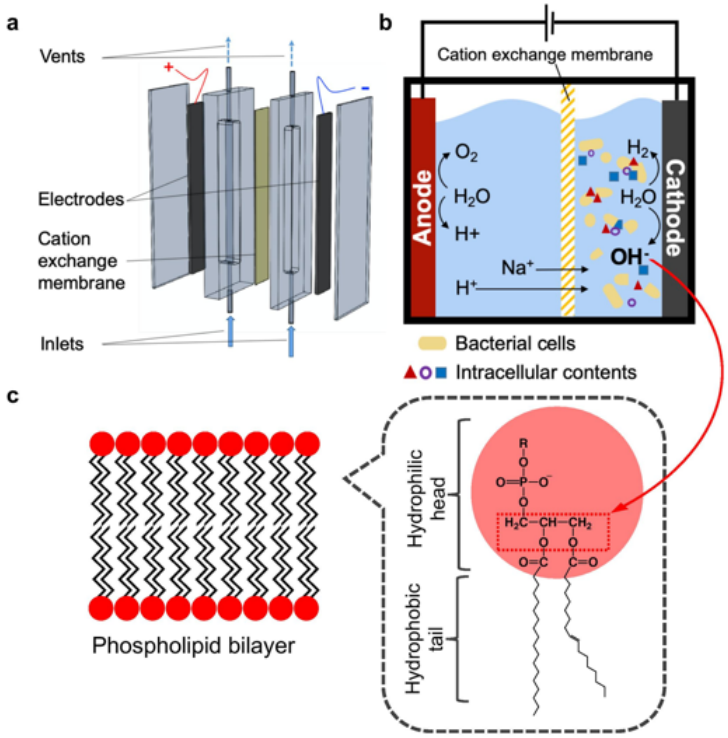

Figure 3.1: Device and mechanism of electrochemical cell lysis. (a) Electrochemical cell lysis device. (b) Schematics of electrochemical cell lysis with cation exchange membrane between anodic and cathodic chambers. (c) Phospholipid bilayer, the major component of bacterial cell membranes, and the chemical structure of phospholipids. The fatty acid-glycerol ester bonds in phospholipids (highlighted in red box) can be hydrolyzed by the locally generated OH^- at cathode.

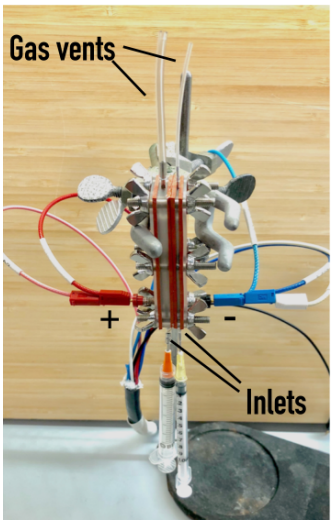

Figure 3.2: The photograph of electrochemical cell lysis (ECL) device.

3.2.4 Analysis of Cell Lysis by Fluorescent Microscope

Following ECL reaction, a 500 µL aliquot of each bacterial sample was harvested by centrifugation at 10,000g for 10 min at 20 °C. The resulting pellets were then washed with PBS three times and resuspended in PBS to a final volume of 500 µL. The Live/Dead Baclight Viability kit (Invitrogen by Thermo Fisher Scientific, USA) was used for bacterial staining. Two staining dyes are included in this kit, the green-fluorescent nucleic acid stain Syto9, which stains both live and dead cells, and the red-fluorescent nucleic acid stain propidium iodide (PI), which can penetrate and stain only dead cells due to their compromised membrane (Boulos *et al*., 1999). The viability of bacterial cells was monitored by these two dyes. PI-staining of dead cells does not indicate the complete rupture of cell membranes, but merely their permeability for PI. Since completely lysed cells cannot be stained by Syto9, the extent of cellular lysis was measured by counting cells stained by Syto9 before and after ECL, as shown in the Eq. (3.1) below:

$$Lysis\ efficiency\ (\%) = \frac{N_{total\ cells\ in\ initial\ sample} - N_{total\ cells\ in\ ECL\ sample}}{N_{total\ cells\ in\ initial\ sample}} \times 100 \qquad (3.1)$$

where N is the counted number of the cells that stained by Syto9. According to the manufacturer's instruction, equal volumes (1.5 µL) of Syto9 (0.33 mM) and PI (2 mM) were added into each 100 µL sample. Each stained sample was added onto a glass slide with cover and examined under a fluorescence microscope (Leica DMi8, Germany). An objective with ×20 magnification was used for analyses. Five images were randomly taken from different areas on each slide and counted by ImageJ software (National Institute of Health, USA).

3.2.5 DNA Quantification by qPCR

To measure the DNA released by ECL, the suspended DNA was collected from the supernatant of each sample by centrifugation at 10,000g for 10 min. As a negative control, an aliquot of the initial sample without ECL was treated in the same way to remove all the cells. Another aliquot of the initial sample was extracted for each bacterial strain using a commercial DNA extraction kit (PureLink® Genomic DNA Mini Kit, Invitrogen by Thermo Fisher Scientific, USA) as a positive control. Real-time PCR (qPCR, MasterCycler RealPlex 4, Eppendorf, USA) was used to quantify the presence of the universal bacterial 16S rRNA gene and to analyze DNA extraction efficiency

for all the above samples. Each sample was tested in triplicates, using a similar protocol as reported previously (Xie *et al*., 2016; Zhu *et al*., 2018). The protocol will be also briefly described in Section 3.6.1, along with other necessary information for qPCR quantification including amplification curves, qPCR standard curves and PCR efficiencies. The cycle numbers above the background fluorescence threshold (C_T) were directly measured and analyzed after PCR reaction, using instrument specific software (Eppendorf, USA). The higher the DNA concentration in the template, the lower the C_T value because the background threshold can be reached with less cycles of PCR amplification. To evaluate the DNA extraction efficiency, ΔC_T values of the ECL treated samples were calculated by subtracting C_T values of the suspended DNA in the ECL treated samples from those in the untreated ones. With a comparison, ΔC_T values of the samples extracted by the commercial kit were calculated similarly, by subtracting C_T values of the total DNA extracted by the commercial kit from those of the suspended DNA in the untreated samples. For each bacterial strain, the higher ΔC_T values were expected for higher DNA extraction efficiency.

3.2.6 pH Effect Tests

The investigation of pH effects on cell lysis was conducted for one gram-negative bacterial species (*E. coli*) and one gram-positive species (*E. durans*) without ECL reaction. *E. coli* and *E. durans* were cultivated as described above. Then, several aliquots of 1 mL bacteria suspensions were harvested by centrifugation at 5000 rpm to obtain pellets. After removal of the culture media, 500 µL of NaOH with different concentrations (0.1 mM, 1 mM, 10 mM, 100 mM, and 1 M) were directly added to the cell pellets, respectively, and resuspended immediately. As a negative control, 1 mL of 50 mM Na_2SO_4 was added to the cell pellets of initial samples for both species and mixed well. 500 µL of HCl with varied concentrations (0.1 mM, 1 mM, 10 mM, 100 mM, and 1 M) were then added to neutralize the alkaline samples, correspondingly, after different sample contact times with alkaline solution (30 s, 1 min, 2 min, 5 min and 10 min). All the neutralized samples were centrifuged at 10,000g for 10 min to remove all the intact cells. The supernatants were then purified by the PureLink® Genomic DNA Mini Kit. An aliquot of the control was extracted by the same commercial DNA extraction kit as a comparison. Another aliquot was treated the same as other samples after alkaline lysis. Then all the purified samples were quantified by qPCR, and ΔC_T values were calculated with the same methods described in the Section 3.2.5.

3.2.7 Electrochemical Cell Lysis of Bacteria in Environmental Water Samples

Three different environmental water samples were tested to evaluate the performance of the ECL technique on DNA extraction of bacteria from ambient environmental water. Pond water was collected from the turtle pond on Caltech campus (Pasadena, CA). The treated and untreated latrine wastewater was collected from a previously described solar-powered recycling electrochemical toilet system located at Caltech with 550 mg/L of chemical oxygen demand (COD) and 28 mM NH_4^+ as major pollutants (Yang and Hoffmann, 2016; Jasper *et al*., 2017). The latrine wastewater was treated by an electrochemical oxidation process to remove >90% of NH_4^+ and COD. Effluent was collected and denoted as "treated water" in this study. Pond water was directly added into the cathodic chamber for ECL reaction, without any pretreatment while 50 mM Na_2SO_4 was added into the anodic chamber. Both types of wastewater samples were first filtered, using sterilized filter papers with 8.0 μm pore size (diameter, 55 mm; Cat No., 1002 055; Whatman) to remove big particles and to enhance the reproducibility between each experiment. Then, the filtered wastewater was added into cathodic chamber for ECL reaction while 50 mM Na_2SO_4 was added into the anodic chamber. The suspended DNA of total bacteria from all the environmental water samples were then collected by centrifugation at 10,000g for 10 min. All the above environmental water samples were also extracted by the same commercial DNA extraction kit (PureLink® Genomic DNA Mini Kit) as the positive control. The same qPCR method was used for DNA quantification and evaluation of DNA extraction efficiency.

3.3 Theory and Simulations

COMSOL Multiphysics (COMSOL Inc., USA), a commercial finite element modeling software, was used to study the fate and transport of hydroxide ions inside the cathodic chamber. The fluid in the cathodic chamber was modeled as a 3 × 5 × 50 mm^3 block, with the electrode surface and the cation exchange membrane represented by the two 5 × 50 mm^2 sides. The gas vent hole on the top was represented by a cylindrical extrusion with a diameter of 1 mm and a height of 0.1 mm. OH^- and H^+ are generated with the hydrogen and oxygen evolution reactions at the cathode and anode, respectively:

$$\text{anode: } 2H_2O \leftrightarrow 4H^+ + 4e^- + O_2 \tag{3.2}$$

$$\text{cathode: } 4H_2O + 4e^- \leftrightarrow 4OH^- + 2H_2 \quad (3.3)$$

The generation and venting of H_2 during electrolysis induces fluid movements in the cathodic chamber. The resulting flow field was first calculated, and then, the convective and diffusive OH^- transport was simulated. Molar influx of H_2 gas at the cathode surface was theoretically half of the OH^- generation rate R_{in}^{cat}, which was calculated by (Bard *et al*., 1980):

$$R_{in}^{cat} = \frac{i}{nFA} \quad (3.4)$$

where i is the supplied current (40 mA), n is the number of electrons used to generate a hydroxide ion, which is 1, F is the Faraday constant, and A is the surface area. Simultaneously, H^+ was produced at the anode surface at the same rate as OH^- was generated, and cations were forced across the cation exchange membrane. It was assumed that sodium ions were the dominant species transported across the membrane due to their concentration dominance over protons, until sodium ions were depleted to a concentration comparable to the protons; at this point, protons were the preferred ions for membrane transport due to their smaller size. For the cathodic chamber, the influx of H^+ was considered as the sink of OH^- and the contribution of water dissociation was negligible to mass transfer trough the membrane (Simons, 1979; Krol *et al*., 1999; Tanaka *et al*., 2012). With the initial pH set at 7.5, time-dependent OH^- concentration profiles were simulated over the whole geometry. The transient pH profiles of the vertical mid-plane across the electrode and the membrane were generated, while the bulk solution pH was estimated from the volume average of $[OH^-]$. More details on the modules and equations used in this simulation will described in Section 3.6.2.

3.4 Results and Discussion

3.4.1 Electrochemical Cell Lysis of Different Bacteria

Four different bacteria, *E. coli*, *S.* Typhi, *B. subtilis*, and *E. durans*, with the initial concentrations of approximately 10^8 cells/mL, were effectively lysed using the ECL method at different durations. ΔC_T values of four different bacteria treated by ECL with 30 s-10 min are shown in Figure 3.3, along with a comparison of those extracted by the commercial kit. After 30 s of ECL, the averaged

ΔC_T values of all the bacterial strains were significantly increased to 3.6-8.1. The highest ΔC_T values of the ECL treated bacterial samples all lay in the duration of 1 min as the optimized ECL condition, with the range of 6.5-9.8. In general, the DNA extraction efficiencies of all the bacterial cells decreases after 2 min of ECL. This could be mainly due to DNA damage during the ECL process (*e.g.*, the local high pH which will be further discussed later with simulation in this study), as we preclude PCR inhibition caused by electrolyzed cathodic effluents. The details will be discussed in Section 3.6.3. The pH of the catholyte increased rapidly from the average of 7.4 (± 0.2) to 12.5 (± 0.1) after 1 min of ECL, which is consistent with the increase of ΔC_T values. It confirms that the generation of OH^- at cathode is the mechanism of ECL. All the PCR mixtures containing cathodic effluents (after ECL) were able to be adjusted to a pH range of 8.4-8.7 by the PCR reagents prior to qPCR measurements. Thus, no additional neutralization step was necessary before detection. The optimized ECL duration of 1 min is much faster than most of the commercial DNA extraction kits based on chemical lysis (*e.g.*, at least 30 min for lysis step with the PureLink® Genomic DNA Mini Kit following the manufacturer instruction by Invitrogen by Life Technologies, 2012). The optimal processing time by ECL is also faster than the typical processing time of 5-30 min by the bead beating method, when using a flat pad vortex mixer, which is the least expensive bead beating technique (van Burik *et al*., 1998; Ho *et al*., 2008). In addition, the required voltage input is *ca.* 5 V, which is ~10-1000-fold lower than that of electrical lysis, reported previously (Experton *et al*., 2016; Lee and Cho, 2007; Bahi *et al*., 2010; Haberl *et al*., 2013).

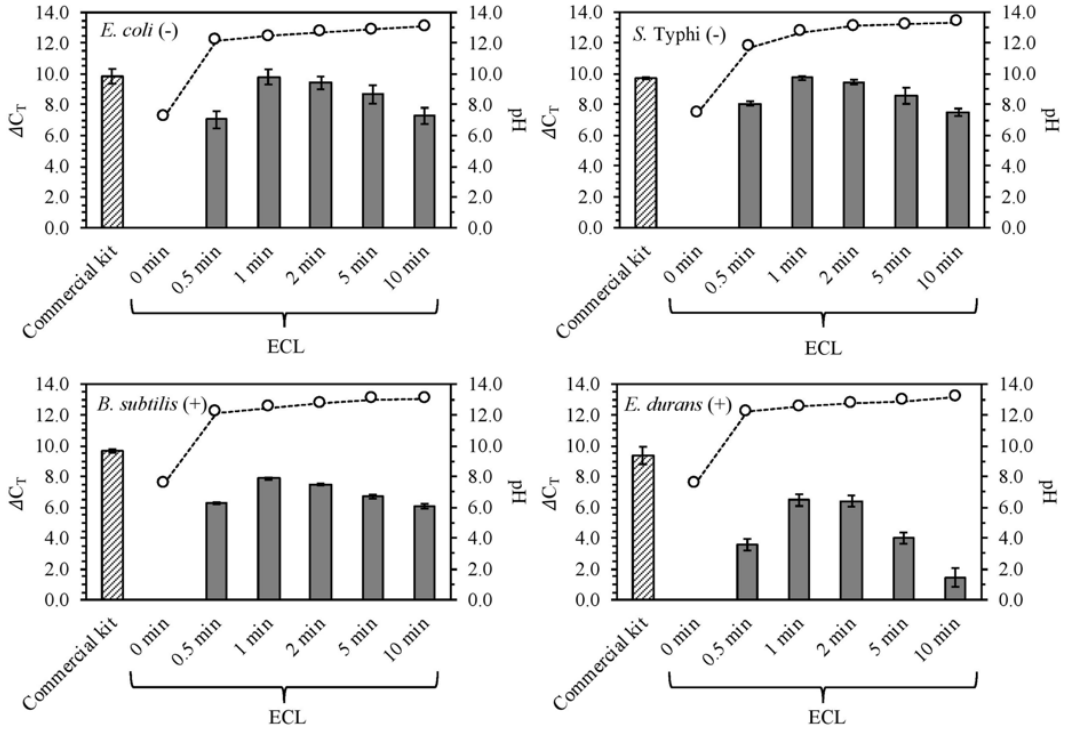

Figure 3.3: ΔC_T values of 4 different bacterial cells lysed by ECL as a function of times (▬) and of those extracted by a commercial DNA extraction kit (▨) as a comparison; and the average pH values measured in the cathodic effluents (-o-). For the ECL-treated samples, ΔC_T values were calculated by subtracting C_T values of the suspended DNA in ECL treated samples from those in the untreated samples. For the samples extracted by the commercial kit, ΔC_T values were calculated by subtracting C_T values of the total DNA extracted by the commercial kit from those of the suspended DNA in the untreated samples.

DNA extraction by ECL was especially efficient for the two gram-negative bacterial strains. The averaged ΔC_T values increased to 9.8 and 9.7 with 1 min of ECL for *E. coli* and *S.* Typhi, respectively. There is no significant difference between the ΔC_T values of the samples treated by 1 min of ECL and of those extracted by the commercial kit ($P = 0.72$ for *E. coli* and $P = 0.48$ for *S.* Typhi). Lower DNA extraction efficiencies were observed for the two gram-positive bacterial strains with the optimized 1 min of ECL. Compared to the samples extracted by the commercial kit, the differences of ΔC_T values ($= \Delta C_{T,\text{ commercial kit}} - \Delta C_{T,\text{ 1 min of ECL}}$) are 1.8 and 2.9 for *B. subtilis* and *E. durans*, respectively. However, the ΔC_T values after 1 min of ECL were still increased significantly to 7.9 and 6.5 for *B. subtilis* and *E. durans*, respectively, which was sufficient for

downstream qPCR detection in this study. The lower lysis efficiency for gram-positive bacteria than for gram-negative bacteria was not only observed by using ECL in our present study, but also by other lysis methods reported previously. For example, a lysis method based on cold atmospheric-pressure plasma was reported to have only 0.6 $\log_{10}$ reduction for *B. subtilis* after 10 min treatment, while 3.3-3.6 $\log_{10}$ reduction for other three gram-negative bacteria with the same treatment duration (Mai-Prochnow *et al*., 2016). And 10-100 times higher detection limits were determined for gram-positive bacteria than for gram-negative bacteria by applying a hybrid chemical/mechanical lysis method on a microfluidic chip (Mahalanabis *et al*., 2009). The differences in DNA extraction efficiency between the gram-positive and gram-negative bacteria can be explained by their different cell wall structures. The cell walls of gram-negative bacteria are composed of phospholipid bilayers (*i.e.*, cell membranes) that can be readily hydrolyzed by hydroxide ions, while the cell walls of the gram-positive bacteria are predominantly composed of multilayers of peptidoglycan, which provide stronger protection for gram-positive bacteria (Bruslind, 2018; Ghuysen and Hakenbeck, 1994; Hammond *et al*., 2012). In addition, the cell wall thickness of gram-positive bacteria, *e.g.*, ~55.4 nm for *B. subtilis* (Matias and Beveridge, 2005; Hayhurst *et al*., 2008; Vollmer *et al*., 2008), is generally much higher than that of gram-negative bacteria as well, *e.g*., ~8.2 nm for *Enterobacter cloacae* (Coward and Rosenkranz, 1975; Eumkeb and Chukrathok, 2013).

The successful cell lysis by ECL was further confirmed for all the bacteria via fluorescence microscopy. The fluorescence images visualizing the bacteria viability with ECL treatment, monitored by PI (in red) and Syto9 (in green), are shown for *E. coli* as an example in Figure 3.4. It was observed clearly that cells were completely lysed by ECL after the cell death. Because the number of dead cells (in red) significantly increased after only 30 s of ECL, but reduced after 1 min. So did most of the total intact cells (in green) disappear after 1 min, which is an evidence for complete cell wall breakdown. The images in fluorescent green also show that the number of total intact cells decreased significantly after 30 s of ECL and only a few can be observed after 1 min, which has an agreement with the increase of ΔC_T values measured by qPCR. The cell numbers for both live and dead cells were calculated for all the bacteria with different ECL durations and are shown in Figure 3.5. For gram-negative bacteria, the lysis efficiencies are close to 100% after 2

min of ECL, while efficiencies over 50% for both of the gram-positive bacteria were obtained after 5 min. The lysis efficiencies keep increasing over time until an apparent equilibrium is achieved. Apparently, the cell number measurement by fluorescent microscope showed the efficient performance of ECL on cell lysis more straightforwardly, due to the absence of complex factors related to DNA detection, *e.g.*, potential DNA damage after release from cells and PCR inhibition.

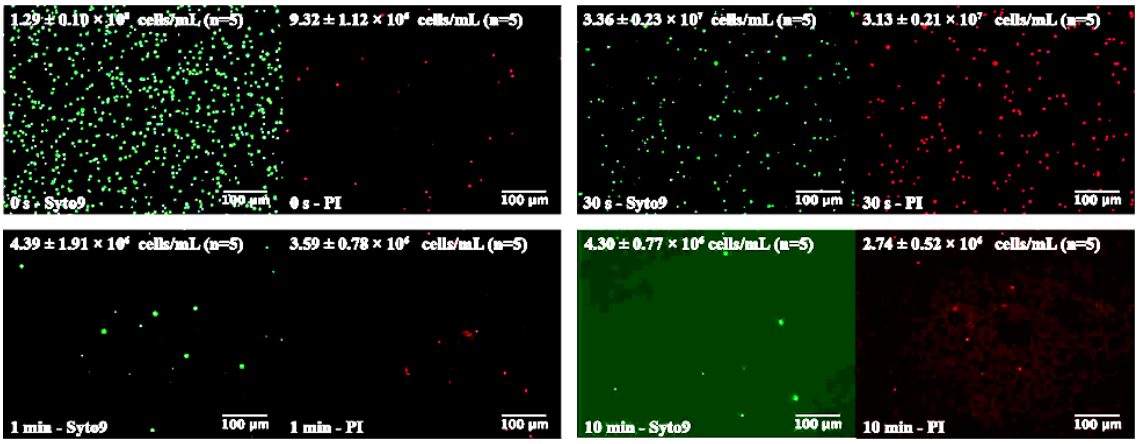

Figure 3.4: Fluorescent microscope images of *E. coli* cells stained by Syto9 (green) and PI (red) with different durations of ECL.

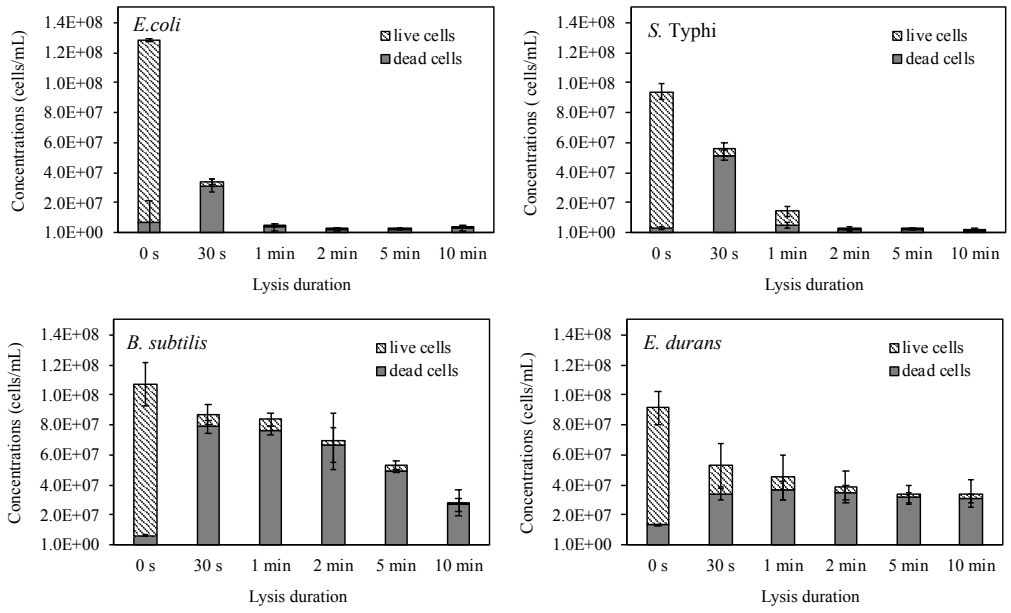

Figure 3.5: The cell concentrations of 4 different bacteria in control and electrochemical lysed samples with the measurement by fluorescence image counting.

3.4.2 pH Effects on Cell Lysis and DNA Extraction

To further understand how pH affects cell lysis and DNA extraction, bacterial cells were treated by homogeneous alkaline lytic reagent at various pH values, *i.e.*, NaOH with varied concentrations of 0.1 mM – 1 M, without ECL. *E. coli* and *E. durans* were selected as models for gram-negative and gram-positive bacteria, respectively. Homogeneous alkaline lysis is not efficient for *E. durans* at all investigated pH values (10 to 14). The ΔC_T values of *E. durans* treated by NaOH were all lower than 3.0 (data not shown), while those extracted by the commercial kit were 11.6 as an average. The ΔC_T values of *E. coli* cells treated by NaOH at varied pH from 10 to 14 as a function of contact times, are shown in Figure 2.6. *E. coli* cells were barely lysed at pH 10 with ΔC_T values close to 0, while higher DNA extraction efficiency was observed at pH 11 with ΔC_T values around 2. Among all the conditions, the highest DNA extraction efficiency for *E. coli* cells was achieved at pH 13 with an averaged ΔC_T value of 5.6 at 2 min contact time. However, ΔC_T values decreased at contact times longer than 2 min. When pH increased to an even higher level, *i.e.*, at pH 14, C_T values of NaOH treated cells were even lower than initial samples after 2 min of contact time, although the samples were neutralized after a defined contact time. Consequently, ΔC_T values were negative and cannot be seen in Figure 3.6. This suggests that the DNA might be damaged by high pH conditions above pH 13, which has an agreement with the DNA damage observed in the ECL experiments with longer durations than 2 min. On the other hand, there was no decrease of ΔC_T values observed for NaOH treated *E. coli* cells at pH 12 within contact times of 10 min. The ΔC_T values at pH 12 were quite close to those at pH 13 after 5 min of contact time and even out performed those at pH 13 later on. Therefore, it appears that a pH between 12 and 13 may provide optimal conditions for DNA extraction from bacterial cells; this result is consistent with a previously reported optimal pH range of 11.5-12.5 for cell lysis (Lee *et al*., 2010; Harrison, 1991). Plasmid DNA isolation via alkaline lysis was also previously reported to be most efficient within a pH range of 12.0-12.6 (Birnboim and Doly, 1979; Birnboim, 1983). These values are also in good agreement with the bulk pH (12.47-12.76) measured under optimized conditions during ECL extraction.

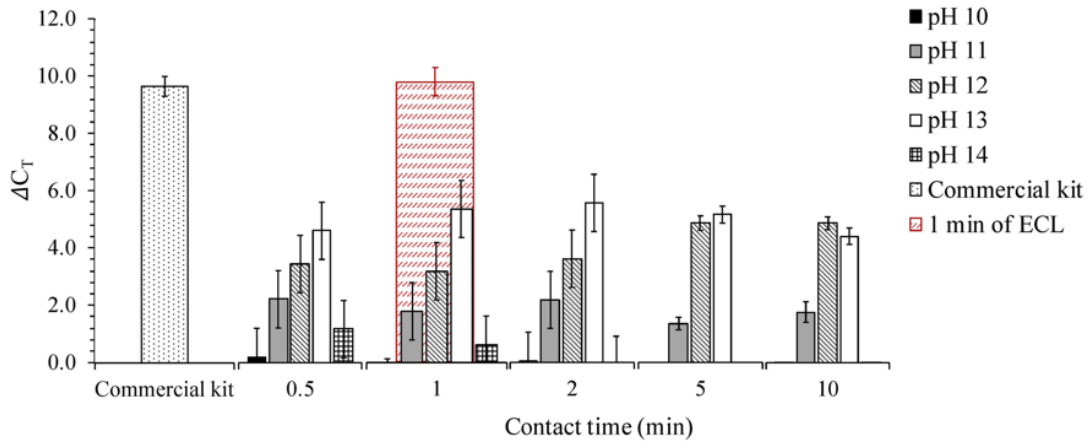

Figure 3.6: ΔC_T values of *E. coli* cells under varied pH conditions as a function of contact times, with comparison of those extracted by the commercial DNA extraction kit and 1 min of ECL.

As a comparison, the highest averaged ΔC_T value achieved by alkaline lysis (pH 13, 2 min) is 4.2 less than of that measured after 1 min of ECL, as highlighted in Figure 4. And *E. coli* cells extracted by the commercial kit in this pH test were detected as similar ΔC_T values (9.7 ± 0.3) to those treated by 1 min of ECL. Besides, ECL is also capable of lysing gram-positive bacteria while conventional alkaline lysis cannot. These results emphasize that the ECL method is faster and much more efficient for DNA extraction from gram-negative and gram-positive bacterial cells, compared to alkaline cell lysis.

3.4.3. Simulations of pH Profiles at the Cathode

To gain more mechanistic insight of the ECL process, pH profiles for the vertical mid-plane of the cathodic chamber were simulated for different contact times and are shown in Figure 3.7a. These simulations show that the local pH value near the cathode surface increases rapidly within 1 min of ECL and that an ideal pH range for cell lysis (pH 12-13) is predicted. After 2 min of ECL operation, the pH in most of the upper volume reaches 13. This simulation is consistent with the DNA loss observed during ECL tests on different bacteria. Hydrogen gas is also generated, as protons are consumed and OH^- is produced at the cathode surface. Gas evolution helps mixing the solution (the calculated flow field is shown in the Figure 3.8), which in turn leads to a larger volume that has a suitable pH for cell lysis after 30 s and 1 min of operation (Figure 3.7a). The simulated pH profiles for the bulk-phase cathodic solutions as a function of time is shown in Figure

3.7b. The simulation results are in line with the measured bulk pH values of the cathodic effluents during different ECL tests. The results also highlight that there is a higher pH at the cathode surface than in the bulk electrolyte. It is speculated that cells were efficiently lysed near the cathode surface. The released DNA molecules with negative charge were likely repelled from the cathode, and subsequently preserved in the bulk electrolyte at a lower pH. This may explain the much more efficient DNA extraction by ECL than that by direct alkaline lysis, which was found in the pH effect tests (*vide supra*). Detailed understanding of this phenomenon awaits further study.

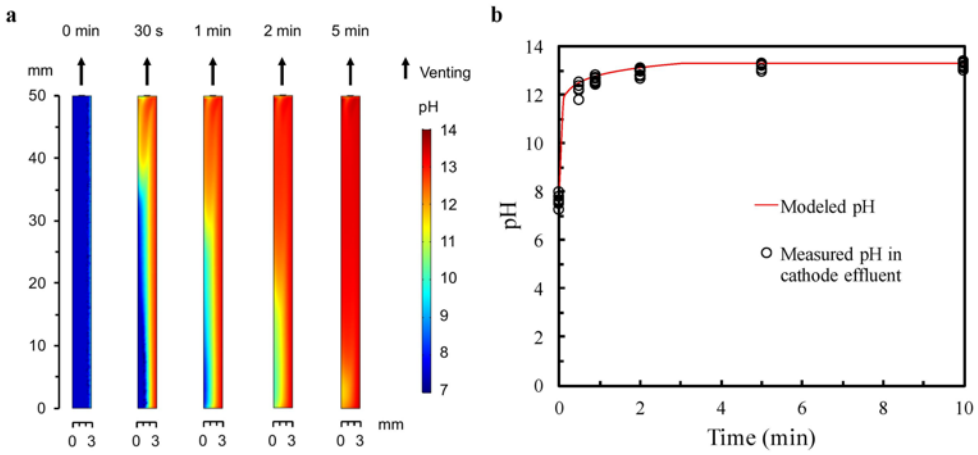

Figure 3.7: Computational simulation results for the distribution of pH in the cathodic ECL chamber and corresponding pH values of cathodic effluents. (a) Simulation of pH value distribution for the vertical mid-plane in the cathodic chamber with the cation exchange membrane on the left and the cathode on the right. (b) Modeled and measured pH for the cathode effluents as a function of electrochemical reaction time.

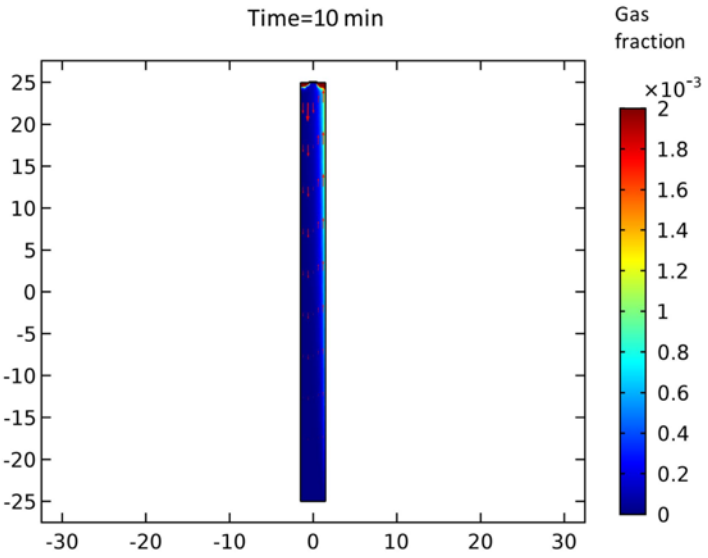

Figure 3.8: Simulated steady-state flow field of the vertical mid-plane across the electrode and the membrane. The gas fraction and velocity field shown in the plot rapidly reached steady-state within 0.1 s, the shortest time step in the simulation. The color surface represents the volume fraction of gas phase. In the superimposed 2D arrow plot of velocity field, it is observed that upward fluid momentum close to the electrode surface (the right edge) was induced by gas motion, and that downward motion on the other side was driven by mass conservation. The fluid in the upper volume was notably accelerated and would boost convective transport of OH^- ions.

3.4.4. Electrochemical Cell Lysis in Environmental Water

Figure 3.9 shows the optimal ΔC_T values of total bacteria in natural pond water, treated and untreated latrine wastewater treated by ECL, with the comparison of those of *E. coli* (~10^8 cells/mL) in 50 mM Na_2SO_4 treated by ECL (*vide supra*). The initial cell concentrations of total bacteria were approximately 8.0×10^5, 3.0×10^6, 2.1×10^7 cells/mL for pond water, treated and untreated wastewater, respectively, as measured by qPCR with the calibration curve of *E. coli* (shown in Figure 3.12 of Section 3.6.1). The optimal DNA extraction efficiency achieved ΔC_T values of 4.4 ± 0.4 for pond water after 1 min of ECL. For the treated and the untreated wastewater samples, the optimal ΔC_T values of 2.6 ± 0.3 and 4.1 ± 0.2 were obtained after 10 min and 15 min of ECL, respectively. These results show that the bacteria in both pond water and wastewater were rapidly and efficiently lysed by ECL with ΔC_T values comparable to those obtained with the commercial kit. The differences of ΔC_T values between ECL and the commercial kit are generally less than 0.3 for different water types. Clearly, the required lysis/extraction times for environmental water

samples are longer than those for pure cell samples reported herein. It could be mainly taken account of the more complex composition in real environmental water samples which has buffer capacity. Therefore, it takes longer reaction time to achieve the ideal pH range for cell lysis in the cathodic chamber. For example, it was reported previously that there was 17 mM of $HCO_3^- + CO_3^{2-}$, 0.6 mM of total phosphate and 13 mM of NH_4^+, with buffer capacity of 0.79, 0.09 and 2.71 mequiv/(L· pH), respectively, for the wastewater collected from the same onsite electrochemical wastewater treatment system as this study (Cid *et al*., 2018). However, the ECL process is still much faster than most of the conventional DNA extraction kits (*vide supra*), additionally with much more simplified operational procedure.

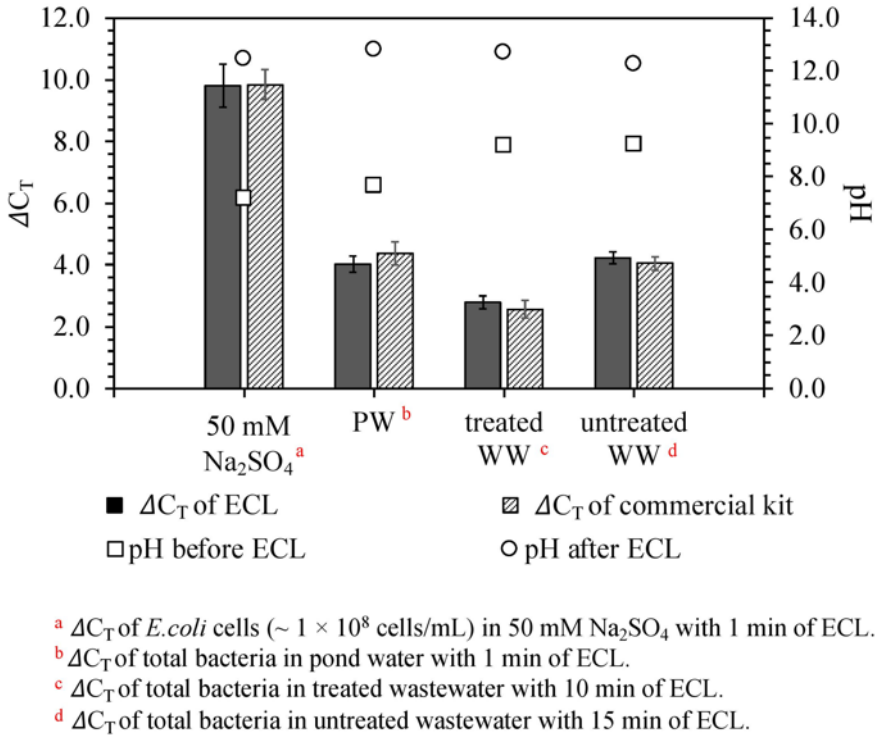

[a] ΔC_T of *E.coli* cells (~ 1×10^8 cells/mL) in 50 mM Na_2SO_4 with 1 min of ECL.
[b] ΔC_T of total bacteria in pond water with 1 min of ECL.
[c] ΔC_T of total bacteria in treated wastewater with 10 min of ECL.
[d] ΔC_T of total bacteria in untreated wastewater with 15 min of ECL.

Figure 3.9: ΔC_T values of bacterial cells in 50 mM Na_2SO_4, pond water (PW), treated wastewater (treated WW) and untreated wastewater (untreated WW) extracted by ECL and the commercial kit.

The optimized DNA extraction efficiencies for the environmental water samples by ECL treatment were in a pH range from 12 to 13. These results suggest that the pH can be used as an indicator to determine the optimal residence time of ECL for DNA extraction in the field. Additionally, in this

study, a centrifugation step (at 10,000g for 10 min) was applied after each ECL reaction because the cell lysis by PCR process needs to be excluded for measuring the DNA extraction efficiency by ECL *per se*. The thermal cycling process of PCR could also cause some of the cells lysed and thereby increased the DNA extraction efficiency. Figure 3.10 shows that the qPCR C_T values are 0.4-1.0 lower for different environmental water samples without any further treatment after the optimized ECL than with the centrifugation step. This result is somewhat counter-intuitive since higher C_T values (lower DNA concentrations) were expected for the samples without post-ECL treatment due to the potential inhibitors in environmental samples. However, any post-treatments after lysis could also cause sample loss, which might explain the lower C_T values (higher DNA concentrations) detected in this study. Therefore, for application of ECL in the field, the centrifugation after ECL might not be necessary. In case that a treatment might be necessary to reduce PCR inhibition, a filtration step with a 0.2 μm syringe filter (13 mm, nylon, Pall Corporation, USA) was also tested after ECL as an alternative post-treatment to centrifugation. Because it is much easier to be realized in the field. Centrifugation and filtration as a post-ECL step resulted in no significant differences of qPCR C_T values (P = 0.62, 0.25 and 0.48 for pond water, treated and untreated wastewater, respectively) for the three different types of environmental water samples (shown in Figure 3.10).

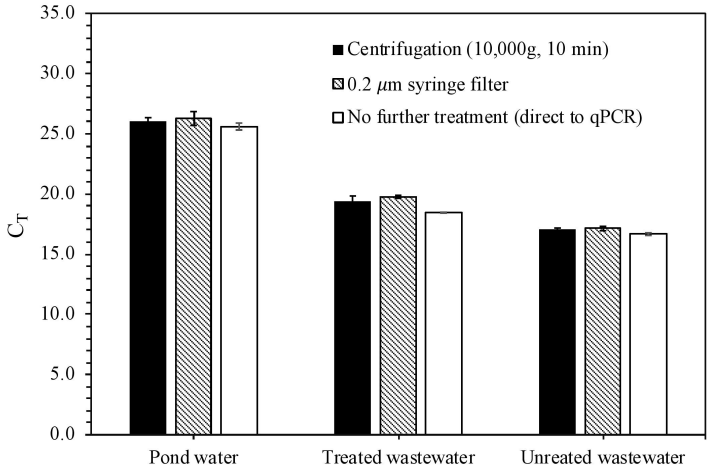

Figure 3.10: The qPCR C_T values of total bacteria in environmental water samples with different post-treatment following the optimized ECL reactions (1 min, 10 min and 15 min for pond water, treated and untreated latrine wastewater, respectively).

3.5 Conclusion

In summary, we developed an ECL device for the rapid extraction of DNA from waterborne bacteria, using low-cost materials. The efficient cell lysis by ECL was demonstrated for both gram-positive and gram-negative bacteria with a short but optimal lysis duration of 1 min, at a constant DC of 40 mA (~5 V of voltage). Extraction by ECL was more efficient and quicker than direct alkaline lysis. The successful application of ECL on different environmental water samples suggests the potential application of ECL as a rapid and reagent-free sample preparation technique with a low voltage requirement for microbial monitoring in the field. In addition, ECL as applied to cell lysis has the potential to significantly reduce the overall cost for nucleic acid-based microbial monitoring. For example, a conventional DNA extraction kit, based on chemical lysis, *e.g.*, PureLink® Genomic DNA Mini Kit, costs approximately $3 per preparation, using the required instrumentation (*e.g.*, centrifuge ($2,000-20,000 provided by Eppendorf) and vortex mixer (>$300 available through VWR)). The bead beating method costs *ca.* $2 per sample prep using 0.1 mm diameter beads (Gene Rite, LLC) and a bead milling instrument with a price range from $300 to $12,000 (MP Biomedicals, LLC website, https://www.mpbio.com/; Biospec Product Inc website, https://biospec.com; OMNI Inc website, https://www.omni-inc.com; Qiagen website, https://www.qiagen.com; Hopkins, 1991). The ECL device developed in this study, on the other hand, can be produced for as little as $4.20 per unit. The estimated total cost includes a) polycarbonate reactor ($0.44), b) an anode ($0.8 for an IrO_2/Ti anode with an estimated lifetime of 4.3 yrs at 25 mA/cm^2, as reported previously by Yang *et al.*, 2016), c) $0.54 for the Ti-cathode and, d) a cation exchange membrane ($2.42 for Nafion 117 with estimated lifetime of > 60,000 hrs, Rozière and Jones, 2003; Cheng *et al.*, 2006). For field sampling, the ECL device E

3.6 Supporting Information

3.6.1 Detailed Methods and Information of qPCR Measurements

Real-time PCR (qPCR, MasterCycler RealPlex 4, Eppendorf, USA) was used to quantify the universal bacterial 16S rRNA gene. Each 20 µL reaction mixture contains 2 µL of sample, 10 µL of PerfeCTa® qPCR ToughMix® (Quanta BioSciences Inc.), 0.25 µM of both forward (1369F, 5′CGG TGA ATA CGT TCY CGG3′, where Y is either C or T, Integrated DNA Technologies Inc., USA) and reverse primers (1492R, 5′GGW TAC CTT GTT ACG ACT T3′, where W is either

A or T, Integrated DNA Technologies Inc., USA) and 0.25 μM of TaqMan probe (FAM-5′CTT GTA CAC ACC GCC CGT C3′, Integrated DNA Technologies Inc., USA). The thermal cycling was 3 min at 95 °C followed by 40 cycles of 15 s at 95 °C for denaturation and 30 s at 55 °C for annealing/extension. The PCR amplification curves are shown as an example in Figure 3.11. A non-template control (NTC) was set up with each qPCR test. The average C_T values for all the NTCs were 35.8 (± 0.50, n=9), which meets the requirement suggested by the EPA protocol "Method B: *Bacteroidales* in Water by TaqMan® Quantitative Polymerase Chain Reaction (qPCR) Assay" (U.S. Environmental Protection Agency, 2010). As a control test, 50 mM Na_2SO_4 was injected into the cathodic chamber after three-times wash following an ECL experiment with bacterial cells. The effluent was collected after 10 min and detected by qPCR. The average qPCR C_T values are 32.0.

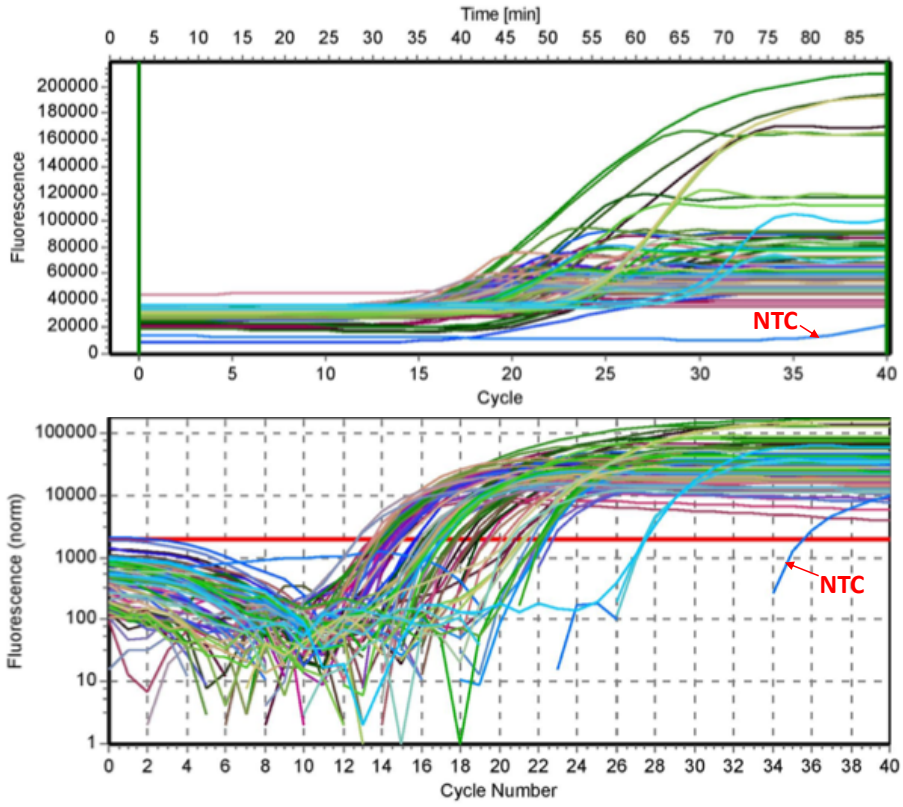

Figure 3.11: The qPCR amplification curves.

The qPCR calibration curves were prepared for all the four bacterial strains as follows: After the 12-14 hrs cultivation of the bacteria, cells were harvested by centrifugation at 5,000 rpm for 5 min to remove the culture media. PBS buffer was then added and mixed well to achieve the concentration of approximately 8×10^8 cells/mL as the calibration solution I (CS-I) and the optical density at the wavelength of 600 nm (OD_{600}) was measured by Nanodrop 2000C (Thermo Fisher Scientific). The cell density was estimated by assuming that the OD_{600} of 1.0 equals 8×10^8 cells/mL and that the cell density is proportional to the OD_{600} values within the range of 0.1-1.0. The CS-I was then progressively diluted with PBS to achieve five calibration solutions with the cell concentration range from 8×10^8 to 8×10^4 cells/mL. The cell densities of the calibration solutions were calculated by the cell density of CS-I times the respective dilution rates. The five calibration solutions were detected by qPCR in triplicates based on the same method described in the Section 3.2.5. The average PCR cycles numbers (C_T) for calibration solutions and the estimated cell densities were used to prepare the calibration curves of C_T - $\log_{10}$ cell concentrations. The linear regression coefficients (R^2) of the calibration curves range from 0.994 to 0.999 and PCR efficiencies are 90.2%-95.7% for all the four bacteria strains tested in this study (shown in Figure 3.12).

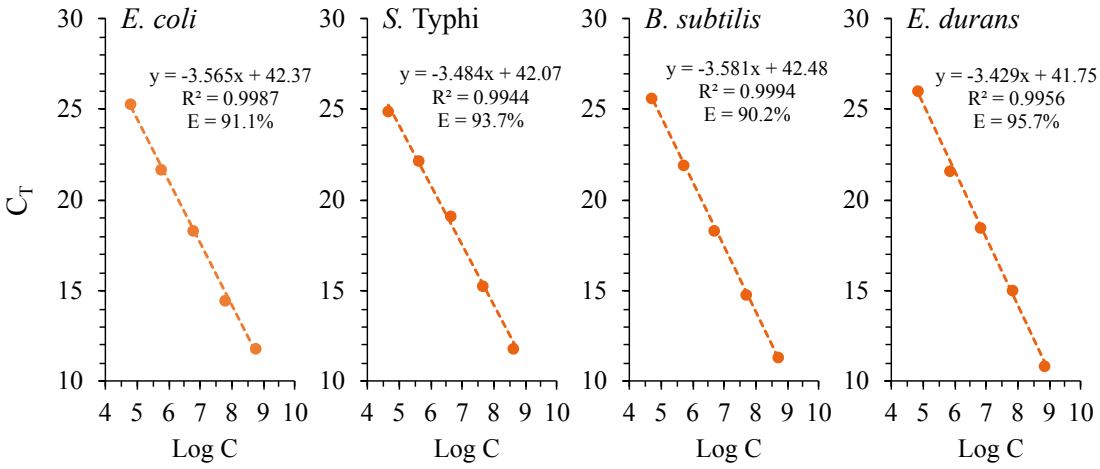

Figure 3.12: The qPCR calibration curves for four different bacteria with R^2 and percentage PCR efficiency (E, $E = 10^{(-1/slope)} - 1$ where the slope is derived from the linear fitted line of the standard curve).

3.6.2 Detailed Simulation Methods

The flow field within the cathodic chamber was first simulated by *laminar bubbly-flow* module, which calculates the fluid movement induced by the generation and venting of H_2 during electrolysis. The convective and diffusive OH^- transport under the calculated flow field was then modeled by *transport of dilute species* module. Free tetrahedral mesh calibrated for fluid dynamics was used with predefined element size, which was set as fine for all boundary surfaces and as normal for the rest of the geometry.

For flow field simulation, *laminar bubbly-flow* module uses Euler-Euler model to solve two-phase flow macroscopically by tracking phase averaged parameters and volume fraction of each phase (Vera and Ruiz, 2012). Molar influx of H_2 gas at the cathodic electrode surface was theoretically half of hydroxide ion generation rate R_{in}^{cat} at the cathode surface, calculated by (Bard *et al.*, 1980):

$$R_{in}^{cat} = \frac{i}{nFA} \tag{3.5}$$

where i is the supplied current at 40 mA, n is the number of electrons used to generate a hydroxide ion, which is 1, F is Faraday's constant, and A is the surface area. The bubble diameter was set at 100 μm which is a typical size reported by Matsushima *et al.*, 2006, 2009.

For *transport of dilute species* interface, OH^- generation from the cathodic electrode surface was represented by a uniform inward flux of R_{in}^{cat}, calculated by Equation (3.5) at 1.66×10^{-3} mol/(s·m^2). Simultaneously, in the anodic chamber with 50 mM Na_2SO_4 buffer solution, H^+ ions were produced from the anode surface at the same rate as OH^- generation, and cations were forced across the cation exchange membrane. It was assumed that sodium ions were the dominant species transported across the membrane due to their concentration dominance over protons, until sodium ions were transferred down to a concentration comparable to the proton; at this point protons are the preferred ions for membrane transport due to their smaller size. For the cathodic chamber, the influx of H^+ was considered as the sink of OH^- and the contribution of water dissociation was negligible to mass transfer through the membrane (Simons, 1979; Krol *et al.*, 1999; Tanaka *et al.*,

2012).Therefore, the flux of hydroxide ions at the membrane, R_{in}^{mem}, was approximated as a step function:

$$R_{in}^{mem} = \begin{cases} 0 & t < t_c \\ -R_{in}^{cat} & t \geq t_c \end{cases} \tag{3.6}$$

where t is time and t_c is the critical time when protons become favored for cross membrane transport. The value of t_c was approximated by the time of complete consumption of sodium ion in the anodic chamber. The initial pH was set at 7.5. The time-dependent concentration profile of OH^- was analyzed with the diffusion coefficient of OH^- in water set at 5×10^{-5} cm^2/s (Lee and Rasaiah, 2011). From the simulated hydroxide ion concentrations, the transient pH profiles of the cut plane across the electrode and the membrane were generated, while the bulk solution pH was estimated from the volume average of $[OH^-]$.

3.6.3 The ECL Effects on DNA Damage and PCR Inhibition

In order to further understand the decrease of the DNA extraction efficiency with longer ECL durations, the effects of ECL on DNA damage was first investigated. The extracted DNA was used to conduct the ECL experiments instead of bacterial cells. And the DNA samples were collected from *E. coli* cells in 50 mM Na_2SO_4 (~10^8 cells/mL) after 5 min of bead beating in a pre-loaded bead tube (S0205-50, GeneRite, USA) followed by 10 min of centrifuge at 10,000g to remove cell debris. Then the extracted DNA samples were injected into the cathodic chamber and subjected to ECL with different durations from 30 s-30 min. To exclude any potential PCR inhibition effects, the cathodic effluents were purified by a commercial DNA extraction kit (PureLink® Genomic DNA Mini Kit, Invitrogen by Thermo Fisher Scientific, USA) and then measured by qPCR. The DNA concentrations in all the samples were estimated using the calibration curve of C_t-Log C for *E. coli* shown in Figure 3.12. Then the percentages of DNA loss compared to the initial DNA sample in function of ECL durations are calculated and shown in Figure 3.13. Approximately 60% less DNA than in the initial sample was detected after 30 min of ECL. This confirms the contribution of DNA damage to the decrease in DNA extraction efficiency, shown in Figure 3.3 of Section 3.4.1.

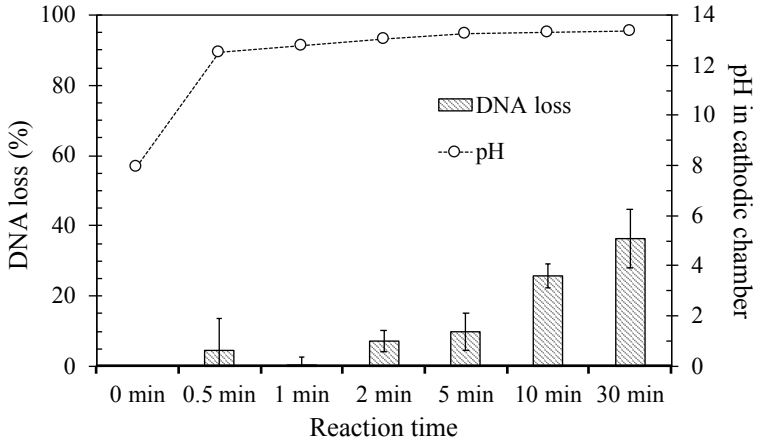

Figure 3.13: Effects of ECL on DNA damage.

On the other hand, to investigate the influence of PCR inhibition, 50 mM Na_2SO_4 was added into both anodic and cathodic chambers, and the electrolyzed cathodic solutions (ECS) were collected after ECL durations of 30 s-30 min. The extracted DNA samples were prepared in the same way as in the DNA damage test above. Then the extracted DNA samples were mixed with different ECS in a ratio of 1:1. All the mixture and the initial DNA samples without adding any ECS were detected by qPCR and qPCR C_T values are shown in Figure S4. There was no significant difference observed between the DNA samples mixed with different ECS and the initial DNA sample. It suggests that there were barely any PCR inhibitors generated in the ECS, which could contribute to the decrease in the DNA extraction efficiency. Additionally, all the PCR assays containing ECL samples with different durations were measured as a pH range of 8.4-8.7 (*vide supra*). So, the increased pH in the ECS with different ECL durations should not have an inhibition effect on qPCR detection, either. Therefore, it suggests that the decreased DNA extraction efficiencies with longer ECL durations were predominately resulted by DNA damage during ECL process, *e.g.* the local high pH generated at cathode.

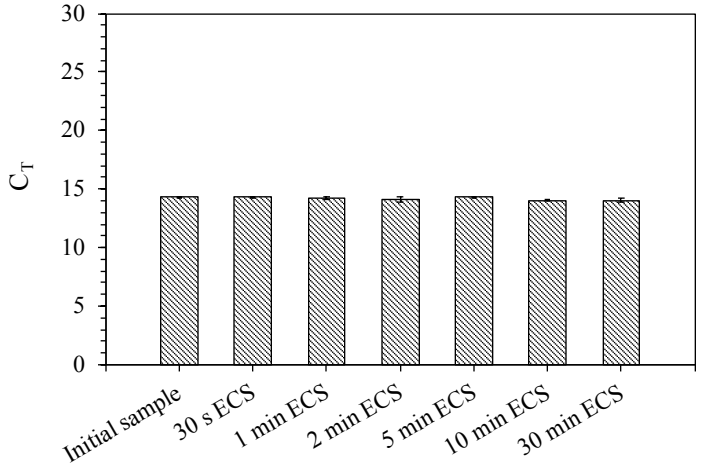

Figure 3.14: Effects of electrolyzed cathodic solution (ECS) with varied ECL durations on qPCR detection. The extracted DNA samples in 50 mM Na_2SO_4 was added in different ECS with a ratio of 1:1.

3.6.4 Summary of experimental setups for previous studies on ECL

Table 3.1: Summary of experimental setups for previous studies on ECL.

ECL conditions					***Cell lysis/DNA Extraction Efficiency***	***Device***					***Target cell***	**Concentration (cells/mL)**	**Reference**
AC or DC	Voltage	Electrodes	Electrolyte	Lysis time		Type	Volume	Batch or Flow-through	Flow rate (μL/min)	Other structure			
DC	2.6 V (40 V/cm)	Cathode: Pd; Anode: Ti	PBS buffer	Varied	N.A.	10-chamber arrays	0.36 uL for each chamber	Flow-through	~20	PDMS filter for trapping cells (2 μm)	Red blood cells; HeLa (Human tumor line); Chinese hamster Ovary cells(CHO)	1.5×10^6	Di Carlo *et al*., 2004
DC	2.5 V (~11 V/cm)	Cathode: Pt Anode: Ti	PBS buffer	>5 min	~100% (~7 min at 2.6 V)	Microfluidic lysis on chip	11 nL for each chamber	Flow-through	~7.5	U-shape cell traps	HeLa MCF-7 Jurkat CHO-K1	$1\sim5\times10^6$	Nevill *et al*., 2007
DC	5 V	Cathode: Pt Anode: Ti	100 mM NaCl	40 s	[a] ΔC_t=7.3 for *E.coli*; [a] ΔC_t=4.8 for [b] *P .putida*; [a] ΔC_t=3.9 for [c] *S. epidermidis*; [a] ΔC_t=3.5 for [d] *S. mutans.*	Micro-device	10 μL for cathodic chamber	Batch	N.A.	Negatively charged ion exchange polymer for accumulating OH^-	*E. coli* (gram-negative); [b] *P .putida* (gram-negative); [c] *S. epidermidis* (gram-positive); [d] *S. mutans* (gram-positive); Chinese hamster ovary cells (mamallian cells)	10^8	Lee *et al*., 2009
DC	5 V	Au-interdigitated electrode	PBS buffer	5 min	N.A.	Micro-chip	50 μL	Flow-through	5		MCF-10A (human cell)	10^6	Jha *et al*, 2009
DC	5 V	Au-interdigitated electrode	PBS buffer		N.A.	Micro-chip		Flow-through	5		MCF-10A (human cell)		Jha *et al*., 2011
DC	5 V		PBS buffer(0.1 % Tween 20 added for Bacillus)		N.A.	Integrated PCR microfluidic chip	50 μL	Flow-through	5		MCF-10A & MCF-7 (human cell)	10^6	Jha *et al*, 2012

[a] $\Delta C_t = C_t$ (control)-C_t (sample); [b] *P .putida: Pseudomonas putida;* [c] *S. epidermidis: Staphylococcus epidermidis;* [d] *S. mutans: Streptococcus mutan; N.A.: not available.*

Chapter 4

SUNLIGHT-ACTIVATED PROPIDIUM MONOAZIDE PRETREATMENT FOR DIFFERENTIATION OF VIABLE AND DEAD BACTERIA BY QUANTITATIVE REAL-TIME POLYMERASE CHAIN REACTION

Xie, X.; Wang, S.; Jiang, S. C.; Bahnemann, J.; Hoffmann, M. R. (2016). Sunlight-Activated Propidium Monoazide Pretreatment for Differentiation of Viable and Dead Bacteria by Quantitative Real-Time Polymerase Chain Reaction. In: *Environmental Science & Technology Letters* 2016, 3, (2), 57-61. https://doi.org/10.1021/acs.estlett.5b00348.

Abstract

Polymerase chain reaction (PCR)-based methods have been developed and increasingly used for rapid and sensitive detection of pathogens in water samples to better protect public health. A propidium monoazide (PMA) pretreatment can help to differentiate between viable and dead cells, but the photo-activation of PMA normally requires the use of an energy consuming halogen light, which is not suitable for off-the-grid applications. Herein, we investigate sunlight as an alternative light source. Our results suggest that sunlight can successfully activate PMA, and the sunlight-activated PMA pretreatment can effectively reduce the amplification of DNA derived from dead cells in PCR assays. Potentially, a sunlight-activated PMA pretreatment unit can be integrated into a lab-on-a-chip (LOAC) PCR device for off-the-grid microbial detection and quantification.

4.1 Introduction

Waterborne diseases due to consumption of pathogen contaminated drinking water supply are the major cause of human mortality and morbidity in the world. Mortality rate attributed to the waterborne diseases is estimated at about 2,000 people every day (Pruess-Ustuen *et al*., 2014). To better protect public health, rapid detection and accurate quantification of pathogens in water is critical. The traditional cultivation based method for detection of microbial pathogens on selective media is time-consuming, labor intensive, and often requires standard lab facilities and complicated biochemical testing to confirm the pathogenicity of the isolates. Moreover, the cultivation method is insensitive to viable but non-culturable cells (Li *et al*, 2014). To overcome

these limitations, polymerase chain reaction (PCR)-based methods have been developed and increasingly used for rapid, sensitive, and specific detection of pathogens (Girones *et al*., 2010; He and Jiang, 2005; Heid *et al*., 1996). In addition, lab-on-a-chip (LOAC) devices are being developed to utilize PCR techniques in the field where standard lab facilities are not readily available (Cai *et al*., 2014; Xu *et al*., 2015; Hawtin *et al*., 2005; Kim *et al*., 2009; Lee *et al*., 2006). A major challenge for PCR-based methods is that they cannot differentiate between viable and dead cells, because 1) target DNA fragments may remain intact even though the cell is dead, 2) DNA may persist in the environment for days to weeks, and 3) all target DNA fragments, extracted from cells either viable or dead, will be amplified during PCR (Blaser *et al*., 1986; Butler *et al*., 1987; Josephson *et al*., 1993). As a result, PCR-based methods may produce false-positive results and overestimate the infectious cell concentration. For the same reason, PCR-based methods are not suitable for measuring water samples after disinfection treatments, during which the dead cells are inactivated but not removed.

A propidium monoazide (PMA) pretreatment before PCR can help to discriminate DNA from dead cells whose cell membranes are irreversibly damaged (Nocker *et al*., 2006a). The mechanism is that PMA penetrates the compromised cell membrane but is excluded from the viable cells with intact cell membranes (Nocker *et al*., 2006a). Once inside the cell, PMA binds to DNA by intercalating between the bases (Waring, 1965). When exposed to bright light, the azide group is converted to a highly reactive nitrene, which reacts with the DNA bases forming a stable covalent nitrogen-carbon bond (Hixon *et al*., 1975). Cross-linked DNA strands become insoluble and can be easily removed during subsequent DNA extraction process (Nocker *et al*., 2006a). Due to the structural change in nucleotide angle, the remaining DNA strands are also unavailable for elongation by polymerase, thus not amplified during PCR (Nocker *et al*., 2006b). The residual photo-activated PMA in solution is simultaneously quenched in a reaction with water molecules and the resulting hydroxylamine is no longer capable of forming covalent bond with DNA (Detraglia *et al*., 1978; Kell *et al*., 1998). The DNA strands extracted afterwards from viable cells are therefore not affected by the inactivated PMA and available for PCR amplification. This PMA pretreatment method has been successfully integrated in qPCR assays to differentiate between viable and dead cells of various bacteria (Nocker *et al*., 2006a; Varma *et al*., 2009; Pan and Breidt,

2007; Kobayashi *et al*., 2009; Cawthorn and Witthuhn, 2008; Bae and Wuertz, 2009; Zhang *et al*., 2015; Wu *et al*., 2015; Banihashemi *et al*., 2015).

In a typical PMA pretreatment process, the photo-activation of PMA requires the use of a halogen light source (Nocker *et al*., 2006a; Nocker *et al*., 2007a; Sanchez *et al*., 2014; Seinige *et al*., 2014; Taylor *et al*., 2014). When a 600-W commercial halogen lamp is used to generate an illuminated area of ~0.25 m^2 at distance of 20 cm from the light source, the light intensity is measured to be in the range of ~500-2000 W/m^2 depending on distance from the center. The generation of light using a halogen lamp is energy intensive and requires a grid-based source of electricity. Next generational lab-on-a-chip PCR devices for detection and quantification of microbial concentrations in water samples will be portable and powered by batteries or solar energy (Jiang *et al*., 2014; Agrawal *et al*., 2007; Norian *et al*., 2014), so that they can be readily applied off the grid where the measurement is most needed, *e.g.*, epidemic areas in developing countries and places after natural disasters. In order to integrate PMA pretreatment into such devices, it is critical to investigate an alternative light source that runs without grid electricity and consumes minimal energy. In this study, we first applied sunlight for the photo-activation of PMA. The peak solar irradiance on the earth's surface at AM1.5 (1.5 atmosphere thickness) is about 1000 W/m^2. Compared to the output spectrum of a typical halogen light, the solar spectrum is shifted slightly toward the ultraviolet range, where photons have shorter wavelengths and higher energies. We optimized the pretreatment conditions and studied the effect of sunlight intensity and multiple sequential treatments. The potential integration of photolytic PMA pretreatment for use in LOAC qPCR devices is also proposed and discussed for the first time.

4.2 Materials and Methods

4.2.1 Bacterial Sample Preparation

The bacterial strains used in this study include *Escherichia coli* (ATCC 10798), *Enterobacter cloacae* (ATCC 700323), *Enterococcus durans* (ATCC 6056), and *Bacillus subtilis* (ATCC 6051). The cultivation conditions are listed in Table 4.1. The cultures were grown for 14-16 hours in a shaker at 200 rpm at the given temperature. Bacterial concentrations were quantified by spreading 100 μL of diluted samples on corresponding agar plates, incubating the plates for 24 h at their corresponding temperatures, and counting the colony forming units (CFU). All culture media were

purchased from Fisher Scientific. Dead cells were prepared by placing bacterial cultures in a dry bath at 90 °C for 10 minutes. The effectiveness of the inactivation was confirmed by cultivating treated culture samples on agar plates. In all PMA-qPCR experiments, each bacterial sample contained 500 μL of viable or dead cells. Specifically, the samples for validation of PMA pretreatment were prepared using different ratio of viable and dead *E. coli* cells: the percentage of viable cells in samples ranged from 1% to 100%. All samples were tested in triplicate. Real wastewater samples were collected from the solar-powered toilet on Caltech campus (Cho and Hoffmann, 2014).

Table 4.1: Bacterial species used and growth conditions.

Species (Gram stain)	Media	T (°C)	ATCC No.
Escherichia coli (G^-)	Fisher BioReagents, LB Broth, Miller	37	10798
Enterobacter cloacae (G^-)	BD Difco™, Tryptic Soy Broth	30	700323
Enterococcus durans (G^+)	BD™ Bacto™, Brain Heart Infusion Broth	37	6056
Bacillus subtilis (G^+)	BD Diagnostics, Nutrient Broth	30	6051

4.2.2 PMA Treatment

A typical PMA pretreatment includes the following three steps: 1) add PMA stock solution (20 mM in water, Biotium Inc.) to samples to a final concentration of 80 μM in an ice bath; 2) incubate samples in dark for 10 min; and 3) expose samples to light for 10 min to photo-activate PMA. A solar simulator was used as the light source (Sun 2000, Abet Technologies Inc.). The light spectrum of the solar simulator is very similar to natural sunlight (Figure 4.1). The light intensity was set at 1000 W/m^2 in different experiments, so that the results could be comparable.

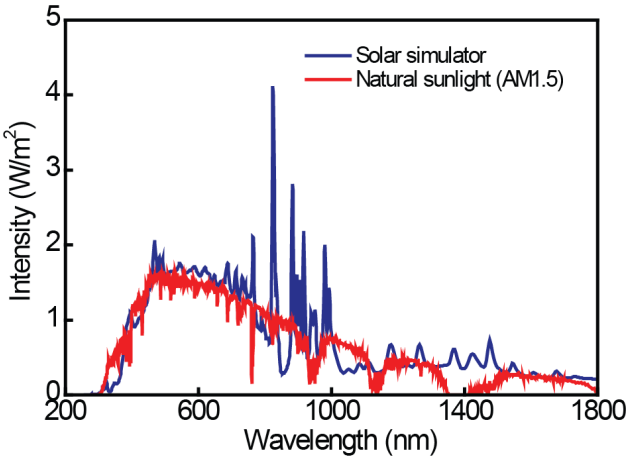

Figure 4.1: Spectrum of the solar simulator (provided by vendor: Sun 2000, Abet Technologies Inc.) and natural sunlight at AM1.5 (downloaded from National Renewable Energy Laboratory website: http://rredc.nrel.gov/solar/spectra/am1.5/).

In experiments for optimizing the pretreatment condition, PMA concentrations varied from 10 to 100 μM and light exposure time varied from 1 to 20 min. In experiments for investigating the effect of sunlight intensity, light intensities varied from 100 to 2500 W/m^2. Lower intensities (100, 300, and 500 W/m^2) were obtained by adding UV-NIR Neutral Density Filters (Edmund Optics Inc.), while higher intensities (1600 and 2500 W/m^2) were achieved by placing sets of UV Plano-Convex Lens (Edmund Optics Inc.). The exposure time was adjusted according to the light intensities and varied from 0.8 to 20 min. In experiments for testing the effect of multiple sequential treatments, the final accumulated PMA concentration was 80 μM, and the total dark incubation time and total light exposure time were both 10 min. For example, when 4 pretreatments were applied, 20 μM PMA was added each time, and the dark incubation time and light exposure time were both reduced to 2.5 min each time. In experiments using real wastewater samples, natural sunlight was applied for PMA activation. Experiments were performed on Caltech campus (Pasadena, CA) around noon on two different days: a sunny day (October 21, 2015) and a cloudy day (October, 19, 2015). Light intensities during experiments were 973±6 W/m^2 and 70±10 W/m^2, respectively, measured by a light meter (Amprobe, LM-120).

4.2.3 DNA Extraction and qPCR Measurement

Bacteria cells were collected from both PMA treated and untreated control samples by centrifugation at 17,000×g for 10 min (Centrifuge 5424, Eppendorf Inc.). Genomic DNA was

extracted using the PureLink® Genomic DNA Mini Kit (Thermo Fisher Scientific Inc.) following the manufacturer's instructions. Real-time PCR assays were performed with MasterCycler RealPlex 4 (Eppendorf Inc.) to quantify the presence of universal bacterial 16S rRNA gene. The reaction mixture contains 10 μL PerfeCTa® qPCR ToughMix® (Quanta BioSciences Inc.), 0.25 μM forward primer (1369F, 5′CGGTGAATACGTTCYCGG3′, where Y is either C or T, Integrated DNA Technologies Inc.), 0.25 μM reverse primer (1492R, 5′GGWTACCTTGTTACGACTT3′, where W is either A or T, Integrated DNA Technologies Inc.), 0.25 μM TaqMan probe (FAM-5′CTTGTACACACCGCCCGTC3′, Integrated DNA Technologies Inc.), 1 μL template DNA, and nuclease-free water (Promega Corporation) to a final volume of 20 μL (Suzuki *et al*., 2000). For the thermal cycling, the initialization was 3 min at 95 ^{o}C, followed by 40 cycles of 15 s at 95 ^{o}C for denaturation and 30 s at 55 ^{o}C for annealing/extension.

4.2.4 Data Analysis

Instrument specific software (Eppendorf Inc.) was used to define the threshold cycle (C_t) values. The PMA-qPCR to discriminate between viable and dead cells was made by comparing the C_t values from samples containing different percentages of viable cells to the expected C_t values based on 100% efficiency of amplification of viable cells without any interference from dead cells. Linear regression analysis was performed to determine the slopes and regression coefficients (R^2) of the fitting curves. The effect of PMA treatment under different experimental conditions was indicated by ΔC_t, which was calculated by subtracting C_t value of PMA untreated sample from that of treated sample. Error bars in diagrams represent standard deviations from three independent replicates.

4.3 Results and Discussion

4.3.1 Validation of Sunlight-Activated PMA Pretreatment

The *E. coli* concentration reached ~1.0×10^9 CFU/mL after 14-16 h cultivation. The heating protocol effectively killed the cells, as no colony growth was observed on the agar plates. Samples with different ratios of viable and dead cells were tested and the threshold cycles (C_t) obtained from qPCR assays are shown in Figure 4.2. The C_t values indicate the target DNA concentration in the sample: higher C_t values suggest that more cycles are necessary for detecting a signal above

the background when the DNA concentration is lower. For the PMA-treated samples, the measured C_t values are all fall in the vicinity of the expected Ct values (black dashed line, Figure 4.2). The plot of C_t value versus the logarithm of viable cell percentage reveals a linear correlation with R^2 value close to ~0.99. This suggests that the signal of DNA derived from dead cells was successfully reduced, and thus the C_t value obtained from qPCR provided a good estimation of the concentration of viable bacteria cells in the sample. However, for the samples without a PMA pretreatment, the measured C_t values did not change significantly between samples containing 1% and 100% viable cells. The C_t values were significantly below the expected values in samples containing less than 10% of viable cells (Figure 4.2). Obviously, without a PMA pretreatment, a significant amount of DNA derived from dead cells was amplified by PCR, causing false-positive results and overestimation of viable cells. The slight signal reduction (C_t increase) is probably due to the loss of DNA integrity in the heat-killed dead cells samples.

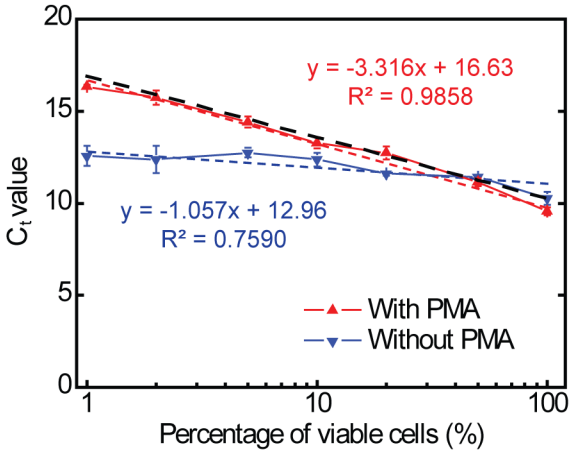

Figure 4.2: C_t values obtained from PMA-qPCR experiments using bacterial samples contained ~1.0×10^9 CFU/mL *E. coli* with different ratio of viable and dead cells. PMA (80 μM) was photo-activated by 10-min exposure of sunlight generated by a solar simulator. The black dashed line indicates the expected C_t values for 100% efficiency of amplification of viable cells without any interference from dead cells. The red and blue curves are the C_t values from the experiments with and without PMA treatment, respectively. The equation of the regression curves and the R^2 values are indicated.

4.3.2 Optimization of Pretreatment Conditions

PMA pretreatment reduces the qPCR signal of DNA derived from dead cells. The extent of PMA induced signal reduction, indicated by the difference between the C_t value of PMA treated sample

and that of untreated sample (ΔC_t), is a function of both the PMA concentration and exposure time. Therefore, we optimized the pretreatment condition by measuring the ΔC_t values when treating samples containing ~1.0×10^9 CFU/mL viable or dead *E. coli* cells with various PMA concentrations (10, 20, 50, 100 μM) and exposure times (1, 2, 5, 10, 20 min). The goal was to find a condition resulting in the highest ΔC_t value for dead cells but lowest ΔC_t values for viable cells. In general, the ΔC_t value for dead cells increased with PMA concentration and exposure time (Figure 4.3A). However, a moderate DNA loss for viable cells (positive ΔC_t in Figure 4.3B) was observed for PMA concentrations above 80 μM. Considering that fast pretreatment is preferred for practical applications, we chose a PMA concentration of 80 μM and an exposure time of 10 min as the optimized pretreatment condition. Such conditions are similar to those reported when halogen light was used as the light source (Nocker *et al*., 2006a; Bae and Wuertz, 2009). With this optimized condition, PMA pretreatments were applied to samples containing different bacterial species, including *Escherichia coli*, *Enterobacter cloacae*, *Enterococcus durans*, and *Bacillus subtilis*. The ΔC_t values achieved for the dead cells were in the range of 2.6-10.0 (Figure 4.4), which are similar to the level reported in the literature (Seinige *et al*., Salam *et al*., Rawthorne *et al*., 2009; Soejima *et al*., 2011). Experiments with *Bacillus* obtained the highest ΔC_t value for dead cells, but the ΔC_t value for viable cells (2.4) is also the highest, which suggests that the cell membrane of *Bacillus* is the most permeable to PMA.

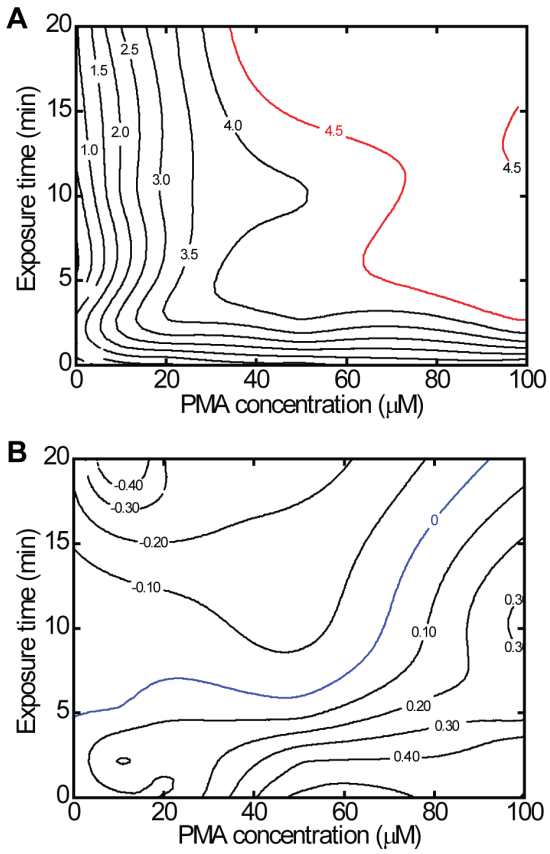

Figure 4.3: Signal reduction (ΔC_t values) in qPCR assays when samples containing dead (A) or viable (B) *E. coli* cells were pretreated with different PMA concentrations (10, 20, 50, 100 μM) and times of sunlight exposure (1, 2, 5, 10, 20 min). The ΔC_t values, calculated by subtracting C_t values of PMA untreated samples from those of treated samples, are represented by the contour lines generated using OriginPro.

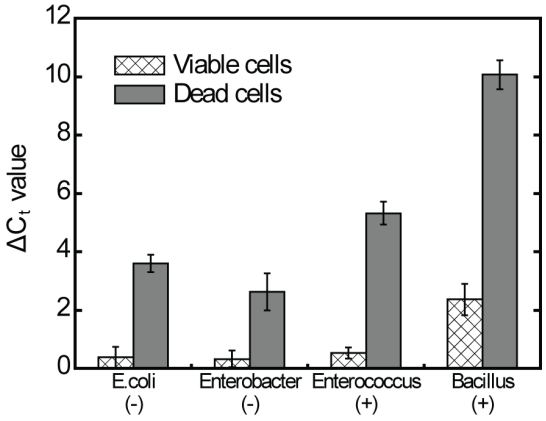

Figure 4.4: Signal reduction (ΔC_t values) in qPCR assays when samples containing various bacterial cells were pretreated with sunlight-activated PMA (80 μM, 10 min). The ΔC_t values were calculated by subtracting C_t values of PMA untreated samples from those of treated samples.

4.3.3 Effect of Light Intensity

The light intensity in the above experiments was set at 1000 W/m^2, a value similar to the peak solar irradiance on the earth surface at AM1.5. However, in reality, the intensity of natural solar irradiance varies from place to place and from time to time. For example, it is lower at dawn or dusk, on a cloudy or rainy day, and at places with higher latitudes. Therefore, it is necessary to investigate the effect of light intensity to the PMA pretreatment. Light intensities from 100 to 2500 W/m^2 were tested and the exposure time was varied depending on the light intensity. For a fixed exposure time of 2 min, the ΔC_t for dead cells increased with light intensity (Figure 3.5A); while for a fixed exposure time of 10 min, the ΔC_t for dead cells first increased with light intensity then decreased when light intensities were over 1000 W/m^2 (Figure 3.5B). These results suggest that when the exposure time is short (*i.e.*, 2 min), increasing the light intensity can enhance the PMA photo-activation thus resulting in higher ΔC_t for dead cells. However, if the exposure time is sufficiently long (*i.e.*, 10 min), a moderate light intensity achieves the highest signal reduction (ΔC_t). A similar phenomenon was revealed by experiments with a fixed light intensity of 2500 W/m^2 (Figure 3.5C). The highest ΔC_t for dead cells was achieved with a moderate exposure time of 2 min. The declined performance was possibly due to the decomposition of PMA caused by the high dose of solar exposure and/or breakdown of the DNA integrity in the dead cells (reduce the signal in untreated samples). These results suggest that in cases when the sunlight intensity is low, we can still maintain the pretreatment performance by either increasing the exposure time or concentrating the light with some optic lenses. Enhancing the sunlight can shorten the time for PMA activation and thus the pretreatment procedure, but overexposure to high intensity sunlight should be avoided. Most of the ΔC_t values for viable cells are within ±1, indicating little effect of PMA pretreatment to the amplification of DNA derived from viable cells in qPCR.

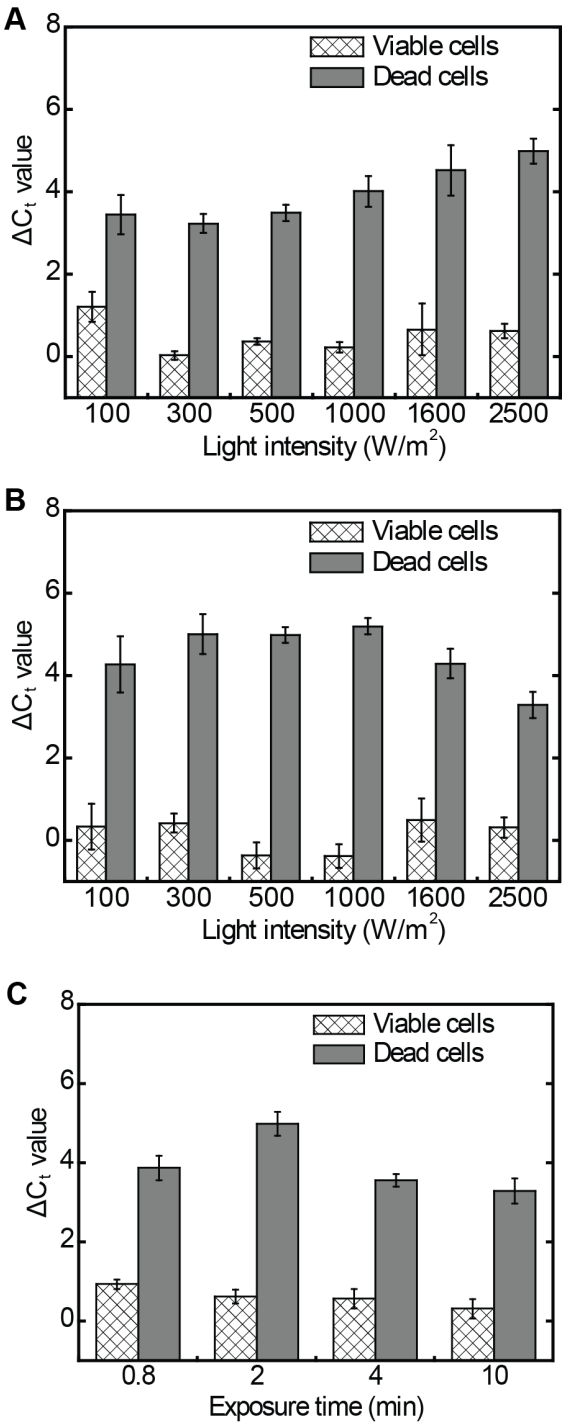

Figure 4.5: Effect of sunlight intensity and exposure time on the signal reduction (ΔC_t values) in PMA-qPCR assays. Bacterial samples containing ~1.0×10^9 CFU/mL *E. coli* were pretreated with 80 μM PMA. (A) Exposure time was fixed at 2 min. (B) Exposure time was fixed at 10 min. (C) Light intensity was fixed at 2500 W/m^2.

4.3.4 Effect of Multiple Sequential Treatments

Double-treatment has been applied in previous studies to improve the signal reduction of dead cells in qPCR (Seinige *et al*., 2014; Minami *et al*, 2010). In this study, we investigated the performance of PMA-qPCR with double, triple, or quadruple PMA treatments. All experiment sets had the same total PMA dose, incubation time, and exposure time. The results (Figure 4.6) show that the ΔC_t values for dead *E.coli* cells were about 4-4.2 with no significant difference regardless of the various number of treatment times. Increasing the treatment times did not show obvious advantages. Conversely, multiple sequential treatments might affect the amplification of DNA from viable cells, indicated by the slightly increased ΔC_t values for viable cells.

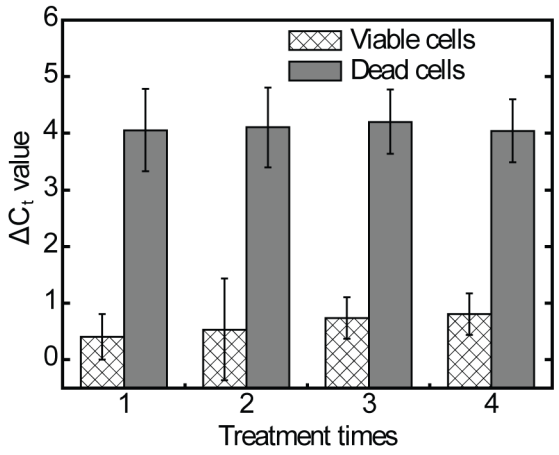

Figure 4.6: Effect of multiple sequential treatments on the signal reduction (ΔC_t values) in PMA-qPCR assays. Bacterial samples contained ~1.0×10^9 CFU/mL *E. coli*. All experiment sets had the same total PMA dose (80 μM), incubation time (10 min), and exposure time (10 min). For example, when 4 pretreatments were applied, 20 μM PMA was added each time, and the incubation time and exposure time were both reduced to 2.5 min.

4.3.5 PMA-qPCR Application on Wastewater Samples

We have also investigated the performance of PMA-qPCR using real wastewater samples and applying 10-min natural sunlight for PMA activation. For experiments on both a sunny day and a cloudy day, the PMA pretreatment effectively reduced the signal of heat-treated wastewater in qPCR with ΔC_t values of 5.9 and 5.0, respectively (Figure 4.7). The results also suggest that, under both weather conditions, 10-min exposure to natural sunlight is sufficient to activate PMA. The

relatively high ΔC_t values (1.9 and 1.2) for unheated samples were probably due to initially dead cells contained in the real wastewater.

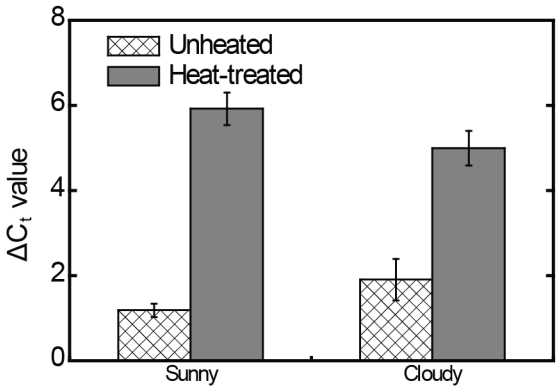

Figure 4.7: Signal reduction (ΔC_t values) in qPCR assays when real wastewater samples were pretreated with sunlight-activated PMA (80 μM, 10 min). The ΔC_t values were calculated by subtracting C_t values of PMA untreated samples from that of treated samples. The light intensities were 973±6 W/m^2 on the sunny day and 70±10 W/m^2 on the cloudy day.

4.4 Conclusion

The sunlight-activated PMA pretreatment can be easily adapted on a LOAC device for off-the-grid microbial detection and quantification. A well-designed LOAC device can provide thoroughly mixing for PMA and treated sample and control the time for dark incubation and light exposure (Bahnemann *et al*., 2013; Rajabi *et al*., 2014). In addition, a light concentration unit can be integrated to enhance the sunlight intensity when it is needed. Multiple sequential treatments can also be realized on a LOAC device by repeating the treatment unit. This increases the complexity of the chip fabrication, but may not improve the PMA treatment according to our experimental results. PMA is considered to be too expensive for routine application (Seinige *et al*., 2014; Taylor *et al*., 2014). However, it could be affordable if applied on a LOAC device, where normally a very small amount of sample is analyzed and thus little PMA consumed. In this case, a sample concentration step may be needed beforehand to achieve more reliable results. The effect of water properties (*e.g.*, present of dead cells, turbidity, salt concentration, pH, *etc*.) on the performance of PMA pretreatment has been reviewed previously (Fittipaldi *et al*., 2012). Specifically, it has been reported that high solid concentration (1000 mg/L) in tested water samples can affect the efficacy of PMA pretreatment (Bae and Wuertz, 2009). In addition, the particles may affect the flow or

even block microfluidic channels. Thus, additional steps to reduce the turbidity of the tested samples are needed before LOAC PMA-qPCR analysis. We also notice that the principle of using PMA to differentiate viable and dead cells is based on membrane integrity. Dead cells without sufficient damage on cell membrane cannot be discriminated by PMA pretreatment (Lee *et al*., 2015; Leifels *et al*., 2015; Nocker *et al*., 2007b).

Chapter 5

CONCLUSION AND FUTURE DIRECTION

5.1 Conclusion

In this thesis, I have presented work on the application of photo- and electro-chemical methods for pathogen treatment and analysis in environmental waters (*i.e.*, natural and engineered waters). From Chapter 2 to 4, each chapter is focused on one technology and evolved from performance assessment, discussion of mechanisms, experimental conditions optimization to the demonstration on ambient and processed water samples. These studies have the potential to be applied for decentralized wastewater treatment or on-site waterborne pathogen monitoring for source-limited conditions.

In Chapter 2, we explored a UV-assisted electrochemical method as a solution for the challenge of reducing the number of antibiotic-resistant bacteria and genes during wastewater treatment. We adopted this combined technique based on the consideration that it could be simply realized by modifying the one existing water treatment unit process with the other, *e.g.,* adding the electrochemical reaction panels in the UV disinfection unit of an existing water treatment facility or adding UV lamps to the electrochemical reaction unit of the Caltech Solar Toilet. The results suggest that the combined UV and electrochemical method presented a higher efficiency on the reduction of antibiotic resistance bacteria (ARB) and antibiotic resistance genes (ARGs) compared with the individual UV irradiation, especially when Cl^- presents in the electrolyte.

Chapter 3 presents the efficient DNA extraction from four different bacteria species by electrochemical cell lysis (ECL) in direct comparison to a commercial DNA extraction kit. The results suggested that ECL has great potential to provide for fast and simplified cell lysis that can be integrated into an automatic, portable and on-site pathogen analysis platform based on nucleic acid detection. The demonstration of ECL on both real environmental water and wastewater both shows high DNA extraction efficiencies for total bacteria. As the highest DNA extraction efficiency occurred at the same pH range near 12.5 for all the tests, we propose to use the pH value

of cathodic effluents as indicators of the optimal operational duration for the pratical application of ECL.

In Chapter 4, we show the potential of applying the sunlight-activated PMA pretreatment in field without electricity grid for live and dead cell differentiation based on real-time PCR measurement. A Lab-on-a-chip device might be an ideal carrier for PMA pretreatment, considering the much smaller volume required for PMA and the thorough mixing which can be realized by well-designed channels.

The advances discussed above also highlight some challenges to be explored in the future. First, most of the techniques set forth in this thesis became problematic or less efficient when demonstrated on real environmental water or wastewater. For example, a less efficient removal by UV-assisted electrochemical treatment was found for the native ARGs in wastewater than in clean buffered samples. The most common water quality parameters that influence the effectiveness of UV disinfection (*e.g.*, the light transmittance of the water, color, and particulate material) may also play an important role in the application of other UV or photolysis methods. Therefore, we suggest that, as in the case of UV-C disinfection, UV-assisted electrochemical methods should also be applied at the last step after other water treatment unit operations and processes for the efficient removal of ARGs in environmental or engineered water. Further work is needed to investigate matrix effects of environmental water samples. We also emphasize the necessity of a field test or a demonstration on real environmental and engineered waters for any practical applications. Second, the complex properties of the environmental water (*e.g.,* turbidity, pH, salt, and suspended solids) as well as the insufficient damage to dead cells that are present in water could also affect differentiation of live and dead cells by solar activated PMA pretreatment followed by qPCR detection. Pretreatment to remove the turbidity of water samples may help improve the performance, however, it cannot solve the problems caused by the insufficient damage to the dead cells because the differentiation of live and dead cells by PMA relies on the integrity of the cell membrane. Development of new dyes that provide more sensitive differentiation or other methods based on difference in motility between live and dead cells, should be explored in the future. Third, the relatively lower DNA extraction efficiency of gram-positive bacteria was found in the buffered samples, which may limit the application of ECL to gram-negative bacteria. It is easy to think of

adding lysozymes to break down the thick cell wall of gram-positive bacteria; however, it would defeat our original intention to use electrochemical methods for *in situ* generation of a lytic reagent and thereby provide a simplified sample preparation method for nucleic acid based detection. It will be challenging yet interesting to take more efforts on improving the DNA extraction efficiency of gram-positive bacteria by electrochemical methods based on different mechanisms (*e.g.,* oxidation) in the future study.

The research field of pathogen detection and control in environment plays a pivotal role in preventing transmission of infectious diseases globally, especially under the ongoing coronavirus disease 2019 (COVID-19) pandemic when this thesis was being prepared. A huge endeavor ahead is waiting for environmental scientists and engineers to approach the problems that threaten the public health with a better fundamental understanding of microbiology and an awareness of the array of advanced technologies that may be brought to bear.

5.2 Future Directions

5.2.1 Development of Electrochemical DNA Sensor for Waterborne Pathogen Detection

5.2.1.1 Introduction

Over the past 30 years, the application of biomolecular techniques has resulted in more rapid, accurate, and sensitive methods for the detection of pathogens in environmental water (Heid *et al*., 1996; Kim *et al*., 2013; Xie *et al*., 2016). Fluorescence-based techniques, such as the polymerase chain reaction (PCR), are the most commonly used biomolecular methods for detection of waterborne pathogens (Law *et al*., 2014). These techniques have the advantage of quick and sensitive analysis, however, involve not only highly precise and expensive instrumentation but also sophisticated numerical algorithms to interpret the data. Therefore, these techniques have been generally limited to use in research laboratories. Electrochemical sensors, in contrast, offer a promising alternative for simplified genetic detection as they eliminate the need for optical equipment, are highly amenable to miniaturization, and can be easily interfaced with integrated circuits and electronic instruments (Drummond *et al*., 2003; Wang, 2006).

According to IUPAC, an electrochemical biosensor is defined as "a self-contained integrated device, which is capable of providing specific quantitative or semi-quantitative analytical information using a biological recognition element (BRE) which is retained in direct spatial contact with an electrochemical transduction element" (Thevenot *et al*., 1999). The first electrochemical biosensor concept was developed by Clark and Lyons in 1962 (Clark and Lyons, 1962). It utilized the oxygen electrode, which was invented by Clark in 1955/56 (Grieshaber *et al*., 2008). The oxygen electrode after modification works as a selective transducer for the detection of an enzymatic reaction, *i.e.*, the oxidation of glucose by glucose oxidase. Since then, various forms of glucose biosensors have been developed and are commercially available for on-site, over the-counter, rapid diagnostic tests, as well as other biosensing technologies and devices. Biosensors have become a valuable tool in numerous other applications, including monitoring of treatment and progression of diseases, environmental monitoring, food safety concerns, drug development, forensics, and biomedical research (Wongkaew *et al*., 2019).

A general layout of electrochemical biosensor is shown in Figure 5.1. Various biorecognition components may be employed using enzymes, antibodies, nucleic acids, cells, and other receptor molecules. Ideally, they should be retained in direct contact with the electrochemical transduction element. The requirements of the biorecognition elements must be strictly considered with respect to sensitivity and selectivity for a target analyte, especially when presents at low concentration in a complex sample matrix, *e.g.*, wastewater. In electrochemical biosensing, the reaction under investigation would either generate a measurable current (amperometric), a measurable potential or charge accumulation (potentiometric), an alteration of conductive properties of a medium (conductometric), a change in impedance (impedimetric), or a field effect. The electrodes play a crucial role in the performance of electrochemical biosensors since the reactions generally occur in close proximity to the electrode surface. The electrode material as well as its surface modification and dimensions could all affect the detection ability. A variety of electrode materials including noble metals, carbon, and conductive polymers are available for specific biosensing applications. Among them, noble metals (*e.g.*, platinum, gold, silver) are widely used due to their excellent conductivity, superior electron transfer kinetics, high stability, and inertness (except for silver). Gold is a highly favored biosensor material that can be used reliably between −0.1 and 1.3

V. It also serves well for microfabrication and immobilization (Grieshaber *et al*., 2008; Wongkaew *et al*., 2019).

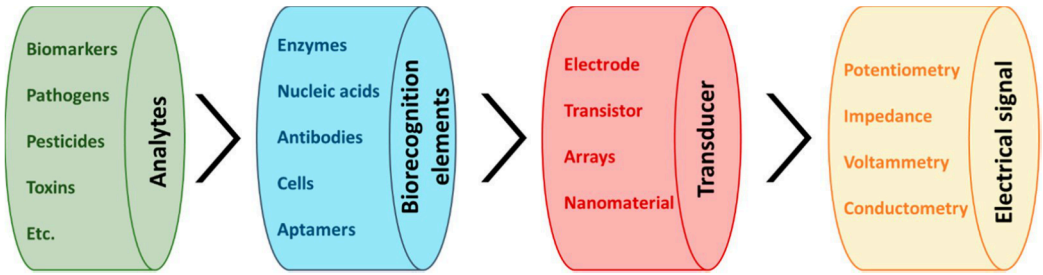

Figure 5.1: Layout of an electrochemical biosensor. Reprinted with permission from Wongkaew *et al*., 2019. Copyright (2019) American Chemical Society.

Sensitive electrochemical signaling strategies based on the direct or catalyzed oxidation of DNA bases (label-free), as well as the redox reactions of reporter molecules (labeled) are shown in Figure 5.2. The earliest electrochemical DNA sensing strategy was based on reduction and oxidation of DNA at a mercury electrode. The amount of DNA reduced or oxidized could quantify the amount of DNA captured. This methodology is quite sensitive, however, it is complicated by significant background currents at the relatively high potentials required for direct DNA oxidation (Drummond *et al*., 2003). On the other hand, several strategies have been pursued in which target DNA sequences are labeled with redox active reporter molecules. In each of these strategies, signal transduction is predicated on changes in the efficiency with which a covalently-attached redox label is able to transfer electrons to or from the electrode surface. Using a redox-labeled DNA strand affords extremely specific and selective detection by combining the specificity of DNA hybridization with the specific redox chemistry of the redox active probe (Kang *et al*., 2009). Given the general paucity of electrochemically active interferants, such sensors have been demonstrated to perform even when challenged with complex media such as blood serum (Lubin *et al*., 2006), crude cellular extracts (Zuo *et al*., 2009), urine, and saliva (Reta *et al*., 2016).

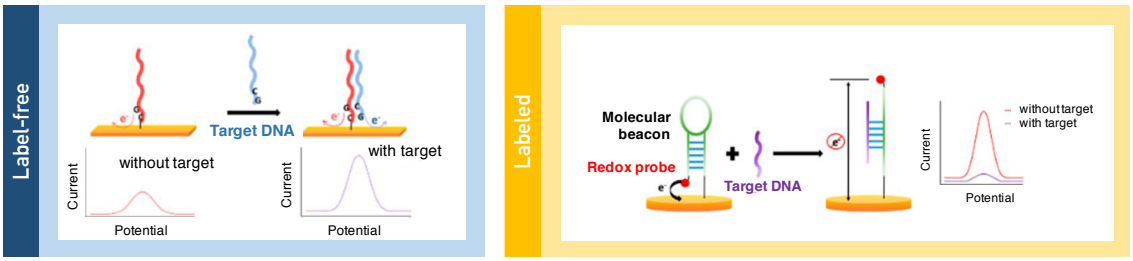

Figure 5.2: Examples of label-free and labeled assays. Adapted with permission from (Wongkaew *et al*., 2019). Copyright (2019) American Chemical Society.

Over the last decade, nanomaterials and nanostructures have attracted increasing attention in electrochemical biosensing. Due to their unique physical and chemical properties, the materials at nanoscale are excellent candidates for high performance electrochemical biosensors (Wongkaew *et al*., 2019). Particularly interesting is the use of nanoporous materials, featuring arrays of nanochannels. These sensing platforms provide several advantages. The large specific surface areas of these materials is expected to enhance the sensitivity of the device (compared to flat electrodes) due to the increase in the number of immobilized bioreceptors and thus available binding site. Additionally, the pore volume and size of nanoporous materials can be controlled in a precise way to facilitate their use as membrane filters of interfering compounds, consequently minimizing matrix effects (Reta *et al*., 2016). In 2011, de la Escosura-Muñiz and Merkoçi (Escosura-Muñiz and Merkoçi, 2011) simply modified a screen-printed carbon electrode surface using an anodized aluminum oxide nanoporous membrane array (Figure 5.3a). A cancer biomarker was detected by the modified electrode and the nanopore arrays reduced the interference from large molecules in blood samples to penetrate into the electrode surface, alleviating electrode fouling. Similarly, Reta *et al.* (Reta *et al*., 2016), modified a gold electrode by flipping over a porous silicon membrane on gold slide, and thereby capturing MS2 bacteriophage by binding to immobilized antibody (Figure 5.3c). Daggumati *et al.* (2016) (Daggumati *et al*., 2016), have exploited the unique features of nanoporous gold electrodes, such as being biofouling resilient, having high electrical conductivity, and having high active surface areas, to develop the purification system for specific DNA sequences, which are possible to serve as a detection system, too (Figure 5.3b). Nanoporous gold electrodes were modified with 26-mer DNA probes via thiol gold-based linker and exposed to a target DNA sequence in a mixture of large interfering DNA

fragments and fetal bovine serum. Excluding the large interfering DNA and proteins by a nanoporous gold structure with a median pore radius of 15 nm could effectively prevent biofouling, giving high purity of target DNA probe hybrids after capturing. Electrochemical cleavage of the thiol−gold linkage facilitated elution of the DNA hybrids for further analysis. The platform offers a great opportunity to integrate both purification and electrochemical detection steps into miniaturized analytical systems. In 2017, Matharu *et al.*,(Matharu *et al.*, 2017) reported on the relationship between pore radii and electrochemical sensing performance of DNA as well as antibiofouling capability (Figure 5.3d). The pore radii were tuned by *in situ* electrochemical coarsening methods realized by CV in which a higher number of CV cycles leads to larger pore sizes. The study demonstrated that an optimum pore radius is required in order to realize high surface areas of the nanostructure and effective biofouling resilience. The nanoporous electrode with too-large pore radii resulted in the penetration of interfering proteins into the pores, potentially blocking access of target DNA, while too-small pore radii lowered the hybridization event.

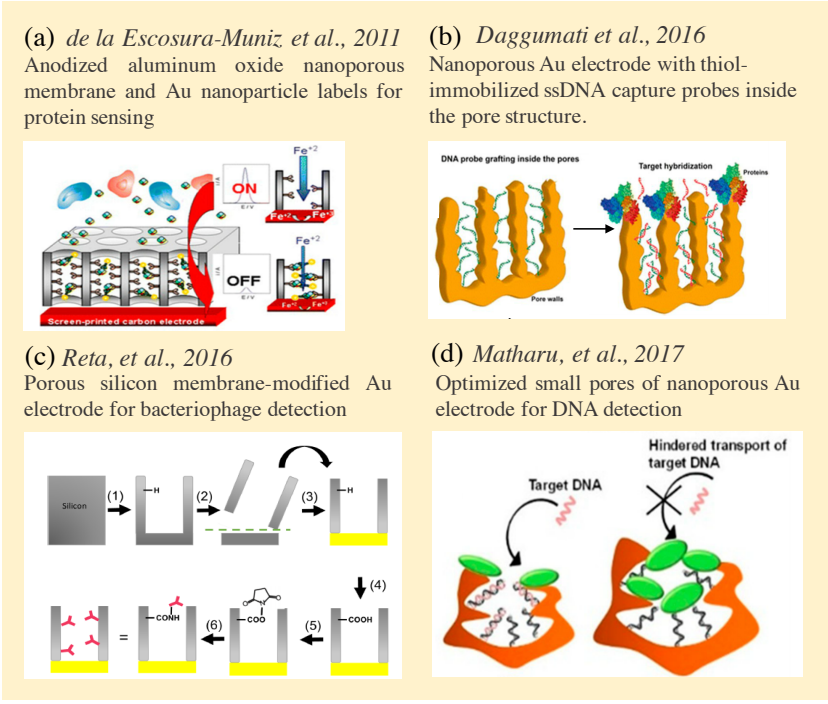

Figure 5.3: Examples of electrochemical sensor assays using nanoporous structures. Reproduced with permission from (a) de la Escosura-Muñiz and Merkoçi, 2011, Copyright (2011) Wiley; (b)

Daggumati *et al*., 2016, Copyright (2016) American Chemcial Society; (c) Reta *et al*., 2016, Copyright (2016) Elsevier; (d) Matharu *et al*., 2017, Copyright (2017) American Chemcial Society.

The superior properties and behavior of certain nanomaterials can result in directly in improved analytical figures of merit such as limit of detection, precision, accuracy, or specificity. Enhanced performance can also be related to a reduction in assay time due to excellent antifouling behavior. The same material in larger dimensions cannot offer the same properties. Yet, we have to note that it is still missing that solid proof of a nanomaterial's superior analytical performance or that important experiments to demonstrate that the new material can indeed to be used under complexed environmental conditions and is stable enough for a long-time run. Moreover, the development of generalizable electrochemical platforms that integrate sample preparation and amplification as well as quantitative and multiplexed detection still remains a challenging and unsolved problem.

Future work will focus on: 1) the development of an electrochemical DNA sensor as the downstream detection after ECL described in Chapter 3 of this thesis, and the modification of gold electrode with a nanoporous structure to potentially achieve DNA purification after cell lysis, thereby enhancing DNA detection sensitivity for waterborne pathogens; 2) the combination of electrochemical cell lysis and DNA sensing, and the development of an integrated electrochemical platform for detecting multiplexed waterborne pathogens, with the goal of a rapid, sensitive, specific, multiplexed on-site microbial monitoring for environmental water; and 3) the demonstration of the integrated electrochemical pathogen detection platform on varied waterborne pathogens and for field study. A summary of the objectives and concept of this prospective work is shown in Figure 5.4.

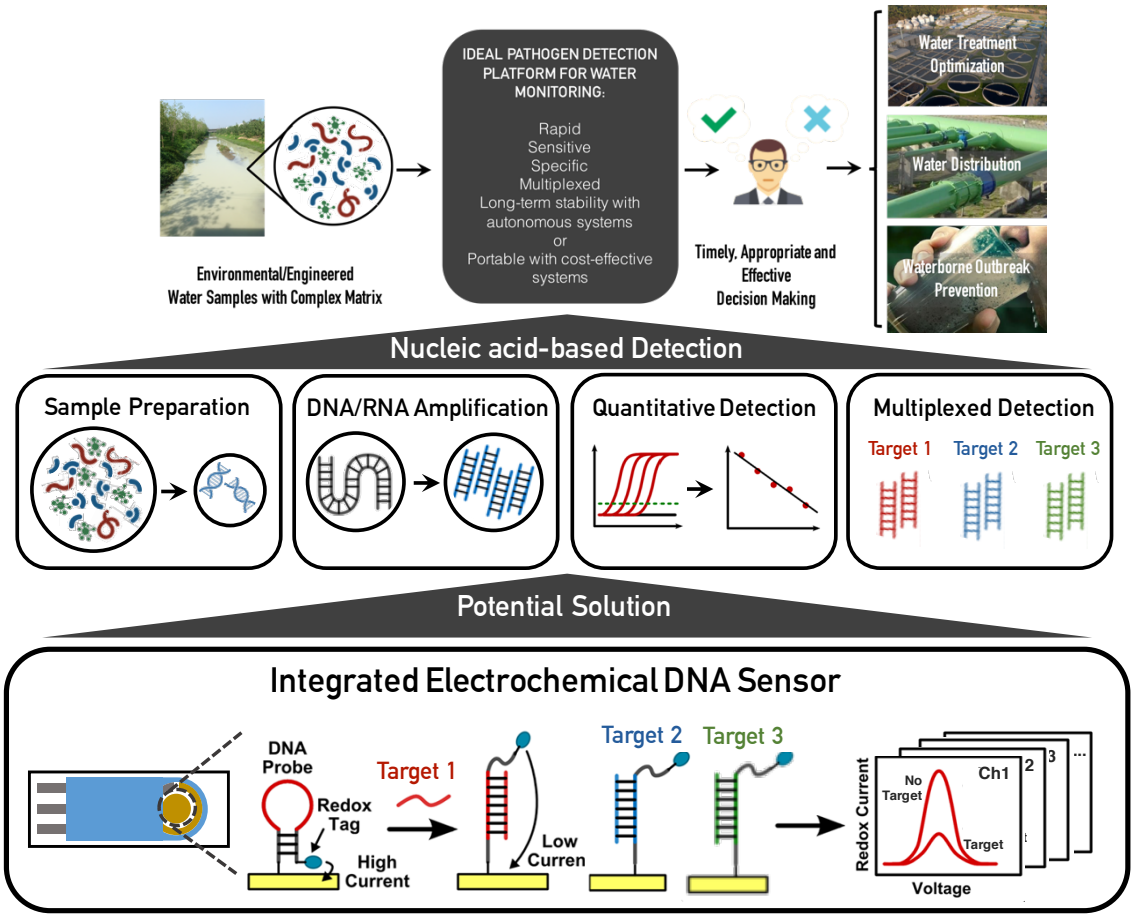

Figure 5.4: Summary of the objectives and concept of the proposal. Some parts of the schematic diagram were adapted with permission from (Hsieh *et al.*, 2015). Copyright (2015) American Chemical Society.

5.2.1.2 Development of Electrochemical DNA Sensor

Nanoporous Electrode Modification

A a direct downstream DNA sensor to the lysed samples by ECL can be envisioned in which an electrochemical DNA sensor with a nanoporous electrode would serve for both sample purification and quantitative detection. A gold electrode will be modified by either simply flipping over a membrane with nanochannels on electrode surface, or gold deposition all over a membrane with nanochannels (Figure 5.5). Regarding the former strategy, membranes including, but not limited to, silicon or conductive polymers could be used for gold electrode modification. Sealing between the membrane and electrode surface would be one of the challenges. The latter strategy may

involve a more complicated fabrication process. But the advantage of this method is its potential for a sample concentration step with a flow-through platform. This would especially benefit the analysis of environmental water samples at low concentrations of target species. Additionally, it should employ an easy cleaning procedure after each detection to allow for a long-term monitoring system.

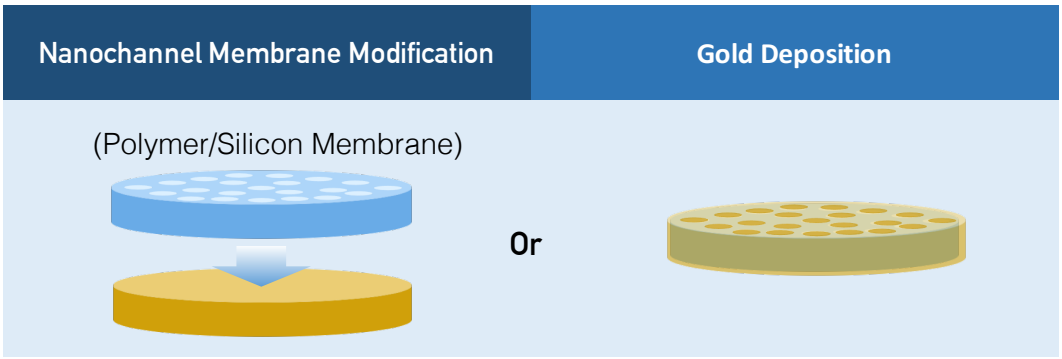

Figure 5.5: Illustration for strategies of electrode modification with nanoporous structure.

Functionalization of Electrode

To take advantage of the large specific area of the modified nanoporous electrode, a single-stranded probe DNA sequence will be immobilized on the wall surface of the nanochannels. The probe DNA will be modified at the 5' terminus with a thiol group for linking with electrode surface and at the 3′-end with an amine group for redox active probe conjugation. Methylene blue and ferrocene are the most commonly used redox active reporters for electrochemical DNA sensors in recent years. I propose to use methylene blue first to label the oligonucleotide probe. Both methylene blue and ferrocene support efficient, sensitive DNA sensing. Ferrocene can slightly improve signal gain and target affinity. Methylene blue has greater stability for long-term storage, which would benefit repeated electrochemical interrogation and repeated sensing/regeneration iterations. This advantage is more apparent when the sensors are employed in realistically complex sample matrices (Kang *et al.*, 2009). Nanoparticle labels will be a backup strategy in case a better signal is needed.

Multiplexed Detection in Environmental Water

The detection of the most studied fecal indicator, *E. coli*, will first be demonstrated on the nanoporous electrochemical DNA sensor. The study will be extended to other pathogens, *e.g.*, *Salmonella* Typhi, and *Enterococcus faecalis*. The capability of the modified electrochemical DNA sensor for detecting ARGs will also be explored, as they remain serious and growing human health challenges, and have drawn attention in recent years (as described in Chapter 2 of this thesis). Different types of environmental water will be tested to evaluate the performance of the modified electrochemical DNA sensor in complexed matrices, which include:

- Wastewater from wastewater treatment plants,
- Surface water,
- Drinking water,
- Recreational water.

5.2.1.3 Integration of Electrochemical DNA Sensing Platform

Given the ECL described in Chapter 3 and the development of an electrochemical DNA sensor in Section 5.2.1.2, an integrated electrochemical DNA sensing platform will be designed and developed. An illustration of the integration concept is shown in Figure 5.6. Water samples will first flow into the cathodic chamber of the cell lysis unit, then the effluent will be distributed onto multiple electrochemical DNA sensors for specific pathogen detection separately. The DNA sensor with a nanoporous electrode will also potentially serve for sample purification and concentration. The platform will be integrated in a hard drive box with USB port which can be connected to either computer or cell phone. The electrical signals generated from multiple sensor channels will be transferred and readout through electrical devices. Therefore, the platform can be potentially controlled remotely. The challenges involving the integrated platform include the pH adjustment for the effluents from the cell lysis unit, miniaturization of power supplies, affordability and scalability, device control, and the development of the suitable working station.

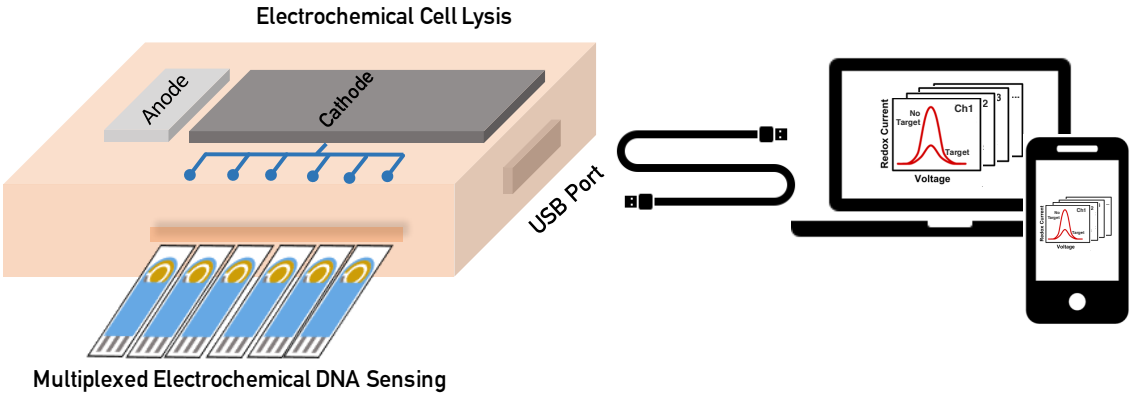

Figure 5.6: Illustration of the integrated electrochemical DNA sensing platform for multiplexed waterborne pathogen detection.

The efforts to develop this integrated electrochemical DNA sensing platform will prospectively realize the on-site waterborne pathogen detection and analysis and solve the challenges of the complex sample preparation, undesirable matrices in environmental water, and the simultaneously multiplexed detection for varied pathogens.

BIBLIOGRAPHY

Agrawal, N.; Hassan, Y. A.; Ugaz, V. M. (2007). "A pocket-sized convective PCR thermocycler". *Angewandte Chemie International Edition*, 46, 4316-4319. https://doi.org/10.1002/anie.200700306.

Ahangari, H.T., Portail, T., Marshall, A.T. (2019). "Comparing the electrocatalytic reduction of CO_2 to CO on gold cathodes in batch and continuous flow electrochemical cells". *Electrochemistry Communications*, 101, 78-81. https://doi.org/10.1016/j.elecom.2019.03.005.

Bahnemann, J.; Rajabi, N.; Fuge, G.; Barradas, O. P.; Muller, J.; Portner, R.; Zeng, A.-P. (2013). "A New Integrated Lab-on-a-Chip System for Fast Dynamic Study of Mammalian Cells under Physiological Conditions in Bioreactor". *Cells*, 2, 349-60. http://doi.org/10.3390/cells2020349.

Bae, S. and Wuertz, S. (2009). "Discrimination of viable and dead fecal bacteroidales bacteria by quantitative PCR with propidium monoazide". *Applied and Environmental Microbiology*, 75, 2940-2944. http://doi.org/10.1128/AEM.01333-08.

Bahi, M.M., Tsaloglou, M.N., Mowlem, M., Morgan, H. (2010). "Electroporation and lysis of marine microalga *Karenia brevis* for RNA extraction and amplification". *Journal of The Royal Society Interface*, 8, 601-608. https://doi.org/10.1098/rsif.2010.0445.

Banihashemi, A.; Van Dyke, M. I.; Huck, P. M. (2015). "Detection of viable bacterial pathogens in a drinking water source using propidium monoazide-quantitative PCR". *Journal of Water Supply: Research and Technology-Aqua*, 64, 139-148. https://doi.org/10.2166/aqua.2014.063.

Bard, A. J., Faulkner, L. R., Leddy, J., Zoski, C. G. (1980). "Electrochemical methods: fundamentals and applications (Vol. 2)". *New York: Wiley*.

Beer K.D., Gargano, J.W., Roberts, V.A., Reses, H.E. Hill, V.R., Garrison, L.E., Kutty, P.K., Hiborn, E.D., Wade, T.J., Fullerton, KE., Yoder, J.S. (2015). "Outbreaks Associated With Environmental and Undetermined Water Exposures — United States, 2011–2012". https://www.cdc.gov/mmwr/preview/mmwrhtml/mm6431a3.htm.

Bielski, B.H.J., Cabelli, D.E., Arudi, R.L., Ross, A.B., (1985). "Reactivity of HO2/O−2 Radicals in Aqueous Solution". *Journal of Physical and Chemical Reference Data*, 14, 1041–1100. https://doi.org/10.1063/1.555739.

Birnboim, H.C. (1983). "A rapid alkaline extraction method for the isolation of plasmid DNA". *Methods in Enzymology*, Academic Press, vol. 100, pp. 243-255. https://doi.org/10.1016/0076-6879(83)00059-2.

Birnboim, H.C. and Doly, J. (1979). "A rapid alkaline extraction procedure for screening recombinant plasmid DNA". *Nucleic acids research*, 7, 1513-1523. https://doi.org/10.1093/nar/7.6.1513.

Blaser, M. J.; Smith, P. F.; Wang, W. L. L.; Hoff, J. C. (1986). "Inactivation of *Campylobacter jejuni* by chlorine and monochloramine". *Applied and Environmental Microbiology*, 51, 307-311.

Bospec Product Inc. website. "Mini bead beater". https://biospec.com.

Boulos, L., Prévost, M., Barbeau, B., Coallier, J., Desjardins, R. (1999). "LIVE/DEAD®BacLight™: application of a new rapid staining method for direct enumeration of viable and total bacteria in drinking water". *Journal of Microbiological Methods*, 37, 77-86. https://doi.org/10.1016/S0167-7012(99)00048-2.

Bruslind, L. (2018). "Bacteria: Cell Walls". *Microbiology*, 4, pp 547.

Burrows, C.J., Muller, J.G. (1998). "Oxidative Nucleobase Modifications Leading to Strand Scission". *Chemical Reviews*. 98, 1109–1152. https://doi.org/10.1021/cr960421s.

Butler, R. C.; Lund, V.; Carlson, D. A. (1987). "Susceptibility of *Campylobacter jejuni* and *Yersinia enterocolitica* to UV-radiation". *Applied and Environmental Microbiology*, 53, 375-378.

Buxton, G.V., Greenstock, C.L., Helman, W.P., Ross, A.B. (1988). "Critical Review of rate constants for reactions of hydrated electrons, hydrogen atoms and hydroxyl radicals (·OH/·O− in Aqueous Solution". *Journal of Physical and Chemical Reference Data* 17, 513–886. https://doi.org/10.1063/1.555805.

Cai, D.; Xiao, M.; Xu, P.; Xu, Y.-C.; Du, W. (2014). "An integrated microfluidic device utilizing dielectrophoresis and multiplex array PCR for point-of-care detection of pathogens. *Lab Chip*, 14, 3917-3924. https://doi.org/10.1039/C4LC00669K.

Catanho, M., Malpass, G.R.P., Motheo, A.J., (2006). "Photoelectrochemical treatment of the dye reactive red 198 using DSA® electrodes". *Applied Catalysis B: Environmental,* 62, 193–200. https://doi.org/10.1016/j.apcatb.2005.07.011.

Cawthorn, D. M. and Witthuhn, R. C. (2008). "Selective PCR detection of viable *Enterobacter sakazakii* cells utilizing propidium monoazide or ethidium bromide monoazide*". Journal of Applied Microbiology*, 105, 1178-1185. https://doi.org/10.1111/j.1365-2672.2008.03851.x.

Centers for Diease Control and Prevention (CDC) (2018). "Global WASH Fast Facts". https://www.cdc.gov/healthywater/global/wash_statistics.html#three.

Centers for Disease Control and Prevention (CDC) (2019). "Antibiotic Resistance Threats In The United States, 2019". https://www.cdc.gov/drugresistance/pdf/threats-report/2019-ar-threats-report-508.pdf.

Chang, P.H., Juhrend, B., Olson, T.M., Marrs, C.F., Wigginton, K.R., (2017). "Degradation of Extracellular Antibiotic Resistance Genes with UV254 Treatment". *Environmental Science & Technology*, 51, 6185–6192. https://doi.org/10.1021/acs.est.7b01120.

Chen, J., Kadlubar, F.F., Chen, J.Z., (2007). "DNA supercoiling suppresses real-time PCR: a new approach to the quantification of mitochondrial DNA damage and repair". *Nucleic Acids Research* 35, 1377–1388. https://doi.org/10.1093/nar/gkm010.

Cheng, X., Peng, C., You, M., Liu, L., Zhang, Y., Fan, Q. (2006). "Characterization of catalysts and membrane in DMFC lifetime testing". *Electrochimica Acta*, 51, 4620-4625. https://doi.org/10.1016/j.electacta.2005.12.043.

Cho, K. and Hoffmann, M. R. (2014). "Urea degradation by electrochemically generated reactive chlorine species: products and reaction pathways". *Environmental Science & Technology*, 48, 11504-11511. http://doi.org/10.1021/es5025405.

Christensen, P.A., Curtis, T.P., Egerton, T.A., Kosa, S.A.M., Tinlin, J.R., (2003). "Photoelectrocatalytic and photocatalytic disinfection of *E. coli* suspensions by titanium dioxide". *Applied Catalysis B: Environmental*, 41, 371–386. https://doi.org/10.1016/S0926-3373(02)00172-8.

Cid, C. A., Jasper, J.T., Hoffmann, M. R. (2018). "Phosphate Recovery from Human Waste via the Formation of Hydroxyapatite during Electrochemical Wastewater Treatment". *ACS Sustainable Chemistry & Engineering*, 6, 3135-3142. https://doi.org/10.1021/acssuschemeng.7b03155.

Clark, L.C., Lyons, C., (1962). "Electrode Systems for Continuous Monitoring in Cardiovascular Surgery". *Annals of the New York Academy of Sciences*, 102, 29–45. https://doi.org/10.1111/j.1749-6632.1962.tb13623.x.

Connick, R.E., (1947). "The Interaction of Hydrogen Peroxide and Hypochlorous Acid in Acidic Solutions Containing Chloride Ion". *Journal of the American Chemical Society*, 69, 1509–1514. https://doi.org/10.1021/ja01198a074.

Coward, J.E. and Rosenkranz, H.S. (1975). "Electron microscopic appearance of silver sulfadiazine-treated *Enterobacter cloacae*". *Chemotherapy*, 21, 231-235. https://doi.org/10.1159/000221863.

Czekalski, N., Imminger, S., Salhi, E., Veljkovic, M., Kleffel, K., Drissner, D., Hammes, F., Bürgmann, H., von Gunten, U., (2016). "Inactivation of Antibiotic Resistant Bacteria and Resistance Genes by Ozone: From Laboratory Experiments to Full-Scale Wastewater

Treatment". *Environmental Science & Technology*, 50, 11862–11871. https://doi.org/10.1021/acs.est.6b02640.

Daggumati, P., Appelt, S., Matharu, Z., Marco, M.L., Seker, E., (2016). "Sequence-Specific Electrical Purification of Nucleic Acids with Nanoporous Gold Electrodes". *Journal of the American Chemical Society*, 138, 7711–7717. https://doi.org/10.1021/jacs.6b03563.

Davalos, R.V. and Rubinsky, B. (2008). "Temperature considerations during irreversible electroporation", *International journal of heat and mass transfer*, 51, 5617-5622. https://doi.org/10.1016/j.ijheatmasstransfer.2008.04.046.

de Lange, N., Tran, T.M., Abate, A.R. (2016). "Electrical lysis of cells for detergent-free droplet assays". *Biomicrofluidics*, 10, 024114. https://doi.org/10.1063/1.4944742.

Detraglia, M. C.; Brand, J. S.; Tometsko, A. M. (1978). "Characterization of azidobenzamidines as photoaffinity labels for trypsin". *Journal of Biological Chemistry*, 253, 1846-1852.

Di Carlo, D., Ionescu-Zanetti, C., Zhang, Y., Hung, P., Lee, L.P. (2005). "On-chip cell lysis by local hydroxide generation". *Lab on a Chip*, 5, 171-178. https://doi.org/10.1039/B413139H.

Drummond, T.G., Hill, M.G., Barton, J.K., (2003). "Electrochemical DNA sensors". *Nature Biotechnology*, 21, 1192–1199. https://doi.org/10.1038/nbt873.

Egan, C.M., Sridhar, S., Wigler, M., Hall, I.M., (2007). "Recurrent DNA copy number variation in the laboratory mouse". *Nature Genetics*, 39, 1384–1389. https://doi.org/10.1038/ng.2007.19.

Escosura-Muñiz, A. de la, Merkoçi, A., (2011). "A Nanochannel/Nanoparticle-Based Filtering and Sensing Platform for Direct Detection of a Cancer Biomarker in Blood". *Small*, 7, 675–682. https://doi.org/10.1002/smll.201002349.

Eumkeb, G. and Chukrathok, S. (2013). "Synergistic activity and mechanism of action of ceftazidime and apigenin combination against ceftazidime-resistant *Enterobacter cloacae*". *Phytomedicine*, 20, 262-269. https://doi.org/10.1016/j.phymed.2012.10.008.

Experton, J., Wilson, A.G., Martin, C.R. (2016). "Low-Voltage Flow-Through Electroporation in Gold-Microtube Membranes". *Analytical Chemistry*, 88, 12445-12452. https://doi.org/10.1021/acs.analchem.6b03820.

Feng, Y., Yang, L., Liu, J., E. Logan, B., (2016). "Electrochemical technologies for wastewater treatment and resource reclamation". *Environmental Science: Water Research & Technology*, 2, 800–831. https://doi.org/10.1039/C5EW00289C.

Fittipaldi, M.; Nocker, A.; Codony, F. (2012). "Progress in understanding preferential detection of live cells using viability dyes in combination with DNA amplification". *Journal of Microbiological Methods*, 91, 276-289. https://doi.org/10.1016/j.mimet.2012.08.007.

Fleming, A., (1942). Nobel lecture, December 11, 1945. Nobel Lectures, Physiology or Medicine, 1962, 83–93.

Fujishima, A., Honda, K., (1972). "Electrochemical Photolysis of Water at a Semiconductor Electrode". *Nature*, 238, 37–38. https://doi.org/10.1038/238037a0.

Gabardo, C.M., Kwong, A.M., Soleymani, L. (2015). "Rapidly prototyped multi-scale electrodes to minimize the voltage requirements for bacterial cell lysis". *Analyst*, 140, 1599-1608. https://doi.org/10.1039/C4AN02150A.

Gao, J., Yin, X.-F., Fang, Z.-L. (2004). "Integration of single cell injection, cell lysis, separation and detection of intracellular constituents on a microfluidic chip". *Lab on a Chip*, 4, 47-52. https://doi.org/10.1039/B310552K.

Geng, T. and Lu, C. (2013). "Microfluidic electroporation for cellular analysis and delivery". *Lab on a Chip*, 13, 3803-3821. https://doi.org/10.1039/C3LC50566A.

Ghuysen, J.M. and Hakenbeck, R. (1994), "Bacterial cell wall", *Elsevier*.

Gibson, D.G., Young, L., Chuang, R.Y., Venter, J.C., Hutchison, C.A., Smith, H.O., (2009). "Enzymatic assembly of DNA molecules up to several hundred kilobases". *Nature Methods*, 6, 343–345. https://doi.org/10.1038/nmeth.1318.

Gilbert, B.C., Stell, J.K., Peet, W.J., Radford, K.J., (1988). "Generation and reactions of the chlorine atom in aqueous solution". *Journal of the Chemical Society, Faraday Transactions*, 1, 84, 3319–3330. https://doi.org/10.1039/F19888403319.

Girones, R.; Antonia Ferrus, M.; Luis Alonso, J.; Rodriguez-Manzano, J.; Calgua, B.; de Abreu Correa, A.; Hundesa, A.; Carratala, A.; Bofill-Mas, S. (2010). "Molecular detection of pathogens in water - the pros and cons of molecular techniques". *Water Research*, 44, 4325-4339. https://doi.org/10.1016/j.watres.2010.06.030.

Grebel, J.E., Pignatello, J.J., Mitch, W.A., (2010). "Effect of Halide Ions and Carbonates on Organic Contaminant Degradation by Hydroxyl Radical-Based Advanced Oxidation Processes in Saline Waters". *Environmental Science & Technology*, 44, 6822–6828. https://doi.org/10.1021/es1010225.

Grieshaber, D., MacKenzie, R., Vörös, J., Reimhult, E., (2008). "Electrochemical Biosensors - Sensor Principles and Architectures". *Sensors*, 8, 1400–1458. https://doi.org/10.3390/s80314000.

Guo, C., Wang, K., Hou, S., Wan, L., Lv, J., Zhang, Y., Qu, X., Chen, S., Xu, J., (2017). "H2O2 and/or TiO2 photocatalysis under UV irradiation for the removal of antibiotic resistant bacteria and their antibiotic resistance genes". *Journal of Hazardous Materials*, 323, 710–718. https://doi.org/10.1016/j.jhazmat.2016.10.041.

Guo, M.T., Yuan, Q.B., Yang, J., (2015). "Distinguishing Effects of Ultraviolet Exposure and Chlorination on the Horizontal Transfer of Antibiotic Resistance Genes in Municipal Wastewater". *Environmental Science & Technology*, 49, 5771–5778. https://doi.org/10.1021/acs.est.5b00644.

Guo, M.T., Yuan, Q.B., Yang, J., (2013). "Microbial selectivity of UV treatment on antibiotic-resistant heterotrophic bacteria in secondary effluents of a municipal wastewater treatment plant". *Water Research*, 47, 6388–6394. https://doi.org/10.1016/j.watres.2013.08.012.

Graham D.W., Olivares-Rieumont, S., Knapp, C.W., Lima, L., Werner, D., Bowen, E. (2011). "Antibiotic Resistance Gene Abundances Associated with Waste Discharges to the Almendares River near Havana, Cuba". *Environmental Science & Technology*, 45, 418-424. https://doi.org/10.1021/es102473z.

Haberl, S., Jarc, M., Štrancar, A., Peterka, M., Hodžić, D., Miklavčič, D. (2013). "Comparison of Alkaline Lysis with Electroextraction and Optimization of Electric Pulses to Extract Plasmid DNA from *Escherichia coli*". *The Journal of Membrane Biology*, 246, 861-867. https://doi.org/10.1007/s00232-013-9580-5.

Hammond, S.M., Lambert, P.A., Rycroft, A. (2012). "The bacterial cell surface". Springer Science & Business Media.

Harrison, S.T.L. (1991). "Bacterial cell disruption: A key unit operation in the recovery of intracellular products". *Biotechnology Advances*, 9, 217-240. https://doi.org/10.1016/0734-9750(91)90005-G.

Hawtin, P.; Hardern, I.; Wittig, R.; Mollenhauer, J.; Poustka, A.; Salowsky, R.; Wulff, T.; Rizzo, C.; Wilson, B. (2005). "Utility of lab-on-a-chip technology for high-throughput nucleic acid and protein analysis". *Electrophoresis*, 26, 3674-3681. https://doi.org/10.1002/elps.200500166.

Hayhurst, E.J., Kailas, L., Hobbs, J.K., Foster, S.J. (2008). "Cell wall peptidoglycan architecture in Bacillus subtilis". *Proceedings of the National Academy of Sciences*, 105, 14603-14608. https://doi.org/10.1073/pnas.0804138105.

Harper, J.C., Christensen, P.A., Egerton, T.A., Curtis, T.P., Gunlazuardi, J., (2001). "Effect of catalyst type on the kinetics of the photoelectrochemical disinfection of water inoculated with *E. coli*". *Journal of Applied Electrochemistry*, 31, 623–628. https://doi.org/10.1023/A:1017539328022.

Hasegawa, K., Neta, P., (1978). "Rate constants and mechanisms of reaction of chloride (Cl2-) radicals". *The Journal of Physical Chemistry*, 82, 854–857. https://doi.org/10.1021/j100497a003.

Hawkins, C.L., Davies, M.J., (1998). "Degradation of Hyaluronic Acid, Poly- and Mono-Saccharides, and Model Compounds by Hypochlorite: Evidence for Radical Intermediates and Fragmentation". *Free Radical Biology and Medicine*, 24, 1396–1410. https://doi.org/10.1016/S0891-5849(98)00009-4.

Hayes, F., (2003). "The Function and Organization of Plasmids, in: Casali, N., Preston, A. (Eds.), *E. Coli* Plasmid Vectors: Methods and Applications, Methods in Molecular Biology™". *Humana Press*, Totowa, NJ, pp. 1–17. https://doi.org/10.1385/1-59259-409-3:1.

He, H., Zhou, P., Shimabuku, K.K., Fang, X., Li, S., Lee, Y., Dodd, M.C., (2019). "Degradation and Deactivation of Bacterial Antibiotic Resistance Genes during Exposure to Free Chlorine, Monochloramine, Chlorine Dioxide, Ozone, Ultraviolet Light, and Hydroxyl Radical". *Environmental Science & Technology*, 53, 2013–2026. https://doi.org/10.1021/acs.est.8b04393.

He, J. W. and Jiang, S. (2005). "Quantification of enterococci and human adenoviruses in environmental samples by real-time PCR". *Applied and Environmental Microbiology*, 71, 2250-2255. https://doi.org/10.1128/AEM.71.5.2250-2255.2005.

Heid, C.A., Stevens, J., Livak, K.J., Williams, P.M. (1996). "Real time quantitative PCR". *Genome Research*, 6, 986-994. http://doi.org/ 10.1101/gr.6.10.986.

Hixon, S.C.; White, W.E.; Yielding, K.L. (1975). "Selective covalent binding of an ethidium analog to mitochondrial-DNA with production of petite mutants in yeast by photoaffinity labeling". *Journal of molecular biology*, 92, 319-329. http://doi.org/10.1016/0022-2836(75)90231-4.

Ho, C.W., Tan, W.S., Yap, W.B., Ling, T.C., Tey, B.T. (2008). "Comparative evaluation of different cell disruption methods for the release of recombinant hepatitis B core antigen from *Escherichia coli*". *Biotechnology and Bioprocess Engineering*, 13, 577-583. https://doi.org/10.1007/s12257-008-0020-9.

Hoffmann, M.R., Martin, S.T., Choi, Wonyong., Bahnemann, D.W., 1995. "Environmental Applications of Semiconductor Photocatalysis". *Chemical Reviews*, 95, 69–96. https://doi.org/10.1021/cr00033a004.

Hopkins, T.R. (1991). "Physical and chemical cell disruption for the recovery of intracellular proteins". *Bioprocess Technol*, 12, 57-83.

Hsieh, K., Ferguson, B.S., Eisenstein, M., Plaxco, K.W., Soh, H.T., (2015). "Integrated Electrochemical Microsystems for Genetic Detection of Pathogens at the Point of Care". *Accounts of Chemical Research*, 48, 911–920. https://doi.org/10.1021/ar500456w.

Hu, Y., Zhang, T., Jiang, L., Yao, S., Ye, H., Lin, K., Cui, C., (2019). "Removal of sulfonamide antibiotic resistant bacterial and intracellular antibiotic resistance genes by UVC-activated

peroxymonosulfate". *Chemical Engineering Journal*, 368, 888–895. https://doi.org/10.1016/j.cej.2019.02.207.

Iakovides, I.C., Michael-Kordatou, I., Moreira, N.F.F., Ribeiro, A.R., Fernandes, T., Pereira, M.F.R., Nunes, O.C., Manaia, C.M., Silva, A.M.T., Fatta-Kassinos, D., (2019). "Continuous ozonation of urban wastewater: Removal of antibiotics, antibiotic-resistant Escherichia coli and antibiotic resistance genes and phytotoxicity". *Water Research*, 159, 333–347. https://doi.org/10.1016/j.watres.2019.05.025.

Invitrogen by Life Technologies (2012). "User guide for PureLink® Genomic DNA Kit: For purification of genomic DNA". http://tools.thermofisher.com/content/sfs/manuals/purelink_genomic_man.pdf.

Jaikla, S., Maturos, T., Pogfay, T., Neatpisarnvanit, C., Sritongkham, P., Tuantranont, A. (2012). "On-chip irreversible electroporation for bacterial cell membrane rupture". *The 5th 2012 Biomedical Engineering International Conference, Ubon Ratchathani,* pp. 1-5. https://doi.org/10.1109/BMEiCon.2012.6465456.

Jasper, J.T., Yang, Y., Hoffmann, M.R. (2017). "Toxic Byproduct Formation during Electrochemical Treatment of Latrine Wastewater". *Environmental Science & Technology*, 51, 7111-7119. https://doi.org/10.1021/acs.est.7b01002.

Jayson, G.G., Parsons, B.J., Swallow, A.J., (1973). "Some simple, highly reactive, inorganic chlorine derivatives in aqueous solution. Their formation using pulses of radiation and their role in the mechanism of the Fricke dosimeter". *Journal of the Chemical Society, Faraday Transactions*, *1: Physical Chemistry in Condensed Phases*, 69, 1597–1607. https://doi.org/10.1039/F19736901597.

Jha, S.K., Chand, R., Han, D., Jang, Y.-C., Ra, G.-S., Kim, J.S., Nahm, B.-H., Kim, Y.-S. (2012). "An integrated PCR microfluidic chip incorporating aseptic electrochemical cell lysis and capillary electrophoresis amperometric DNA detection for rapid and quantitative genetic analysis". *Lab on a Chip*, 12, 4455-4464. https://doi.org/10.1039/C2LC40727B.

Jha, S.K., Joo, G.-S., Ra, G.-S., Lee, H.H., Kim, Y.-S. (2011). "Development of PCR microchip for early cancer risk prediction". *IEEE Sensors Journal*, 11, 2065-2070. https://doi.org/10.1109/JSEN.2011.2105262.

Jiang, L.; Mancuso, M.; Lu, Z.; Akar, G.; Cesarman, E.; Erickson, D. (2014). "Solar thermal polymerase chain reaction for smartphone-assisted molecular diagnostics". *Scientific Report*, 4, 4137. http://doi.org/10.1038/srep04137.

Josephson, K. L.; Gerba, C. P.; Pepper, I. L. (1993). "Polymerase chain-reaction detection of nonviable bacterial pathogens". *Applied and Environmental Microbiology*, 59, 3513-3515.

Joy, S.R., Li, X., Snow, D.D., Gilley, J.E., Woodbury, B., Bartelt-Hunt, S.L. (2014). "Fate of antimicrobials and antimicrobial resistance genes in simulated swine manure storage". *Science of The Total Environment*, 481, 69–74. https://doi.org/10.1016/j.scitotenv.2014.02.027.

Kang, D., Zuo, X., Yang, R., Xia, F., Plaxco, K.W., White, R.J. (2009). "Comparing the Properties of Electrochemical-Based DNA Sensors Employing Different Redox Tags". *Analytical Chemistry*, 81, 9109–9113. https://doi.org/10.1021/ac901811n.

Karkman, A., Do, T.T., Walsh, F., Virta, M.P.J. (2018). "Antibiotic-Resistance Genes in Waste Water". *Trends in Microbiology*, 26, 220–228. https://doi.org/10.1016/j.tim.2017.09.005

Kell, D. B.; Kaprelyants, A. S.; Weichart, D. H.; Harwood, C. R.; Barer, M. R. (1998). "Viability and activity in readily culturable bacteria: a review and discussion of the practical issues". *Antonie Van Leeuwenhoek*, 73, 169-187. http://doi.org/10.1023/A:1000664013047.

Kennedy, L.J., Moore, K., Caulfield, J.L., Tannenbaum, S.R., Dedon, P.C. (1997). "Quantitation of 8-Oxoguanine and Strand Breaks Produced by Four Oxidizing Agents". *Chemical Research in Toxicology*, 10, 386–392. https://doi.org/10.1021/tx960102w.

Kim, J.; Byun, D.; Mauk, M. G.; Bau, H. H. (2009). "A disposable, self-contained PCR chip". *Lab Chip*, 9, 606-612. https://doi.org/10.1039/B807915C.

Kim, J., Lim, J., Lee, C. (2013). "Quantitative real-time PCR approaches for microbial community studies in wastewater treatment systems: Applications and considerations". *Biotechnology Advances*, 31, 1358-1373. https://doi.org/10.1016/j.biotechadv.2013.05.010.

Kläning, U.K., Wolff, T. (1985). "Laser Flash Photolysis of HClO, ClO−, HBrO, and BrO− in Aqueous Solution. Reactions of Cl- and Br-Atoms". *Berichte der Bunsengesellschaft für physikalische Chemie*, 89, 243–245. https://doi.org/10.1002/bbpc.19850890309.

Kobayashi, H.; Oethinger, M.; Tuohy, M. J.; Hall, G. S.; Bauer, T. W. (2009). "Improving clinical significance of PCR: use of propidium monoazide to distinguish viable from dead *Staphylococcus aureus* and *Staphylococcus epidermidis*". *Journal of Orthopaedic Research*, 27, 1243-1247. https://doi.org/10.1002/jor.20872.

Koo, M.S., Cho, K., Yoon, J., Choi, W. (2017). "Photoelectrochemical Degradation of Organic Compounds Coupled with Molecular Hydrogen Generation Using Electrochromic TiO2 Nanotube Arrays". *Environmental Science & Technology*, 51, 6590–6598. https://doi.org/10.1021/acs.est.7b00774.

Kostić, T., Stessl, B., Wagner, M., Sessitsch, A. (2011). "Microarray analysis reveals the actual specificity of enrichment media used for food safety assessment". *Journal of Food Protection*, 74, 1030–1034. https://doi.org/10.4315/0362-028X.JFP-10-388.

Kotnik, T., Frey, W., Sack, M., Meglič, S.H., Peterka, M., Miklavčič, D. (2015). "Review: Electroporation-based applications in biotechnology". *Trends in Biotechnology*, 33, 480-488. https://doi.org/10.1016/j.tibtech.2015.06.002.

Krol, J.J., Wessling, M., Strathmann, H. (1999). "Concentration polarization with monopolar ion exchange membranes: current–voltage curves and water dissociation". *Journal of Membrane Science*, 162, 145-154. https://doi.org/10.1016/S0376-7388(99)00133-7.

Law, J.W.-F., Ab Mutalib, N.-S., Chan, K.-G., Lee, L.-H. (2014). "Rapid methods for the detection of foodborne bacterial pathogens: principles, applications, advantages and limitations". *Frontiers in Microbiology*, 5, 770. https://doi.org/10.3389/fmicb.2014.00770.

Lee, D.W. and Cho, Y.-H. (2007). "A continuous electrical cell lysis device using a low dc voltage for a cell transport and rupture". *Sensors and Actuators B: Chemical*, 124, 84-89. https://doi.org/10.1016/j.snb.2006.11.054.

Lee, E.-S.; Lee, M.-H.; Kim, B.-S. (2015). "Evaluation of propidium monoazide-quantitative PCR to detect viable *Mycobacterium fortuitum* after chlorine, ozone, and ultraviolet disinfection". *International Journal of Food Microbiology*, 210, 143-148. https://doi.org/10.1016/j.ijfoodmicro.2015.06.019.

Lee, H.J., Kim, J.-H., Lim, H.K., Cho, E.C., Huh, N., Ko, C., Park, J. C., Choi, J.-W., Lee, S.S. (2010). "Electrochemical cell lysis device for DNA extraction". *Lab on a Chip*, 10, 626-633. https://doi.org/10.1039/B916606H.

Lee, J. G.; Cheong, K. H.; Huh, N.; Kim, S.; Choi, J. W.; Ko, C. (2006). "Microchip-based one step DNA extraction and real-time PCR in one chamber for rapid pathogen identification". *Lab Chip*, 6, 886-895. https://doi.org/10.1039/B515876A.

Lee, S.H. and Rasaiah, J.C. (2011). "Proton transfer and the mobilities of the H^+ and OH^- ions from studies of a dissociating model for water". *The Journal of chemical physics*, 135, 124505. https://doi.org/10.1063/1.3632990.

Lee, Y., Imminger, S., Czekalski, N., von Gunten, U., Hammes, F. (2016). "Inactivation efficiency of Escherichia coli and autochthonous bacteria during ozonation of municipal wastewater effluents quantified with flow cytometry and adenosine tri-phosphate analyses". *Water Research*, 101, 617–627. https://doi.org/10.1016/j.watres.2016.05.089.

Leifels, M.; Jurzik, L.; Wilhelm, M.; Hamza, I. A. (2015). "Use of ethidium monoazide and propidium monoazide to determine viral infectivity upon inactivation by heat, UV-exposure and chlorine". *International Journal of Hygiene and Environmental Health*, 218, 686-693. https://doi.org/10.1016/j.ijheh.2015.02.003.

Li, J., Chen, C.-B., Wang, D.-D., Li, C.-X., Zhang, F., Li, D.-B., Min, D., Li, W.-W., Lam, P.K.S., Yu, H.-Q. (2018). "Solar-Driven Synchronous Photoelectrochemical Sulfur Recovery and

Pollutant Degradation". *ACS Sustainable Chemistry & Engineering*, 6, 9591–9595. https://doi.org/10.1021/acssuschemeng.8b02678.

Li, L.; Mendis, N.; Trigui, H.; Oliver, J. D.; Faucher, S. P. (2014). "The importance of the viable but non-culturable state in human bacterial pathogens". *Frontiers in Microbiology*, 5, 258. https://doi.org/10.3389/fmicb.2014.00258.

Lin, C.-H., Chen, Y.-C., Pan, T.-M. (2011). "Quantification Bias Caused by Plasmid DNA Conformation in Quantitative Real-Time PCR Assay". *PLOS ONE*, 6, e29101. https://doi.org/10.1371/journal.pone.0029101.

Lin, W., Li, S., Zhang, S., Yu, X. (2016). "Reduction in horizontal transfer of conjugative plasmid by UV irradiation and low-level chlorination". *Water Research*, 91, 331–338. https://doi.org/10.1016/j.watres.2016.01.020.

Linsebigler, A.L., Lu, Guangquan., Yates, J.T. (1995). "Photocatalysis on TiO2 Surfaces: Principles, Mechanisms, and Selected Results". *Chemical Reviews*, 95, 735–758. https://doi.org/10.1021/cr00035a013.

Lu, H., Schmidt, M.A., Jensen, K.F. (2005). "A microfluidic electroporation device for cell lysis". *Lab on a Chip*, 5, 23-29. https://doi.org/10.1039/B406205A.

Lubin, A.A., Lai, R.Y., Baker, B.R., Heeger, A.J., Plaxco, K.W. (2006). "Sequence-Specific, Electronic Detection of Oligonucleotides in Blood, Soil, and Foodstuffs with the Reagentless, Reusable E-DNA Sensor". *Analytical Chemistry*, 78, 5671–5677. https://doi.org/10.1021/ac0601819.

Ma, S., Zhan, S., Jia, Y., Shi, Q., Zhou, Q. (2016). "Enhanced disinfection application of Ag-modified g-C3N4 composite under visible light". *Applied Catalysis B: Environmental*, 186, 77–87. https://doi.org/10.1016/j.apcatb.2015.12.051.

Mahalanabis, M., Al-Muayad, H., Kulinski, M.D., Altman, D., Klapperich, C.M. (2009). "Cell lysis and DNA extraction of gram-positive and gram-negative bacteria from whole blood in a disposable microfluidic chip". *Lab on a Chip,* 9, 2811-2817. https://doi.org/10.1039/B905065P.

Mai-Prochnow, A., Clauson, M., Hong, J., Murphy, A.B. (2016). "Gram positive and Gram negative bacteria differ in their sensitivity to cold plasma". *Scientific reports*, 6, 38610. https://doi.org/10.1038/srep38610.

Malpass, G.R.P., Miwa, D.W., Miwa, A.C.P., Machado, S.A.S., Motheo, A.J. (2009). "Study of photo-assisted electrochemical degradation of carbaryl at dimensionally stable anodes (DSA®)". *Journal of Hazardous Materials*, 167, 224–229. https://doi.org/10.1016/j.jhazmat.2008.12.109.

Malpass, G.R.P., Miwa, D.W., Miwa, A.C.P., Machado, S.A.S., Motheo, A.J. (2007). "Photo-Assisted Electrochemical Oxidation of Atrazine on a Commercial Ti/Ru0.3Ti0.7O2 DSA Electrode". *Environmental Science & Technology*, 41, 7120–7125. https://doi.org/10.1021/es070798n.

Matias, V.R.F. and Beveridge, T.J. (2005). "Cryo-electron microscopy reveals native polymeric cell wall structure in *Bacillus subtilis* 168 and the existence of a periplasmic space". *Molecular microbiology*, 56, 240-251. https://doi.org/10.1111/j.1365-2958.2005.04535.x.

Matsushima, H., Fukunaka, Y., Kuribayashi, K. (2006). "Water electrolysis under microgravity: Part II. Description of gas bubble evolution phenomena". *Electrochimica Acta*, 51, 4190-4198. https://doi.org/10.1016/j.electacta.2005.11.046.

Mao, F., Leung, W.-Y., Xin, X. (2007). "Characterization of EvaGreen and the implication of its physicochemical properties for qPCR applications". *BMC Biotechnology*, 7, 76. https://doi.org/10.1186/1472-6750-7-76.

Martens, E., Demain, A.L. (2017). "The antibiotic resistance crisis, with a focus on the United States". *The Journal of Antibiotics*, 70, 520–526. https://doi.org/10.1038/ja.2017.30.

Mártire, D.O., Rosso, J.A., Bertolotti, S., Le Roux, G.C., Braun, A.M., Gonzalez, M.C. (2001). "Kinetic Study of the Reactions of Chlorine Atoms and Cl2•- Radical Anions in Aqueous Solutions. II. Toluene, Benzoic Acid, and Chlorobenzene". *The Journal of Physical Chemistry A*, 105, 5385–5392. https://doi.org/10.1021/jp004630z.

Matharu, Z., Daggumati, P., Wang, L., Dorofeeva, T.S., Li, Z., Seker, E. (2017). "Nanoporous-Gold-Based Electrode Morphology Libraries for Investigating Structure–Property Relationships in Nucleic Acid Based Electrochemical Biosensors". *ACS Applied Materials & Interfaces*, 9, 12959–12966. https://doi.org/10.1021/acsami.6b15212.

Matsushima, H., Kiuchi, D., Fukunaka, Y., Kuribayashi, K. (2009). "Single bubble growth during water electrolysis under microgravity". *Electrochemistry Communications*, 11, 1721-1723. https://doi.org/10.1016/j.elecom.2009.07.009.

Matthew, B.M., Anastasio, C. (2006). "A chemical probe technique for the determination of reactive halogen species in aqueous solution: Part 1 - bromide solutions". *Atmospheric Chemistry and Physics*, 6, 2423–2437. https://doi.org/10.5194/acp-6-2423-2006.

McKinney, C.W., Pruden, A. (2012). "Ultraviolet Disinfection of Antibiotic Resistant Bacteria and Their Antibiotic Resistance Genes in Water and Wastewater". *Environmental Science & Technology*, 46, 13393–13400. https://doi.org/10.1021/es303652q.

Michael-Kordatou, I., Andreou, R., Iacovou, M., Frontistis, Z., Hapeshi, E., Michael, C., Fatta-Kassinos, D. (2017). "On the capacity of ozonation to remove antimicrobial compounds, resistant bacteria and toxicity from urban wastewater effluents". *Journal of Hazardous*

Materials, Special Issue on Emerging Contaminants in engineered and natural environment 323, 414–425. https://doi.org/10.1016/j.jhazmat.2016.02.023.

Minami, J.; Yoshida, K.; Soejima, T.; Yaeshima, T.; Iwatsuki, K. (2010). "New approach to use ethidium bromide monoazide as an analytical tool". *Journal of Applied Microbiology*, 109, 900-909. http://doi.org/10.1111/j.1365-2672.2010.04716.x.

Mohammadali, M., Davies, J. (2017). "Antimicrobial Resistance Genes and Wastewater Treatment, in: Antimicrobial Resistance in Wastewater Treatment Processes". *John Wiley & Sons, Ltd*, pp. 1–13. https://doi.org/10.1002/9781119192428.ch1.

Mohite, S.V., Ganbavle, V.V., Rajpure, K.Y. (2017). "Photoelectrochemical performance and photoelectrocatalytic degradation of organic compounds using Ga:WO3 thin films". *Journal of Photochemistry and Photobiology A: Chemistry*, 344, 56–63. https://doi.org/10.1016/j.jphotochem.2017.04.032.

Mollavali, M., Falamaki, C., Rohani, S. (2018). "Efficient light harvesting by NiS/CdS/ZnS NPs incorporated in C, N-co-doped-TiO2 nanotube arrays as visible-light sensitive multilayer photoanode for solar applications". *International Journal of Hydrogen Energy*, 43, 9259–9278. https://doi.org/10.1016/j.ijhydene.2018.03.102.

MP Biomedicals, LLC. website. "FastPrep-24 5G™ High Speed Homogenizer". https://www.mpbio.com/.

Nan, L., Jiang, Z., Wei, X. (2014). "Emerging microfluidic devices for cell lysis: a review". *Lab on a Chip - Miniaturisation for Chemistry & Biology*, 14, 1060-1073. https://doi.org/10.1039/C3LC51133B.

Nevill, J.T., Cooper, R., Dueck, M., Breslauer, D.N., Lee, L.P. (2007). "Integrated microfluidic cell culture and lysis on a chip". *Lab on a Chip*, 7, 1689-1695. https://doi.org/10.1039/B711874K.

NDRL/NIST Solution Kinetics Database [WWW Document], https://kinetics.nist.gov/solution/ (accessed 9.20.19).

Nihemaiti, M., Yoon, Y., He, H., Dodd, M.C., Croué, J.-P., Lee, Y. (2020). "Degradation and deactivation of a plasmid-encoded extracellular antibiotic resistance gene during separate and combined exposures to UV254 and radicals". *Water Research* 115921. https://doi.org/10.1016/j.watres.2020.115921.

Nocker, A. and Camper, A.K. (2006b). "Selective removal of DNA from dead cells of mixed bacterial communities by use of ethidium monoazide". *Applied and Environmental Microbiology*, 72, 1997-2004. http://doi.org/10.1128/AEM.72.3.1997-2004.2006.

Nocker, A.; Cheung, C.Y.; Camper, A.K. (2006a). "Comparison of propidium monoazide with ethidium monoazide for differentiation of live vs. dead bacteria by selective removal of DNA

from dead cells". *Journal of Microbiological Methods*, 67, 310-320. https://doi.org/10.1016/j.mimet.2006.04.015.

Nocker, A.; Sossa-Fernandez, P.; Burr, M.D.; Camper, A.K. (2007a). "Use of propidium monoazide for live/dead distinction in microbial ecology". *Applied and Environmental Microbiology*, 73, 5111-5117. http://doi.org/10.1128/AEM.02987-06.

Nocker, A.; Sossa, K.E.; Camper, A.K. (2007b). "Molecular monitoring of disinfection efficacy using propidium monoazide in combination with quantitative PCR *Journal of Microbiological Methods*, 70, 252-260. http://doi.org/10.1016/j.mimet.2007.04.014.

Norian, H.; Field, R. M.; Kymissis, I.; Shepard, K. L. (2014). "An integrated CMOS quantitative-polymerase-chain-reaction lab-on-chip for point-of-care diagnostics". *Lab Chip*, 14, 4076-4084. http://doi.org/10.1039/C4LC00443D.

Oberoi, A.S., Jia, Y., Zhang, H., Khanal, S.K., Lu, H. (2019). "Insights into the Fate and Removal of Antibiotics in Engineered Biological Treatment Systems: A Critical Review". *Environmental Science & Technology*, 53, 7234–7264. https://doi.org/10.1021/acs.est.9b01131.

OMNI Inc. website. "Bead ruptor". https://www.omni-inc.com.

O'Neill, J. (2014). "Review on AMR. Antimicrobial resistance: tackling a crisis for the health and wealth of nations".

O'Neil, J. (2016). "Review on Antimicrobial Resistance: Tackling drug-resistant infections globally: final report and recommendations".

Pan, Y. and Breidt, F., Jr. (2007). "Enumeration of viable *Listeria monocytogenes* cells by real-time PCR with propidium monoazide and ethidium monoazide in the presence of dead cells". *Applied and Environmental Microbiology*, 73, 8028-8031. http://doi.org/10.1128/AEM.01198-07.

Pang, Y., Huang, J., Xi, J., Hu, H., Zhu, Y. (2016). "Effect of ultraviolet irradiation and chlorination on ampicillin-resistant Escherichia coli and its ampicillin resistance gene". *Frontiers of Environmental Science & Engineering*, 10, 522–530. https://doi.org/10.1007/s11783-015-0779-9.

Park, H., Vecitis, C.D., Hoffmann, M.R. (2009). "Electrochemical Water Splitting Coupled with Organic Compound Oxidation: The Role of Active Chlorine Species". *The Journal of Physical Chemistry C*, 113, 7935–7945. https://doi.org/10.1021/jp810331w.

Pelegrini, R.T., Freire, R.S., Duran, N., Bertazzoli, R. (2001). "Photoassisted Electrochemical Degradation of Organic Pollutants on a DSA Type Oxide Electrode: Process Test for a Phenol Synthetic Solution and Its Application for the E1 Bleach Kraft Mill Effluent". *Environmental Science & Technology*, 35, 2849–2853. https://doi.org/10.1021/es001784j.

Pinhedo, L., Pelegrini, R., Bertazzoli, R., Motheo, A.J. (2005). "Photoelectrochemical degradation of humic acid on a (TiO2)0.7(RuO2)0.3 dimensionally stable anode". *Applied Catalysis B: Environmental*, 57, 75–81. https://doi.org/10.1016/j.apcatb.2004.10.006.

Pliquett, U. (2003). "Joule heating during solid tissue electroporation". *Medical and Biological Engineering and Computing*, 41, 215-219. https://doi.org/10.1007/BF02344892.

Poudineh, M., Mohamadi, R.M., Sage, A., Mahmoudian, L., Sargent, E.H., Kelley, S.O. (2014). "Three-dimensional, sharp-tipped electrodes concentrate applied fields to enable direct electrical release of intact biomarkers from cells". *Lab on a Chip*, 14, 1785-1790. https://doi.org/10.1039/C4LC00144C.

Pruess-Ustuen, A.; Bartram, J.; Clasen, T.; Colford, J. M., Jr.; Cumming, O.; Curtis, V.; Bonjour, S.; Dangour, A. D.; De France, J.; Fewtrell, L.; Freeman, M. C.; Gordon, B.; Hunter, P. R.; Johnston, R. B.; Mathers, C.; Maeusezahl, D.; Medlicott, K.; Neira, M.; Stocks, M.; Wolf, J.; Cairncross, S. (2014). "Burden of disease from inadequate water, sanitation and hygiene in low- and middle-income settings: a retrospective analysis of data from 145 countries". *Tropical Medicine & International Health*, 19, 894-905. https://doi.org/10.1111/tmi.12329.

Prüss-Üstün, A.; Bos, R.; Gore, F.; Bartram, J. (2008). "Safer water, better health: costs, benefits and sustainability of interventions to protect and promote health". World Health Organization, Geneva. https://apps.who.int/iris/bitstream/handle/10665/43840/9789241596435_eng.pdf;jsessionid=FD7503C682C84B60824F7FF6C61792C8?sequence=1.

Qi, F., An, W., Wang, H., Hu, J., Guo, H., Liu, L., Cui, W. (2020). "Combing oxygen vacancies on TiO2 nanorod arrays with g-C3N4 nanosheets for enhancing photoelectrochemical degradation of phenol". *Materials Science in Semiconductor Processing*, 109, 104954. https://doi.org/10.1016/j.mssp.2020.104954.

Qiagen website. "TissueLyser II". https://www.qiagen.com.

Rahn, R.O. (1997). "Potassium Iodide as a Chemical Actinometer for 254 nm Radiation: Use of Iodate as an Electron Scavenger". *Photochemistry and Photobiology*, 66, 450–455. https://doi.org/10.1111/j.1751-1097.1997.tb03172.x.

Ramírez-Castillo, F.Y., Loera-Muro, A., Jacques, M., Garneau, P., Avelar-González, F. J., Harel, J., Guerrero-Barrera, A. L. (2015). "Waterborne pathogens: detection methods and challenges". *Pathogens*， *4*, 307–334. https://doi.org/10.3390/pathogens4020307.

Rajabi, N.; Bahnemann, J.; Tzeng, T.-N.; Barradas, O. P.; Zeng, A.-P.; Mueller, J. (2014). "Lab-on-a-chip for cell perturbation, lysis, and efficient separation of sub-cellular components in a continuous flow mode". *Sensors and Actuators A: Physical*, 215, 136-143. https://doi.org/10.1016/j.sna.2013.12.019.

Rawsthorne, H.; Dock, C. N.; Jaykus, L. A. (2009). "PCR-based method Using propidium monoazide To distinguish viable from nonviable Bacillus subtilis spores". *Applied and Environmental Microbi*ology, 75, 2936-2939. http://doi.org/10.1128/AEM.02524-08.

Reta, N., Michelmore, A., Saint, C., Prieto-Simón, B., Voelcker, N.H. (2016). "Porous silicon membrane-modified electrodes for label-free voltammetric detection of MS2 bacteriophage". *Biosensors and Bioelectronics*, 80, 47–53. https://doi.org/10.1016/j.bios.2016.01.038.

Rozière, J. and Jones, D.J. (2003). "Non-Fluorinated Polymer Materials for Proton Exchange Membrane Fuel Cells". *Annual Review of Materials Research*, 33, 503-555. https://doi.org/10.1146/annurev.matsci.33.022702.154657.

Salam, K.W.; El-Fadel, M.; Barbour, E.K.; Saikaly, P.E. (2014). "A propidium monoazide-quantitative PCR method for the detection and quantification of viable Enterococcus faecalis in large-volume samples of marine waters". *Applied Microbiology and Biotechnology*, 98, 8707-8718. http://doi.org/10.1007/s00253-014-6023-x.

Sanchez, M.C.; Marin, M.J.; Figuero, E.; Llama-Palacios, A.; Leon, R.; Blanc, V.; Herrera, D.; Sanz, M. (2014). "Quantitative real-time PCR combined with propidium monoazide for the selective quantification of viable periodontal pathogens in an *in vitro* subgingival biofilm model". *Journal of Periodontal Research*, 49, 20-28. https://doi.org/10.1111/jre.12073.

Sedgwick, H., Caron, F., Monaghan, P.B., Kolch, W., Cooper, J.M. (2008). "Lab-on-a-chip technologies for proteomic analysis from isolated cells". *Journal of the Royal Society Interface*, 5, S123-S130. https://doi.org/10.1098/rsif.2008.0169.focus.

Seinige, D.; Krischek, C.; Klein, G.; Kehrenberg, C. (2014). "Comparative analysis and limitations of ethidium monoazide and propidium monoazide treatments for the differentiation of viable and nonviable Campylobacter cells". *Applied and Environmental Microbi*ology, 80, 2186-2192. http://doi.org/10.1128/AEM.03962-13.

Shahini, M. and Yeow, J.T. (2013). "Cell electroporation by CNT-featured microfluidic chip". *Lab on a Chip*, 13, 2585-2590. https://doi.org/10.1039/C3LC00014A.

Shehadul Islam, M., Aryasomayajula, A., Selvaganapathy, R.P. (2017). "A Review on Macroscale and Microscale Cell Lysis Methods". *Micromachines*, 8. https://doi.org/10.3390/mi8030083.

Shi, P., Jia, S., Zhang, X.-X., Zhang, T., Cheng, S., Li, A. (2013). "Metagenomic insights into chlorination effects on microbial antibiotic resistance in drinking water". *Water Research*, 47, 111–120. https://doi.org/10.1016/j.watres.2012.09.046.

Simons, R. (1979). "Strong electric field effects on proton transfer between membrane-bound amines and water". *Nature*, 280, 824-826. https://doi.org/10.1038/280824a0.

Soejima, T.; Schlitt-Dittrich, F.; Yoshida, S.-i. (2011). "Polymerase chain reaction amplification length-dependent ethidium monoazide suppression power for heat-killed cells of Enterobacteriaceae". *Analytical Biochemistry*., 418, 37-43. http://doi.org/10.1016/j.ab.2011.06.027.

Souza, F.L., Aquino, J.M., Miwa, D.W., Rodrigo, M.A., Motheo, A.J. (2014). "Photo-assisted electrochemical degradation of the dimethyl phthalate ester on DSA® electrode". *Journal of Environmental Chemical Engineering*, 2, 811–818. https://doi.org/10.1016/j.jece.2014.02.003.

Straub, T.M., Chandler, D.P. (2003). "Towards a unified system for detecting waterborne pathogens". *Journal of Microbiological Methods*, 53, 185–197. https://doi.org/10.1016/s0167-7012(03)00023-x.

Suquet, C., Warren, J.J., Seth, N., Hurst, J.K. (2010). "Comparative study of HOCl-inflicted damage to bacterial DNA ex vivo and within cells". *Archives of Biochemistry and Biophysics*, 493, 135–142. https://doi.org/10.1016/j.abb.2009.10.006.

Suzuki, M. T.; Taylor, L. T.; DeLong, E. F. (2000). "Quantitative analysis of small-subunit rRNA genes in mixed microbial populations via 5 '-nuclease assays". *Applied and Environmental Microbi*ology, 66, 4605-4614. http://doi.org/10.1128/AEM.66.11.4605-4614.2000.

Tanaka, Y., Moon, S.-H., Nikonenko, V.V., Xu, T. (2012). "Ion-exchange membranes". *International Journal of Chemical Engineering, 2012*. http://doi.org/10.1155/2012/906952.

Taylor, M. J.; Bentham, R. H.; Ross, K. E. (2014). "Limitations of using propidium monoazide with qPCR to discriminate between live and dead Legionella in biofilm samples". *Microbiology Insights*, 7, 15-24. http://doi.org/10.4137/MBI.S17723.

Thevenot, D.R., Tóth, K., Durst, R.A., Wilson, G.S. (1999). "Electrochemical Biosensors: Recommended Definitions and Classification". *Pure and Applied Chemistry*, 71, 2333–2348. https://doi.org/10.1351/pac199971122333.

Thomas, C.M., Nielsen, K.M. (2005). "Mechanisms of, and Barriers to, Horizontal Gene Transfer between Bacteria". *Nature Reviews Microbiology*, 3, 711–721. https://doi.org/10.1038/nrmicro1234.

Tsong, T. Y. (1991). "Electroporation of cell membranes". *Biophysical Journal*, 60, 297-306. http://doi.org/10.1016/S0006-3495(91)82054-9.

Umar, M., Roddick, F., Fan, L. (2019). "Moving from the traditional paradigm of pathogen inactivation to controlling antibiotic resistance in water - Role of ultraviolet irradiation". *Science of The Total Environment*, 662, 923–939. https://doi.org/10.1016/j.scitotenv.2019.01.289.

U.S. Environmental Protection Agency (USEPA) (2006). "Ultraviolet disinfection guidance manual for the final long term 2 enhanced surface water treatment rule". https://www.epa.gov/dwreginfo/long-term-2-enhanced-surface-water-treatment-rule-documents.

U.S. Environmental Protection Agency (USEPA) (2010). "Method B: Bacteroidales in Water by TaqMan® Quantitative Polymerase Chain Reaction (qPCR) Assay." https://www.epa.gov/sites/production/files/2019-03/documents/method-b-bacteroidales-2010.pdf.

van Burik, J.A.H., Schreckhise, R.W., White, T.C., Bowden, R.A., Myerson, D. (1998). "Comparison of six extraction techniques for isolation of DNA from filamentous fungi". *Medical Mycology*, 36, 299-303. https://doi.org/10.1080/02681219880000471.

van der Hoek, J.P., Bertelkamp, C., Verliefde, A., Singhal, N. (2014). "Drinking water treatment technologies in Europe: state of the art–challenges–research needs". *Journal of Water Supply: Research and Technology—AQUA*, 63, 124–130. https://doi.org/10.2166/aqua.2013.007.

Varma, M.; Field, R.; Stinson, M.; Rukovets, B.; Wymer, L.; Hauglanda, R. (2009). "Quantitative real-time PCR analysis of total and propidium monoazide-resistant fecal indicator bacteria in wastewater". *Water Research*, 43, 4790-4801. http://doi.org/10.1016/j.watres.2009.05.031.

Ventola, C.L. (2015). "The Antibiotic Resistance Crisis". *P & T: a peer-reviewed journal for formulary management*, 40(4), 277–283. 40, 277–283.

Vera, E. A. and Ruiz, J. R. (2012). "In Comparison Between Turbulent and Laminar Bubbly-Flow for Modeling H_2/H_2O Separation". *COMSOL Conference*, Milan.

Vollmer, W., Blanot, D., De Pedro, M.A. (2008). "Peptidoglycan structure and architecture". *FEMS microbiology reviews*, 32, 149-167. https://doi.org/10.1111/j.1574-6976.2007.00094.x.

Von Sonntag, C., Von Gunten, U. (2012). "Chemistry of ozone in water and wastewater treatment". *IWA publishing*.

Walsh, C.T., Wencewicz, T.A. (2014). "Prospects for new antibiotics: a molecule-centered perspective". *The Journal of Antibiotics*, 67, 7–22. https://doi.org/10.1038/ja.2013.49.

Wang, H.-Y., Bhunia, A.K., Lu, C. (2006). "A microfluidic flow-through device for high throughput electrical lysis of bacterial cells based on continuous dc voltage". *Biosensors and Bioelectronics*, 22, 582-588. https://doi.org/10.1016/j.bios.2006.01.032.

Wang, J. (2006). "Electrochemical biosensors: Towards point-of-care cancer diagnostics". *Biosensors and Bioelectronics*, 21, 1887–1892. https://doi.org/10.1016/j.bios.2005.10.027.

Wang, S., Zhu, Y., Yang, Y., Li, J., Hoffmann, M.R. (2020). "Electrochemical cell lysis of gram-positive and gram-negative bacteria: DNA extraction from environmental water samples". *Electrochimica Acta*, 338, 135864. https://doi.org/10.1016/j.electacta.2020.135864.

Wang, T.X., Margerum, D.W. (1994). "Kinetics of Reversible Chlorine Hydrolysis: Temperature Dependence and General-Acid/Base-Assisted Mechanisms". *Inorganic Chemistry*, 33, 1050–1055. https://doi.org/10.1021/ic00084a014.

Waring, M. J. (1965). "Complex formation between ethidium bromide and nucleic acids". *Journal of molecular biology*, 13, 269-282. http://doi.org/10.1016/S0022-2836(65)80096-1.

Wongkaew, N., Simsek, M., Griesche, C., Baeumner, A.J. (2019). "Functional Nanomaterials and Nanostructures Enhancing Electrochemical Biosensors and Lab-on-a-Chip Performances: Recent Progress, Applications, and Future Perspective". *Chemical Reviews*, 119, 120–194. https://doi.org/10.1021/acs.chemrev.8b00172.

World Health Organization (WHO) (2015). "WHO world water day report". https://www.who.int/water_sanitation_health/takingcharge.html.

World Healrh Organization (WHO) (2016). "Mortility and burden of disease from water and sanitation". https://www.who.int/gho/phe/water_sanitation/burden_text/en/.

Wu, B.; Liang, W.; Kan, B. (2015). "Enumeration of viable non-culturable *Vibrio cholerae* using propidium monoazide combined with quantitative PCR". *Journal of Microbiological Methods*, 115, 147-152. http://doi.org/10.1016/j.mimet.2015.05.016.

Wu, D., Wong, D., Di Bartolo, B. (1980). "Evolution of Cl−2 in aqueous NaCl solutions". *Journal of Photochemistry*, 14, 303–310. https://doi.org/10.1016/0047-2670(80)85102-1.

Xiao, S., Qu, J., Zhao, X., Liu, H., Wan, D. (2009). "Electrochemical process combined with UV light irradiation for synergistic degradation of ammonia in chloride-containing solutions". *Water Research*, 43, 1432–1440. https://doi.org/10.1016/j.watres.2008.12.023.

Xie, X., Wang, S., Jiang, S.C., Bahnemann, J., Hoffmann, M.R. (2016). S"unlight-Activated Propidium Monoazide Pretreatment for Differentiation of Viable and Dead Bacteria by Quantitative Real-Time Polymerase Chain Reaction". *Environmental Science & Technology Letters*, 3, 57–61. https://doi.org/10.1021/acs.estlett.5b00348.

Xu, J., Xu, Y., Wang, H., Guo, C., Qiu, H., He, Y., Zhang, Y., Li, X., Meng, W. (2015). "Occurrence of antibiotics and antibiotic resistance genes in a sewage treatment plant and its effluent-receiving river". *Chemosphere*, 119, 1379–1385. https://doi.org/10.1016/j.chemosphere.2014.02.040.

Xu, P., Janex, M.-L., Savoye, P., Cockx, A., Lazarova, V. (2002). "Wastewater disinfection by ozone: main parameters for process design". *Water Research*, 36, 1043–1055. https://doi.org/10.1016/S0043-1354(01)00298-6.

Xu, X., Cai, J., Zhou, M., Du, X., Zhang, Y. (2020). "Photoelectrochemical degradation of 2,4-dichlorophenoxyacetic acid using electrochemically self-doped Blue TiO2 nanotube arrays with formic acid as electrolyte". *Journal of Hazardous Materials*, 382, 121096. https://doi.org/10.1016/j.jhazmat.2019.121096.

Xu, Y.; Yan, H.; Zhang, Y.; Jiang, K.; Lu, Y.; Ren, Y.; Wang, H.; Wang, S.; Xing, W. (2015). "A fully sealed plastic chip for multiplex PCR and its application in bacteria identification". *Lab Chip*, 15, 2826-2834. https://doi.org/10.1039/C5LC00244C.

Yang, Y. and Hoffmann, M.R. (2016). "Synthesis and Stabilization of Blue-Black TiO2 Nanotube Arrays for Electrochemical Oxidant Generation and Wastewater Treatment". *Environmental Science & Technology*, 50, 11888-11894. https://doi.org/10.1021/acs.est.6b03540.

Yang, Y., Shin, J., Jasper, J.T., Hoffmann, M.R. (2016). "Multilayer Heterojunction Anodes for Saline Wastewater Treatment: Design Strategies and Reactive Species Generation Mechanisms". *Environmental Science & Technology*, 50, 8780-8787. https://doi.org/10.1021/acs.est.6b00688.

Yang, Y., Kao, L.C., Liu, Y., Sun, K., Yu, H., Guo, J., Liou, S.Y.H., Hoffmann, M.R. (2018). "Cobalt-Doped Black TiO2 Nanotube Array as a Stable Anode for Oxygen Evolution and Electrochemical Wastewater Treatment". *ACS Catalysis*, 8, 4278–4287. https://doi.org/10.1021/acscatal.7b04340.

Yang, Y., Zhang, S., Wang, S., Zhang, K., Wang, H., Huang, J., Deng, S., Wang, B., Wang, Y., Yu, G. (2015). "Ball Milling Synthesized MnOx as Highly Active Catalyst for Gaseous POPs Removal: Significance of Mechanochemically Induced Oxygen Vacancies". *Environmental Science & Technology*, 49, 4473–4480. https://doi.org/10.1021/es505232f.

Yoon, Y., C. Dodd, M., Lee, Y. (2018). "Elimination of transforming activity and gene degradation during UV and UV/H2O2 treatment of plasmid-encoded antibiotic resistance genes". *Environmental Science: Water Research & Technology*, 4, 1239–1251. https://doi.org/10.1039/C8EW00200B.

Yoon, Y., Chung, H.J., Wen Di, D.Y., Dodd, M.C., Hur, H.-G., Lee, Y. (2017). "Inactivation efficiency of plasmid-encoded antibiotic resistance genes during water treatment with chlorine, UV, and UV/H2O2". *Water Research*, 123, 783–793. https://doi.org/10.1016/j.watres.2017.06.056.

Yuan, R., Chen, T., Fei, E., Lin, J., Ding, Z., Long, J., Zhang, Z., Fu, X., Liu, P., Wu, L., Wang, X. (2011). "Surface Chlorination of TiO2-Based Photocatalysts: A Way to Remarkably Improve Photocatalytic Activity in Both UV and Visible Region". *ACS Catalysis*, 1, 200–206. https://doi.org/10.1021/cs100122v.

Zehavi, D., Rabani, J. (1972). "Oxidation of aqueous bromide ions by hydroxyl radicals. Pulse radiolytic investigation". *The Journal of Physical Chemistry*, 76, 312–319. https://doi.org/10.1021/j100647a006.

Zhang, C., Ma, J., He, D., Waite, T.D. (2018). "Capacitive membrane stripping for ammonia recovery (CapAmm) from dilute wastewaters". *Environmental Science & Technology Letters*, 5, 43-49. https://doi.org/10.1021/acs.estlett.7b00534.

Zhang, T., Hu, Y., Jiang, L., Yao, S., Lin, K., Zhou, Y., Cui, C. (2019). "Removal of antibiotic resistance genes and control of horizontal transfer risk by UV, chlorination and UV/chlorination treatments of drinking water". *Chemical Engineering Journal*, 358, 589–597. https://doi.org/10.1016/j.cej.2018.09.218.

Zhang, Y., Gu, A.Z., He, M., Li, D., Chen, J. (2017). "Subinhibitory Concentrations of Disinfectants Promote the Horizontal Transfer of Multidrug Resistance Genes within and across Genera". *Environmental Science & Technology*, 51, 570–580. https://doi.org/10.1021/acs.est.6b03132.

Zhang, Y.Y., Zhuang, Y., Geng, J., Ren, H., Zhang, Y., Ding, L., Xu, K. (2015). "Inactivation of antibiotic resistance genes in municipal wastewater effluent by chlorination and sequential UV/chlorination disinfection". *Science of The Total Environment*, 512–513, 125–132. https://doi.org/10.1016/j.scitotenv.2015.01.028.

Zhang, Z., Li, B., Li, N., Sardar, M.F., Song, T., Zhu, C., Lv, X., Li, H. (2019). "Effects of UV disinfection on phenotypes and genotypes of antibiotic-resistant bacteria in secondary effluent from a municipal wastewater treatment plant". *Water Research*, 157, 546–554. https://doi.org/10.1016/j.watres.2019.03.079.

Zhang, Z.; Liu, W.; Xu, H.; Aguilar, Z. P.; Shah, N. P.; Wei, H. (2015). "Propidium monoazide combined with real-time PCR for selective detection of viable *Staphylococcus aureus* in milk powder and meat products". *Journal of Dairy Science*, 98, 1625-1633. http://doi.org/10.3168/jds.2014-8938.

Zhao, X., Lin, C.-W., Wang, J., Oh, D.H. (2014). "Advances in rapid detection methods for foodborne pathogens". *Journal of Microbiology and Biotechnology*, 24, 297–312. https://doi.org/10.4014/jmb.1310.10013.

Zhou, Y., Fan, X., Zhang, G., Dong, W. (2019). "Fabricating MoS2 nanoflakes photoanode with unprecedented high photoelectrochemical performance and multi-pollutants degradation test for water treatment". *Chemical Engineering Journal*, 356, 1003–1013. https://doi.org/10.1016/j.cej.2018.09.097.

Zhu, Y., Huang, X., Xie, X., Bahnemann, J., Lin, X., Wu, X., Wang, S., Hoffmann, M.R. (2018). "Propidium monoazide pretreatment on a 3D-printed microfluidic device for efficient PCR determination of 'live versus dead' microbial cells". *Environmental Science: Water Research & Technology*, 4, 956-963. https://doi.org/10.1039/C8EW00058A.

Zhuang, Y., Ren, H., Geng, J., Zhang, Yingying, Zhang, Yan, Ding, L., Xu, K. (2015). "Inactivation of antibiotic resistance genes in municipal wastewater by chlorination,

ultraviolet, and ozonation disinfection". *Environmental Science and Pollution Research*, 22, 7037–7044. https://doi.org/10.1007/s11356-014-3919-z.

Zuo, X., Xiao, Y., Plaxco, K.W. (2009). "High Specificity, Electrochemical Sandwich Assays Based on Single Aptamer Sequences and Suitable for the Direct Detection of Small-Molecule Targets in Blood and Other Complex Matrices". *Journal of the American Chemical Society*, 131, 6944–6945. https://doi.org/10.1021/ja901315w.

A p p e n d i x A

"NANOFILTRATION" ENABLED BY SUPER-ABSORBENT POLYMER BEADS FOR CONCENTRATING MICROORGANISMS IN WATER SAMPLES

Xie, X.; Bahnemann, J.; Wang, S.; Yang, Y.; Hoffmann, M. R. (2016). " 'Nanofiltration' Enabled by Super-Absorbent Polymer Beads for Concentrating Microorganisms in Water Samples". In: *Scientific Reports* 2016, 6, 20516. https://doi.org/10.1038/srep20516.

A p p e n d i x B

PROPIDIUM MONOAZIDE PRETREATMENT ON A 3D-PRINTED MICROFLUIDIC DEVICE FOR EFFICIENT PCR DETERMINATION OF 'LIVE VERSUS DEAD' MICROBIAL CELLS

Zhu, Y., Huang, X., Xie, X., Bahnemann, J., Lin, X., Wu, X., Wang, S., Hoffmann, M. R. (2018). "Propidium monoazide pretreatment on a 3D-printed microfluidic device for efficient PCR determination of 'live versus dead' microbial cells". In: *Environmental Science: Water Research & Technology* 2018, 4, (7), 956-963. https://doi.org/10.1039/C8EW00058A.